

LITHOFACIES AND CHEMOSTRATIGRAPHIC EVALUATION OF THE WOODFORD  
SHALE IN THE WESTERN ARKOMA AND EASTERN ANADARKO BASINS,  
OKLAHOMA

By

ELI CHRISTIAN REESE

Bachelor of Science in Geology

Oklahoma State University

Stillwater, OK

2013

Submitted to the Faculty of the  
Graduate College of the  
Oklahoma State University  
in partial fulfillment of  
the requirements for  
the Degree of  
MASTER OF SCIENCE  
December, 2016

LITHOFACIES AND CHEMOSTRATIGRAPHIC EVALUATION OF THE WOODFORD  
SHALE IN THE WESTERN ARKOMA AND EASTERN ANADARKO BASINS,  
OKLAHOMA

Thesis Approved:

Dr. Jim Puckette

---

Thesis Adviser

Dr. Jack Pashin

---

Dr. Mary Hileman

---

## ACKNOWLEDGEMENTS

I would like to acknowledge my great appreciation to my thesis adviser, Dr. Jim Puckette. The idea for this project was suggested by Dr. Puckette and his advice and encouragement during the past year helped make this project possible. I cannot express enough gratitude for everything he has done throughout this process. I would also like to thank my committee members, Dr. Jack Pashin and Dr. Mary Hileman for their availability and help during this process, as well as Newfield Exploration and the Oklahoma State University Boone Pickens School of Geology for providing me the tools and data needed to complete this project. Additionally, the support from my wife, family, and friends cannot be understated as they were essential in giving me confidence, encouragement, and advice. Most of all, I would like to thank my lord and savior Jesus Christ for continually blessing me throughout my life and I look forward to what the future holds.

Acknowledgements reflect the views of the author and are not endorsed by committee members or Oklahoma State University.

Name: ELI CHRISTIAN REESE

Date of Degree: DECEMBER, 2016

Title of Study: LITHOFACIES AND CHEMOSTRATIGRAPHIC EVALUATION OF THE  
WOODFORD SHALE IN THE WESTERN ARKOMA AND EASTERN ANADARKO  
BASINS, OKLAHOMA

Major Field: GEOLOGY

Abstract: The purpose of this study was to evaluate the chemo- and lithostratigraphic properties of the Woodford Shale in the Anadarko and Arkoma Basins of Oklahoma. Woodford Shale lithology varies considerably throughout Oklahoma due to depositional history and diagenesis. To understand the chemo- and lithostratigraphic properties of the Woodford, two cores, one from Garvin County in the Anadarko Basin, and another from Coal County in the Arkoma Basin were characterized using geochemical and lithologic properties. The two cores were described in detail at a one foot (30.48 cm) interval to record lithology, sedimentary, biogenic, structural and diagenetic features. Wireline logs were used to evaluate how gamma-ray, neutron, density, and resistivity signatures relate to changes in lithofacies. X-ray diffraction (XRD) and thin section petrography established bulk mineralogy whereas X-ray fluorescence (XRF) identified proxies for paleo-redox conditions during deposition, allowed an estimate of the geochemistry of bottom water, and estimation of frequency of disruption of stratification. The roles of radiolaria and *tasmanites* as sources of silica and organic matter, respectively, were analyzed. The relative abundance of silica and other non-clay components as quantified by XRD were compared to wireline log curves to determine if a set of parameters could be developed whereby conventional log curves could be used to detect and map brittle zones with a propensity to fracture naturally or artificially. If these brittle zones are mappable, log signatures can be used to help explore for and develop oil and gas reserves in the Woodford Shale.



## TABLE OF CONTENTS

Chapter	Page
I. INTRODUCTION.....	1
II. PREVIOUS WORK.....	5
Black Shale.....	7
Woodford Geologic Setting.....	10
Tectonic Setting.....	12
Sedimentology.....	14
III. METHODS & RESULTS.....	19
Williams 1H-7X Core Overview.....	21
McDonald 2H-16E Core Overview.....	33
Chemostratigraphy Overview.....	40
Williams 1H-7X Chemostratigraphic Analysis.....	43
McDonald 2H-16E Chemostratigraphic Analysis.....	48
Wireline Log Analysis.....	49
Williams 1H-7X Wireline Analysis.....	52
McDonald 2H-16E Wireline Analysis.....	55
IV. DISCUSSION & CONCLUSIONS.....	57
REFERENCES.....	70
APPENDICES.....	76

## LIST OF TABLES

Table	Page
1. Key elements and their associated environmental proxies.....	41

## LIST OF FIGURES

Figure	Page
1. Geological provinces of Oklahoma.....	4
2. Stratigraphic nomenclature of part of the Ordovician through Mississippian Section of the southern Anadarko Basin and western Arkoma Basin.....	6
3. Late Devonian paleogeography of Laurussia showing major trade winds.....	9
4. Map of the southwestern United States, showing approximate boundaries of the Oklahoma Basin, Southern Oklahoma Aulacogen, and other major features that existed in early Paleozoic time.....	11
5. The tectonic evolution of the Southern Oklahoma Aulacogen.....	13
6. Water circulation during the Late Devonian eustatic highstand.....	17
7. Lower and upper contacts of the Woodford Shale in the Williams 1H-7X.....	22
8. Description of the Williams 1H-7X core with sedimentary, biogenic, and tectonic features.....	23
9. Mudstone classification ternary diagram of the Williams 1H-7X.....	24
10. Thin section and core photographs of the AM lithofacies of the Woodford Shale, Williams 1H-7X core.....	25
11. Thin section and core photographs of the A-SM lithofacies of the Woodford Shale, Williams 1H-7X core.....	27
12. Thin section and core photographs of the S-DM lithofacies of the Woodford Shale, Williams 1H-7X core.....	28
13. Thin section and core photographs of the SM lithofacies of the Woodford Shale, Williams 1H-7X core.....	30
14. Thin section and core photographs of the P-SM lithofacies of the Woodford Shale, Williams 1H-7X core.....	32
15. Description of the McDonald 2H-16E core with sedimentary, biogenic, and tectonic features.....	34
16. Mudstone classification ternary diagram of the McDonald 2H-16E core.....	35
17. Thin section and core photographs for the AM lithofacies of the Woodford Shale, McDonald 2H-16E core.....	36
18. Thin section and core photographs for the A-SM lithofacies of the Woodford Shale, McDonald 2H-16E core.....	38
19. Thin section and core photographs of the SM lithofacies of the Woodford Shale, McDonald 2H-16E core.....	40
20. Chemostratigraphic profile for the Williams 1H-7X.....	42
21. Chemostratigraphic profile for the McDonald 2H-16E.....	47
22. Digital wireline log across the Woodford Shale showing the characteristics of lithofacies in the Williams 1H-7X.....	51

23. Digital wireline log across the Woodford Shale showing the characteristics of lithofacies in the McDonald 2H-16E.....	54
24. Late Devonian schematic depositional model including cores used in this study.....	59
25. Interpretational paleogeographic map with core locations marked by stars.....	59
26. Current features and associated oxygenated water indicators.....	64
27. Comparison of density and neutron porosity values with increasing clay content in the Williams 1H-7X and McDonald 2H-16E.....	66
28. Comparison of silica percentage with number of fractures in the SM lithofacies of the Williams 1H-7X.....	67

## CHAPTER I

### INTRODUCTION

The Late Devonian-Early Mississippian Woodford Shale is best classified as a mudrock, a sedimentary rock of clay and/or silt-sized constituents that include differing amounts of clay, silica, carbonate, and metals (Arthur and Sageman, 1994). The current interest in shales is the result of natural gas production, which started in the late 1800s, but came of age in the 21<sup>st</sup> century with exploration in formations such as the Barnett Shale in Texas, Marcellus Shale in the Appalachian Basin, Fayetteville Shale in Arkansas, Haynesville/Bossier in Louisiana, and the Woodford Shale in Oklahoma (USGS, 2012). The Woodford Shale and other Upper-Devonian formations including the Marcellus (Pennsylvania, West Virginia), Chattanooga (Tennessee, Kentucky), and Bakken (North Dakota) shales are believed to have sourced nearly 8% of the world's oil and gas reserves (Ulmishek and Klemme, 1990). Each shale reservoir/source is unique in its own way as a result of differences in the geologic settings of each basin during deposition and post-deposition history (USGS, 2012). This research is focused on examining cores from the eastern Anadarko Basin and the western Arkoma Basin in Oklahoma (Figure 1).

The Woodford Shale is a prolific hydrocarbon source rock throughout the southern Midcontinent of the United States (Comer, 1992). Historically, formations such as the

Mississippian Limestone, Hunton Group, and the Misener sandstone have been identified as reservoirs for hydrocarbons sourced from the Woodford Shale. Recent advancements in technology such as horizontal drilling and hydraulic fracturing, have allowed the Woodford Shale to be targeted as a self-sourced reservoir for more than a decade (Cardot, 2012). It is estimated that 70 to 85 percent of commercial oil reserves in central and southern Oklahoma were sourced from the Woodford (Comer, 1992). Though the Anadarko and Arkoma Basins are relatively close geographically, the Woodford Shale between and within these basins display a range of thermal maturities, a variety of sedimentary and biogenic structures, experienced different tectonic histories and paleo-redox conditions, and contains an interesting and informative set of lithofacies. Certain Woodford Shale lithologic characteristics are linked to increased hydrocarbon production. The presence of silica increases rock brittleness leading to natural fractures and the formation of rock properties amenable to hydraulic fracturing and oil and gas production. The origin of silica in the Woodford Shale is attributed to either detrital quartz or dissolution of silicified radiolarians (Cecil, 2016). Locating silica-rich intervals and assessing their impact on rock fabric is critical to interpreting rock brittleness as the occurrence of isolated quartz silt grains surrounded by clay minerals often does not result in a silica-cemented interval. It is the goal of this study to assess the depositional, biogenic, geochemical, tectonic, and diagenetic processes operating during Woodford time in the region that is now known as the transition area between the Anadarko and Arkoma Basins. As the Arkoma and Anadarko Basins, *per se*, did not exist during Woodford time it is expected that the processes operating in both currently defined areas were the same. Based on this premise, the following hypotheses are proposed.

- Since both study sections were deposited in the same basin, they should display similar lithologic, biogenic, and diagenetic features, and if proximal to the upwelling zone, should contain accumulations of radiolarians and phosphate nodules.
- Silica-rich (chert) beds, which are expected in both representative cores, are primarily the result of radiolarian accumulations, and should contain a higher frequency of natural fractures.
- Silica-rich zones, as well as those cemented by carbonates and pyrite will contain less clay minerals and have signatures recognizable on wireline logs.

The following objectives were formulated to test these hypotheses. These objectives address determining both the lithologic character and paleo-redox conditions during deposition and include:

- Establishing a detailed description of the lithologic, biogenic, and diagenetic features of each core,
- Establishing paleo-redox during Woodford deposition from trace elements using XRF and describing how the changes in the sedimentology/lithology relate to changes in geochemical signatures, and
- Determining a set of parameters for conventional log curves that can be used to detect and map brittle zones.

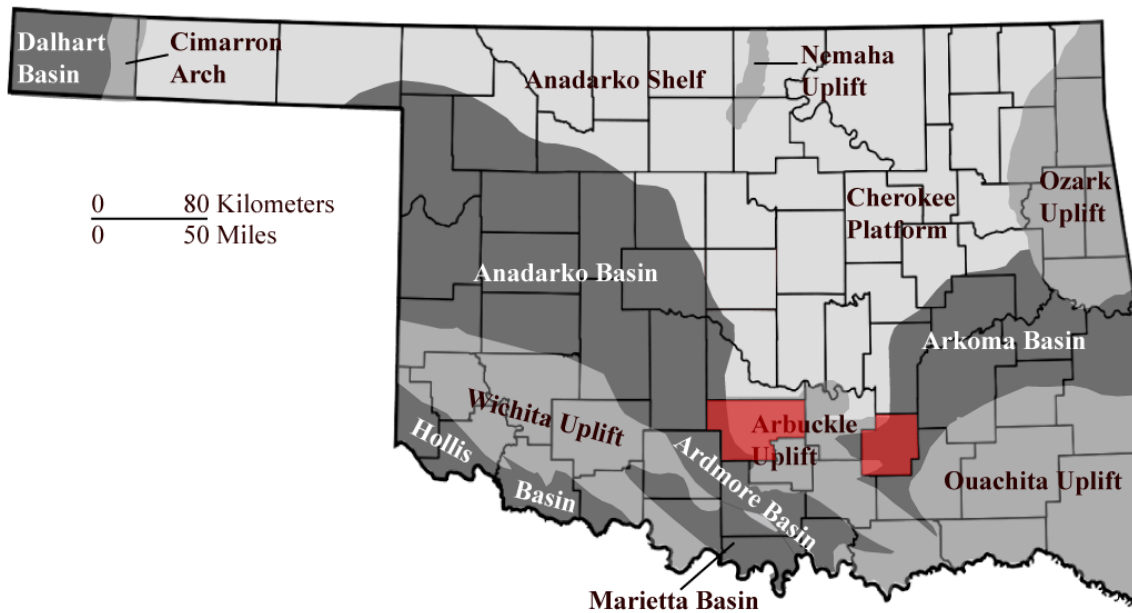


**Figure 1.** Geological provinces of Oklahoma (Modified from Oklahoma Geological Society). Core locations are indicated by highlighted counties in red (OGS, 2016).



## CHAPTER II

### PREVIOUS WORK

The Woodford Shale was originally described as a limy chert interbedded with shales of Upper Devonian in age that correlated with the Chattanooga Shale of eastern Oklahoma, Alabama, and Tennessee (Taff, 1902). Conodont derived ages from measured Woodford Shale sections in Oklahoma showed that the Woodford is mostly Late Devonian (Frasnian-Famennian) in age, with the uppermost part being Early Mississippian in parts of southern Oklahoma (Tournaisian-Kinderhookian) (Hass and Huddle, 1965). Traditionally, the Woodford Shale was subdivided into three units, lower, middle, and upper based on lithology, radioactivity, and electric log patterns (Ellison, 1950). Recent geochemical studies based on total organic carbon (TOC) and mineralogy as well as detailed core descriptions further subdivide the Woodford Shale into well-defined lithofacies (Caldwell, 2011). Seven different lithofacies and fifteen stratigraphic units make up the Woodford Shale in the eastern Anadarko Basin, with the main mineral constituents being quartz, dolomite, and clay (Caldwell, 2011). These Woodford lithofacies are not universally distributed and vary as the result of paleogeography and proximity to upwelling currents (Kvale, 2014; McCullough and Slatt, 2014). The Woodford Shale is easily recognized using wireline logs due to a high gamma-ray signature (>300 API) (Lambert, 1993). This high level of radioactivity in the Woodford is attributed to an abundance of the radiogenic elements thorium, potassium, and mostly uranium (Blackford, 2007). The Woodford Shale is rich in organic matter and its bulk organic composition includes Type II Kerogen (oil

generating), amorphous organic matter, and vitrinite (Cardott, 2013). The high total organic carbon (TOC) contributes to the dark color of the Woodford Shale, which is described as a black, siliceous mudrock containing an abundance of natural fractures caused by its inherent brittleness (Cardott, 2013). The favorable lithological characteristics and organic composition of the Woodford Shale formed a unique “self-sourcing” reservoir that has recently become an important exploration target. Because of the regional pre-Woodford unconformity, the Woodford overlies a number of older strata including the Hunton Group, Sylvan Shale, Viola Limestone, Simpson Sandstone, and Arbuckle Group (McCullough and Slatt, 2014). Where the Woodford Shale overlies the Sylvan Shale, the Woodford tends to be thicker due to erosion of the underlying shale. In contrast, erosion of the Hunton Group or Viola Group is somewhat less. As a result, erosion of the Sylvan Shale formed deeper incised valleys that accommodated thicker intervals of Woodford deposition (McCullough and Slatt, 2014).

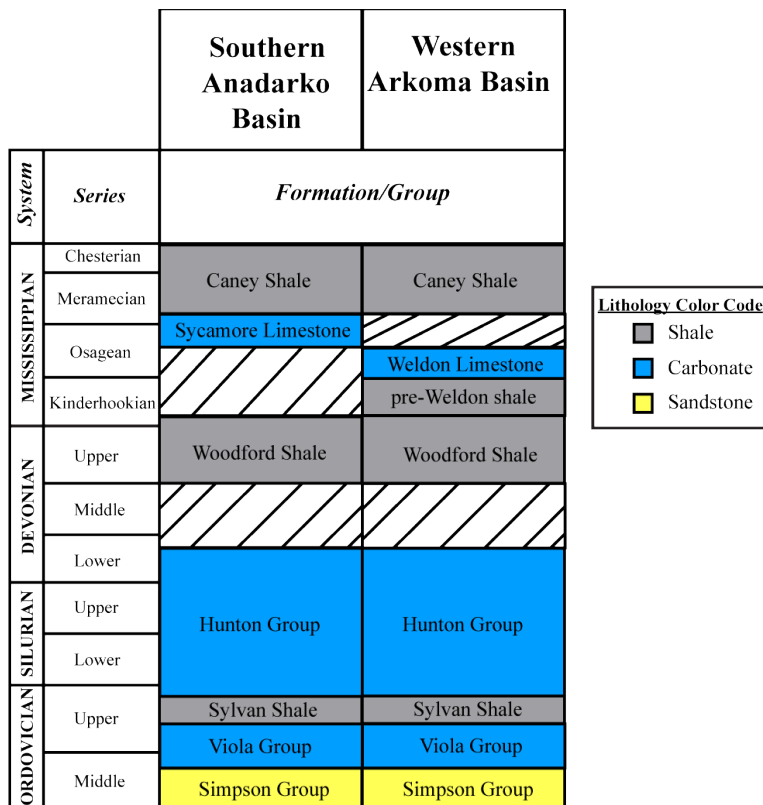


**Figure 2.** Stratigraphic nomenclature of part of the Ordovician through Mississippian section of the southern Anadarko Basin and western Arkoma Basin (Modified from Bebout et al., 1993; Arbenz, 2008; Boardman et al., 2008).

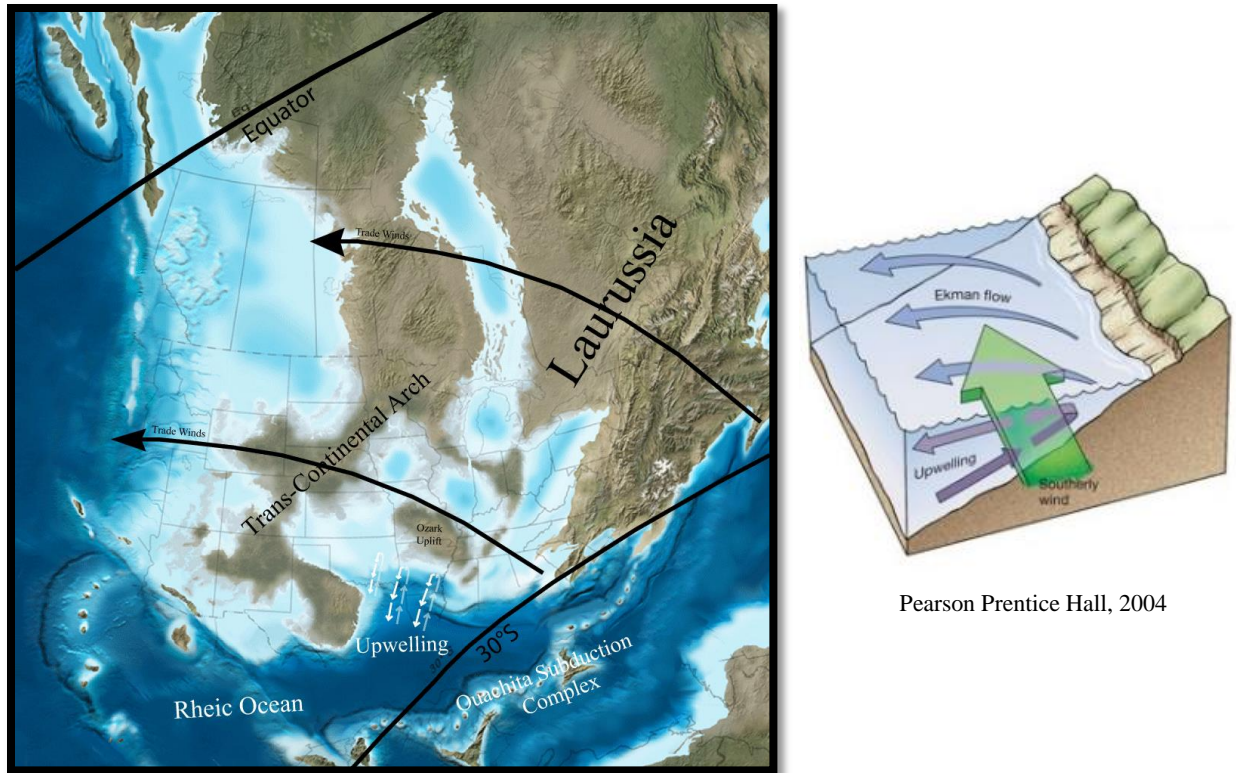
### *Black shale*

The term “black shale” is used for laminated to non-laminated, dark-colored, fine-grained sedimentary rock relatively abundant in organic matter and containing various mineral constituents such as  $\text{CaCO}_3$  and  $\text{SiO}_2$  (Arthur and Sageman, 1994; Meyers and Mitterer, 1986). Black shales differentiate from other mudrocks due to the copious amounts of organic matter (1-30%) which is the primary source for the dark color in ancient shale facies (Trask and Patnode, 1942; Weissert, 1981). Because the amount of organic matter separates black shales from other mudrocks, the definition can be skewed when organic matter is reduced from the mudrock due to thermal maturity or metamorphism (Raiswell and Berner, 1985). Black shales are hydrocarbon source rocks (Meyers and Mitterer, 1986) and as a result, have been of significant interest to the oil and gas industry. If given sufficient exposure to pressure and heat, the source rock is capable of yielding gas, oil, and other by-products due to the conversion of organic matter into hydrocarbons (McCarthy, 2011).

Early interpretations of the depositional conditions that form black shale resorted to the application of uniformitarianism principles by searching for modern analogues of dark, organic carbon-rich muds (Arthur and Sageman, 1994). Most agreed that the conditions for organic-rich mud deposition included an essential supply of organic matter, conditions to preserve the organic matter, and states of anoxia (Arthur and Sageman, 1994; Pettijohn, 1957). The barred basin depositional model was widely accepted due to examples of the Black Sea (deep sea) and Baltic Sea (shallow sea) where steady stratification and/or sills restricted bottom water currents and advanced oxygen deficiency, as well as open marine environments such as coastal upwelling zones (Arthur and Sageman, 1994). The depth at which black mud deposition occurs is widely debated due to the high variability of sea level depths in the modern environments (Arthur and

Sageman, 1994). Vine and Tourtelot (1970) classified the geologic settings of black shales into three generalized model depositional environments: restricted circulation, continental shelf, and open marine. In each of the depositional models, the abundance of organic matter depletes the oxygen and produces conditions where organic rich-sediments and hydrogen sulfide can accumulate (Tourtelot, 1979). Most ancient black shales are believed to have formed in shallow epicontinental marine environments, for which there are no modern analogues (Rezaee, 2015).

The Upper Devonian black shales were deposited during a time of global transgression and greenhouse conditions that resulted in increased levels of carbon dioxide as well as sea level rise that contributed to increased marine organic productivity (Ettensohn, 1992) (Figure 3). In addition, the Upper Devonian embayment located south of the Transcontinental Arch in Laurussia produced paleogeographic and tectonic conditions that culminated in a favorable depositional setting. These included 1) a subtropical position of 15° and 30° south latitude leading to an increase in solar radiation, 2) an Upper Devonian embayment nearly enclosed due to surrounding landmasses that restricted the circulation of oxygenated waters, 3) coastal upwelling and increased organic productivity resulting from a southern trade-wind belt, and 4) the development of a deep foreland basin separated by shallow sills and structural highs provided conditions for black mud to accumulate and prevented dilution by clastics (Ettensohn, 1992). Despite the favorable depositional settings, interpreting depositional environments is complicated due to the lack of modern analogues that compare to the broad epeiric sea that covered most of North America during the Late Devonian (Comer, 1991).



Pearson Prentice Hall, 2004

**Figure 3.** Late Devonian paleogeography of Laurussia showing major trade winds (Modified from Blakey, 2016). Right figure shows formation of upwelling in southern hemisphere (Pearson Prentice Hall, 2004).

The Devonian-Mississippian Woodford Shale occurs across a broad area including Oklahoma, the present Permian Basin of west Texas, and southeastern New Mexico. The Woodford Shale is correlative to the organic-rich Devonian-Mississippian shale mapped as the Chattanooga Shale in eastern Oklahoma, Arkansas, Missouri, and Kansas (Lambert, 1993). Equivalent Devonian-Mississippian-aged formations include the New Albany Shale (Illinois Basin), Marcellus Shale (Appalachian Basin), Ohio Shale (Appalachian Basin), Chattanooga Shale (Appalachian and Black Warrior Basin), Antrim Shale (Michigan Basin), Exshaw Formation (Alberta Basin) and the Bakken Formation (Williston Basin) (O'Brien and others, 1994).

### *Woodford geologic setting*

The Upper Devonian-Lower Mississippian Woodford Shale occurring in Oklahoma, Texas, and New Mexico is “siliceous” due to the abundance of radiolarian bearing bedded cherts and black, fissile, phosphatic shale (Boardman and others, 2008; McCullough and Slatt, 2014). Regionally, the Woodford Shale formed in a shallow epeiric sea called the Oklahoma Basin. The Oklahoma Basin developed over the failed arm of a triple junction referred to as the Southern Oklahoma Aulacogen, and the combined basin along with proximity to the Ouachita Embayment resulted in a variety of facies including novaculitic chert that contains an abundance of biogenically sourced silica (Cecil, 2016)(Figure 4).

Deposition of Woodford sediments began during a transgression that drowned marine embayments and covered subaerially eroded Ordovician to Lower Devonian strata in now what is recognized as the deepest areas of the Anadarko and Arkoma Basins (Comer, 2007). Periodic coastal upwelling supported normal marine planktonic biota in the upper zones of the water column, while anaerobic and dysaerobic conditions developed near the bottom waters due to the formation of halocline and pycnocline layers that restricted water mixing (Comer, 2007) (Figure 6). Organic- and sulfide-rich mud formed due to slow settling of pelagic debris such as radiolarians, conodonts, ammonoids, and fish debris on the oxygen-deficient sea floor; however, turbidity currents from periodic storms and earthquakes would deposit silt and mud to the basin depocenters (Boardman and others, 2008; Comer, 2007). The “siliceous” component of the Woodford Shale is attributed to novaculitic chert and detrital quartz grains with detrital quartz generally increasing to the north. Chert is biogenic and forms mostly from the skeletons of radiolarians that bloomed during upwellings and then were altered in the water column on the

sea floor; chert formed along the margin of the Ouachita Embayment and distal shelves of the Oklahoma Basin, now identified with the Anadarko and Arkoma Basins (Comer, 2007; Jasin, 1992). Comer (2012) suggested that aridity and high evaporation rates were the primary factors that controlled the paleo-upwelling systems; however, Kvale and Bynum (2014) suggest that the major Upper Devonian southeasterly trade wind belts were the essential drivers behind the coastal upwelling systems. Detrital quartz grains, transported from exposed older sources, are found along the northwestern shelf of the Anadarko Basin and in turbidity flows that deposited in the basin depocenters (Comer, 2007). The combination of silica-rich zones with high TOC and favorable thermal maturity generated conditions that resulted in the Woodford Shale being an ideal exploration target.

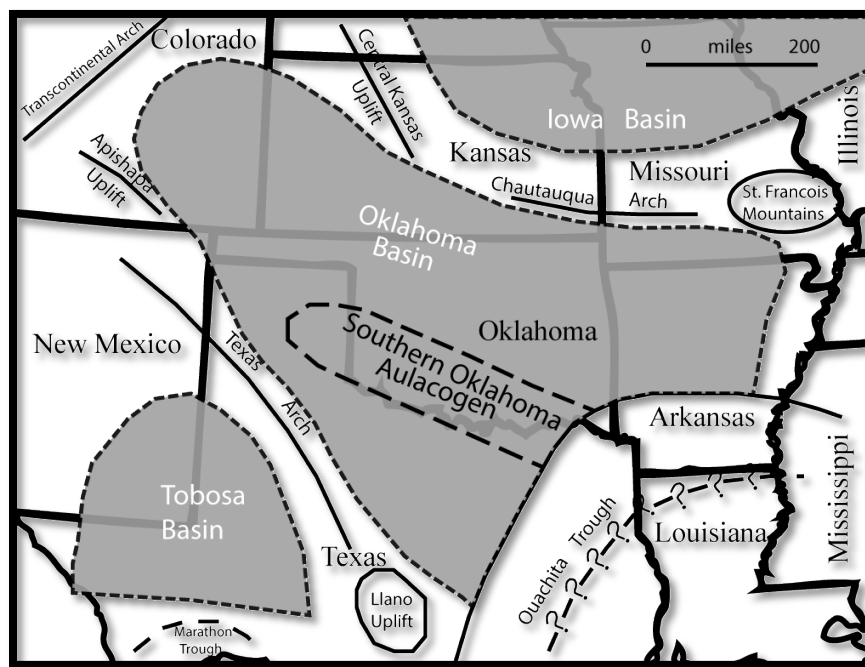


**Figure 4.** Map of southwestern United States, showing approximate boundaries of the Oklahoma Basin, Southern Oklahoma Aulacogen, and other major features that existed in early Paleozoic time (Modified from Northcutt et al., 2001).

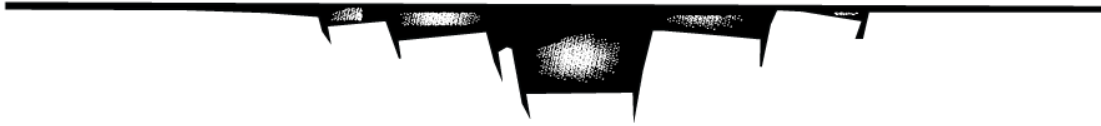
### *Tectonic setting*

Most of the Upper Devonian deposition of black shales occurred during the Acadian Orogeny, a major continent-continent collision that lasted from the Middle Devonian to the Early Mississippian (Ettensohn and Barron, 1981). The Acadian Orogeny was associated with a rise in sea level when Gondwanaland collided with the Avalon-Massachusetts Peninsula; this collision led to the Kaskaskia Sea transgressing over most of the Laurussian supercontinent (Ettensohn and Barron, 1981). According to Sloss and Speed (1974), global sea transgression is associated with periods of plate convergence due to accelerated spreading rates. During accelerated spreading, elevation of the spreading center and ocean bottom causes sea transgression from upward displacement (Sloss and Speed, 1974). During this time, the deposition of organic-rich sediments advanced across the southern Midcontinent's continental arches and cratonic basins adjacent to the Ouachita Embayment of the Rheic Ocean in Oklahoma and Arkansas (Callner, 2014).

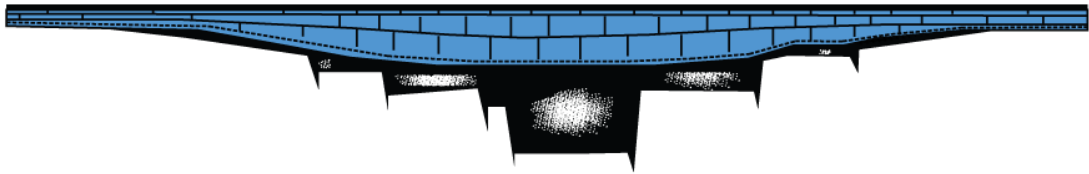
The early Pennsylvanian orogeny contributed to natural fracturing within the silica-rich Woodford Shale (30-87% quartz; Cardott, 2008; Berryman, 2012). Evidence of earlier syndepositional tectonics was reported by Callner (2014) for Woodford Shale formed along the axis of the Anadarko Basin. Fracturing and folding of the Woodford Shale started relatively early, occurring approximately 20 million years after deposition ended during the Early Mississippian (Tournaisian)(Ataman, 2008; Berryman, 2012). The Southern Oklahoma Aulacogen was inverted during the Late Mississippian with the initiation of the Wichita Orogeny, and ended with the onset of the Arbuckle Orogeny in the Vigilian (Hardie, 1990) (Figure 5).



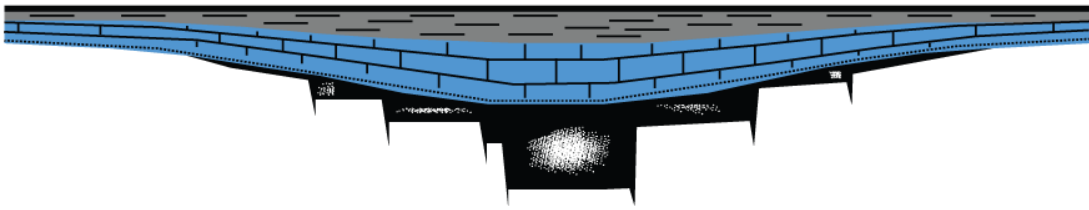
A. Late Proterozoic thru Mid-Cambrian



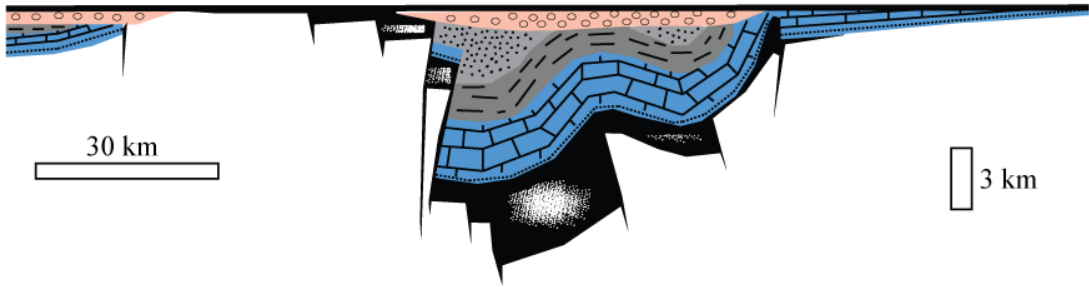
B. Late Cambrian thru Early Devonian



C. Late Devonian thru Mississippian



D. Pennsylvanian thru Permian



30 km

3 km

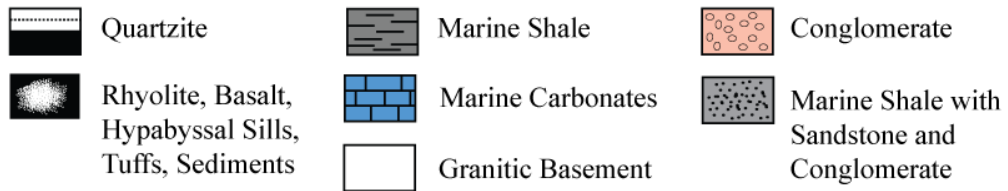


**Figure 5.** The tectonic evolution of the Southern Oklahoma Aulacogen (Modified from Hoffman et al., 1974).

## *Sedimentology*

The siliceous black, fissile Woodford Shale contains a variety of physical and biogenic sedimentary structures that provide an abundance of information concerning the depositional environment. Ripple marks, cross laminae, lag deposits, and inverse and normal grading can indicate upwelling, wave propagation, storm beds, and internal tides (Pashin and Callner, 2014). In marine environments, such as the epicontinental sea in which the Woodford Shale formed, sediments rarely originate from a single source. Comer (2008) classified the variety of Woodford Shale sedimentary features into four different categories based on the origin of the sediment: 1) terrigenous sediment derived from erosion of rocks above sea level, 2) pelagic sediment derived from the accumulation of slow settling marine particles on the sea floor, 3) benthic sediment derived from biota living at or near the benthic zone, and 4) authigenic sediment derived from precipitation of minerals by *in situ* on the sea floor.

Detrital sediments such as quartz, illite, muscovite, feldspar, wood fragments, vitrinite, and heavier minerals (zircon, tourmaline) are recognized as part of the bulk mineralogy of the Woodford Shale. However, biogenic sediments are more common due to the Woodford Shale being deposited in shallow marine settings with low clastic influxes (Comer, 2008). Detrital sediments, especially quartz, are more abundant in areas where Woodford deposition occurred near land such as the inner shelf position of the present Ozark region and northeastern Anadarko Basin and as sediment flows down incised valleys and turbidites in basin depocenters (Comer, 2007).

The abundant accumulation of organic matter in the Woodford Shale was the result of pelagic sediment deposition on anaerobic and dysoxic seafloors. The rich concentration of organic matter coincides with copious deposits of biogenic silica, suggesting that the upper levels

of the water column contained high biologic activity (Comer, 2008). Biogenic silica forms as a result of diagenetic alteration of siliceous microfossils such as radiolarians, diatoms, silicoflagellates, and sponges (Einsele, 2000; Kvale and Bynum, 2014). Presently, the most abundant siliceous organism in modern oceans is diatoms; however, radiolarians have more robust opaline silica skeletons for preservation and are abundant throughout the Woodford Shale at distal parts of major cratonic basins (Anadarko, Arkoma, Ardmore, etc.) (Lisitzin, 1972; Blueford 1989; Comer, 2007; Einsele, 2000). *Tasmanites* algal cysts are common organic fragments in the Woodford Shale and were hollow and easily compacted unless cemented soon after deposition (Comer, 2007). In addition to structured organic matter (*tasmanites*), the Woodford Shale also contains amorphonite, which can be intermingled within the mineral matrices of the shale (Camp and others, 2013). The abundance of amorphous organic matter and algal remains coinciding with limited vitrinite input correlates with marine settings and limited terrestrial input (Furmann, 2013). Index fossils such as conodonts provide the temporal biostratigraphic framework for the Woodford Shale (Ettensohn and others, 1988).

For decades, many interpretations proposed geochemical models representing that only anoxic seafloor conditions existed during Woodford deposition and as a result inhibited all benthic organisms (Johnson and others, 1989). However, recent core analyses show that bioturbation and burrows along with benthic foraminifera occur in the Woodford Shale, indicating periods of oxygenation during deposition (Kennedy, 2014; Snider, 2014; Puckette, 2013). The micro-scale of burrows and their scarcity are evidence that some periods of oxygenation were brief. The presence of burrowing organisms that consumed organic-rich sediments implies mechanisms for oxidizing organic matter using nitrate or sulfate and the

suppression of burrowing resulted in finely laminated structures and high concentrations of organic matter (Peters, 2006).

The Woodford Shale contains an abundance of pyrite in the form of disseminated crystalline pyrite, framboids, and nodules. Isolated smaller pyrite framboids formed authigenically within the water column (Suits and Wilkin, 1998). Larger framboids, disseminated pyrite, and nodules formed diagenetically below the sediment-water interface from microbial sulfate reduction (Berner, 1980, 1984; Pashin and Callner, 2014). Early diagenetic alterations in the Woodford Shale formed pyrite- and chert-filled *tasmanites* cysts, the latter forming due to the dissolution of siliceous radiolaria (Schieber, 1994). Burrows and syneresis cracks, compacted fractures and cemented during early diagenesis (Comer, 1991), are examples of bedding and sedimentary structures that can be infilled by pyrite, calcite, dolomite, or quartz (Comer, 2008). Dolomite, the byproduct of organic matter degradation and dissolution of biogenic calcite, formed penecontemporaneously with the organic-rich Woodford Shale (Comer, 2008). The natural fractures in the Woodford Shale can be infilled with authigenic minerals such as calcite, dolomite, and silica. Calcite precipitation from aqueous solutions was likely sourced from the underlying Hunton Group (Berryman, 2012; Comer, 2007). Phosphate nodule formation was favored by an abundance of skeletal remains for nodule nucleation, a high concentration of  $\text{PO}_4$  ions in upwelling seawater and the generation of thermoclines associated with coastal upwelling (Boardman, 2012) (Figure 6).

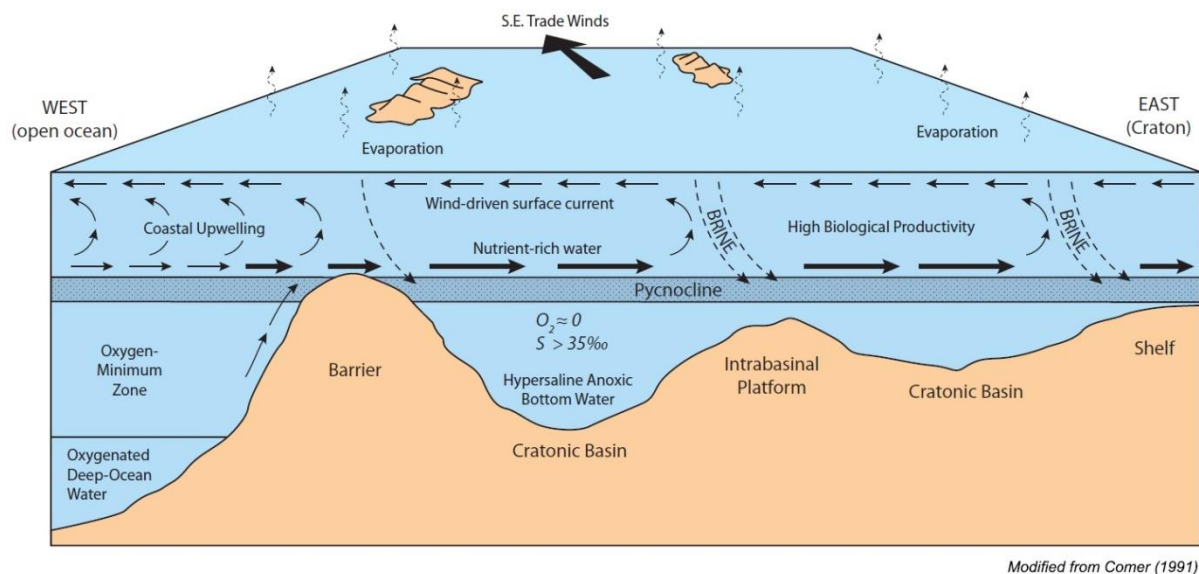


**Figure 6.** Water circulation during the Late Devonian eustatic highstand (Modified from Comer, 1991).

### *Geochemistry*

Organic matter degradation near the sediment-water interface determines the amount of dissolved oxygen in the water column and is the primary controlling factor in determining the state of redox (Musa, 2013). Paleoredox conditions can be reconstructed using selected trace elements due to the varying solubility of the element under oxidizing vs reducing conditions, concentrations influenced by watermass restriction, and preservation from relative immobility in the sediment (Tribovillard et al, 2006; Algeo and Rowe, 2011). An extensive assortment of metallic and nonmetallic elements can differentiate depositional conditions indicated by their enrichment or depletion in organic-rich shale (Rimmer, 2004). Trace metals such as Ag, Cd, Mo, V, Cu, Zn, U, and Ni can be used as proxies to identify redox conditions during deposition

(Arthur and Sageman, 1994). Uranium is an important trace element that serves as a geochemical proxy to estimate depositional conditions and organic-richness of shale. In oxygen-deficient settings, uranium diffused from seawater precipitates into sediments, thereby increasing uranium concentration concurrently with the preservation of associated organic matter (Luning and Kolonic, 2003). Anoxic/dysoxic depositional environments are indicated by high concentrations of U and V, and low concentrations of Mo (Algeo and Rowe, 2011). Euxinic conditions at the sediment-water interface are characterized by high concentrations of U, V, and Mo (Algeo and Maynard, 2004; Tribovillard et al., 2004b, 2005). Enrichment of U, V, and Mo combined with the sedimentary presence of organic matter (Ni and Cu) can distinguish whether anoxic conditions were triggered by an influx of organic matter degradation (Tribovillard et al., 2006). Oxidic depositional conditions are enriched with elements such as Ti and Al (Morford and Emerson, 1999). Detrital input is indicated by cross plotting trace elements versus aluminum or titanium, which are of detrital origin (Tribovillard et al., 2006).

## CHAPTER III

### METHODS AND RESULTS

The focal point of this study is the description and analysis of two Woodford Shale cores provided by Newfield Exploration, the Williams 1H-7X and the McDonald 2H-16E. The Williams 1H-7X is located in Garvin County, OK, in the NW/4 of the SW/4 of Section 19, Township 2 North, Range 3 West. The McDonald 2H-16E is located in Coal County, OK, in the NE/4 of the NW/4 of Section 16, Township 2 North, Range 9 East. Core derived data including total organic carbon (TOC), bulk mineralogy from x-ray diffraction (XRD), thin sections, and spectral gamma-ray curves were provided by Newfield Exploration for the Williams 1H-7X and McDonald 2H-16E. Bulk mineralogy and generalized lithofacies composition were determined from x-ray diffraction (XRD) data. Eighty-six (86) thin sections were described to determine general composition, rock fabric and texture, and biogenic, sedimentary, and diagenetic structures. Thin sections were photographed using a Olympus EX51 epifluorescence microscope. Total and spectral gamma-ray curves were plotted across the entire Woodford interval in both cores to compare lithology, gamma-ray and resistivity signatures, and uranium and thorium concentrations.

X-ray fluorescence (XRF) measurements were collected to establish trace element concentrations. The XRF survey was conducted at 1 foot intervals using a handheld Thermo Scientific Niton™ XL 3t GOLDD device with a sample time of 180 seconds. Additional information regarding the handheld XRF device can be found at <http://www.us-tech.co.za/>. The

device was calibrated every 10 samples using the United States Geological Survey (USGS) Cody Shale (SCo-1) and the National Institute of Standards and Technology (NIST) hard rock mine waste (2780). The calibrations provided a means to establish correction factors for elements of interest and to compensate for instrumental drift. Individual elements were corrected based on the deviation of specific elements from known standard values. The deviation percentage was acquired using this equation:

$$\text{Correction Factor} = \frac{\text{Element}_{\text{USGS Standard Reported Value}}}{\text{Element}_{\text{Average XRF Measured Value}}}$$

Once corrected, the elements were normalized by the concentration of aluminum in order to better proportion for biogenic diluents such as CaCO<sub>3</sub> and opal (Tribovillard, 2006). The XRF device can measure up to 35 different elements including silicon (Si), aluminum (Al), vanadium (V), calcium (Ca), zinc (Zn), chromium (Cr), copper (Cu), molybdenum (Mo), titanium (Ti), potassium (K), nickel (Ni), uranium (U), etc. for each individual sample. Elemental ratios such as V/Cr, U, V, Zr, and Ti were used to determine paleo-redox conditions during Woodford Shale deposition (Rimmer, 2004; Boardman, 2012). Threshold values indicative of oxic, dysoxic, or anoxic paleo-depositional settings were compared to the ratios of V/Cr (Jones and Manning, 1994; Rimmer, 2004). Individual elements such as U and V can indicate deep marine conditions and organic-richness, whereas higher concentrations of elements such as Zr and Ti can be indicative of terrestrial input and more oxic settings (Luning and Kolonic, 2003; Tribovillard, 2006). Descriptions of lithology and physical features were recorded at intervals no larger than one (1) foot (30.48 cm) to capture detailed lithology, sedimentary structures, fractures, and other physical or deformation structures.



*Williams 1H-7X*

The Williams 1H-7X was cored from 12,707.25 feet to 13,005.2 feet (core depth). The core consists of the lower interval of the Caney Shale (12,707.25' to 12,745'), the Woodford Shale (12,744.5' to 12,967.8'), and the top of the Hunton Group (12,967.8' to 13,005.2'). The underlying 37 feet of cored Hunton Group is a medium to medium dark gray (N5-N4, GSA rock color chart) limestone containing an abundance of normal marine invertebrate fossils including brachiopods, echinoderms, and gastropods. The Hunton Group carbonate forms a sloping sharp contact with the base of the Woodford Shale (Figure 7). The contact is marked by an abrupt change from medium dark gray limestone to a grayish black (N2) mudstone containing phosphate nodules, burrows, soft-sediment deformation within interbedded argillaceous medium dark gray bands (N4), pyrite nodules, faulting, and minor gypsum crystals. The bulk of the 223 feet of cored Woodford Shale is grayish black mudstone with numerous intervals enriched in quartz, carbonate, pyrite (laminae, nodules, and disseminated grains), open and mineralized ptigmatic and vertical fractures, micro-faulting, minor burrowing and skeletal fragments (Figure 8). A phosphatic glauconitic zone at 12,744.5' indicates the unconformable contact with the overlying Caney Shale (Figure 7). Thirty-eight feet of the Caney Shale were cored consisting of a medium dark gray to medium gray (N4-N5) mudstone with abundant burrowing, fossils, and disseminated pyrite.

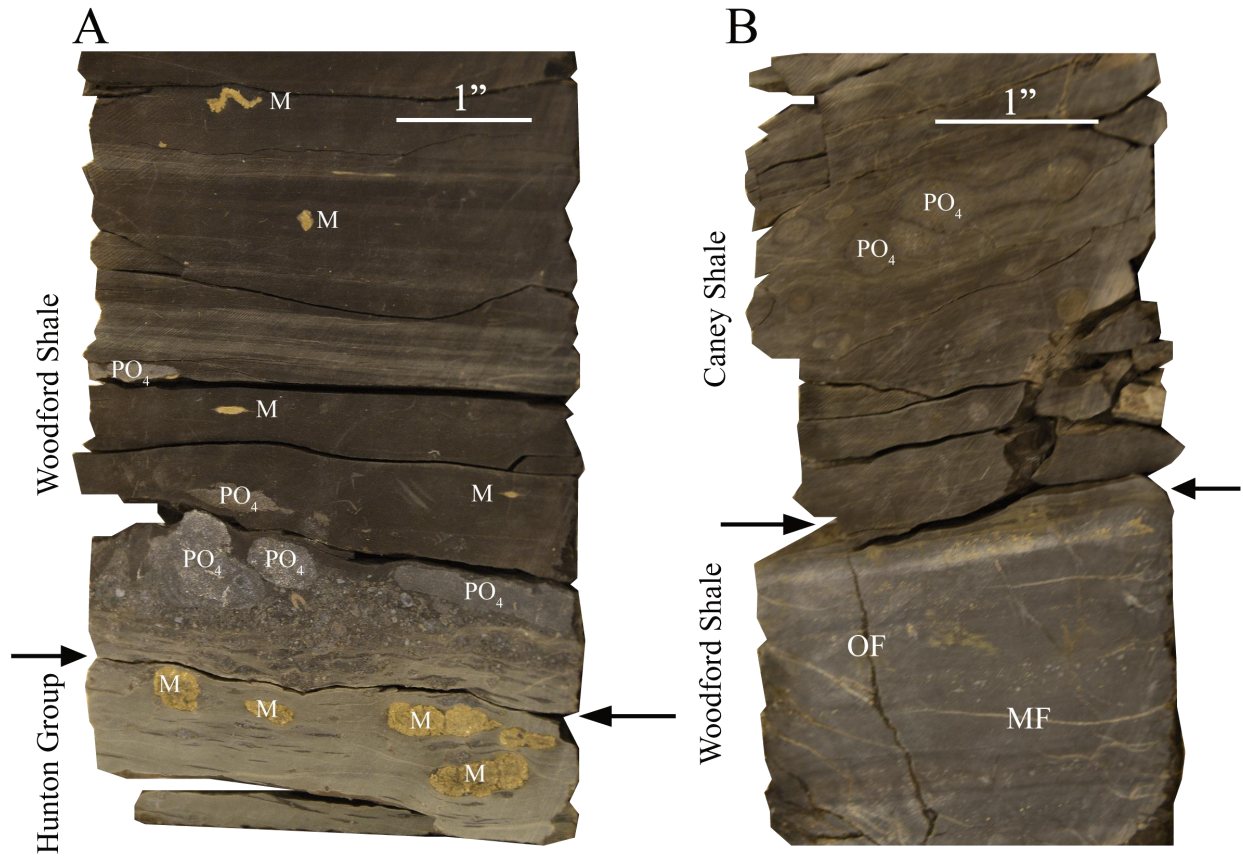


**Figure 7.** Lower and upper contacts of the Woodford Shale in the Williams 1H-7X. A) Sharp, sloping erosional contact of the Woodford/Hunton, depth 12,967.8 feet. B) Sharp, sloping erosional contact of the Woodford/Caney, depth 12,744.5 feet.

**M:** Marcasite Nodules, **PO<sub>4</sub>:** Phosphate Nodules, **OF:** Open Fractures, **MF:** Mineralized Fractures

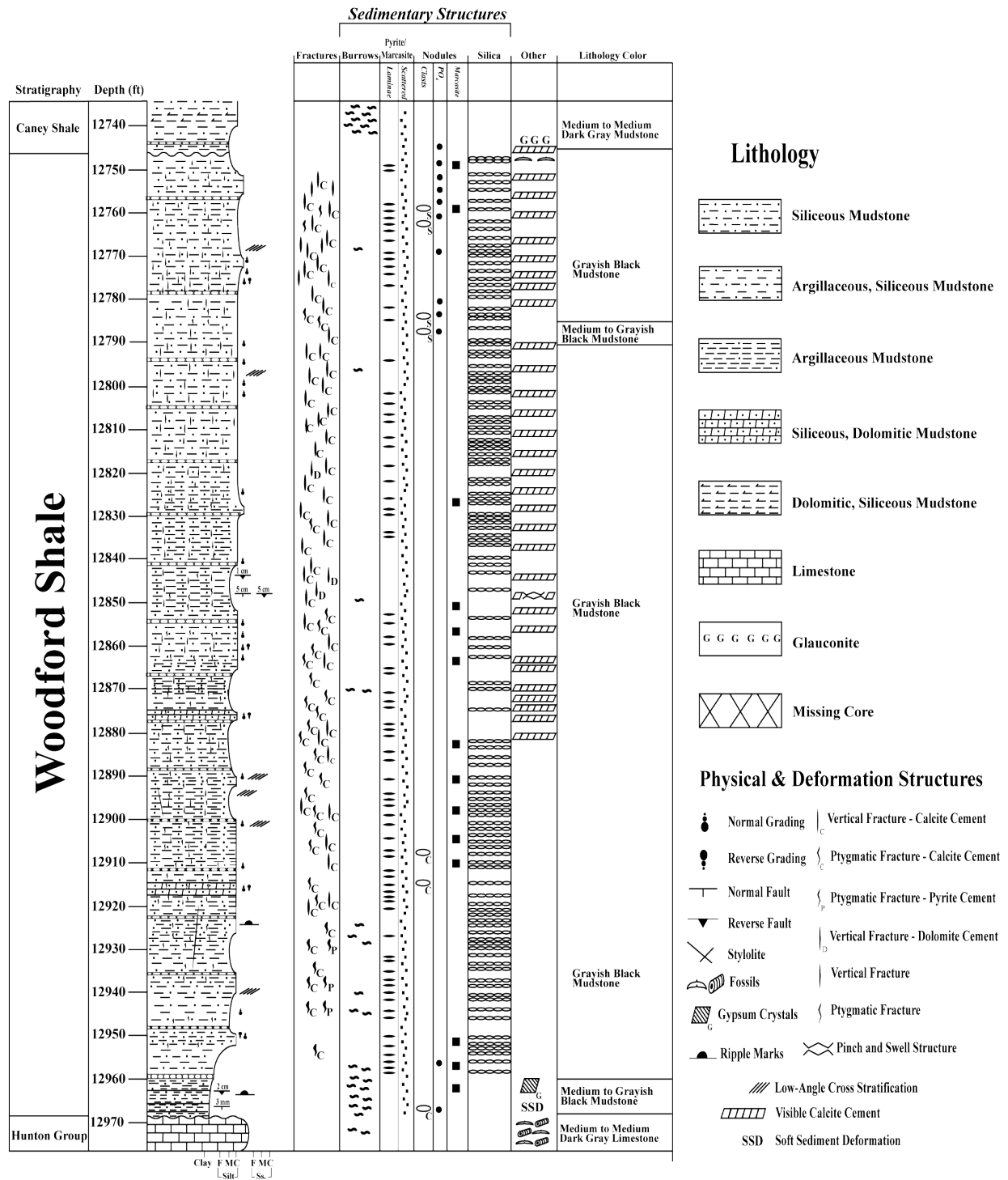


**Figure 8.** Description of the Williams 1H-7X core with sedimentary, biogenic, and tectonic features.

Based on core description, thin section petrography and XRD, five different lithofacies were recognized for the Woodford Shale interval of the Williams 1H-7X. The mudstone classification of Caldwell (2012) was used to name facies: siliceous mudstone, phosphatic, siliceous mudstone, argillaceous, siliceous mudstone, siliceous, dolomitic mudstone, and argillaceous mudstone (Figure 9).

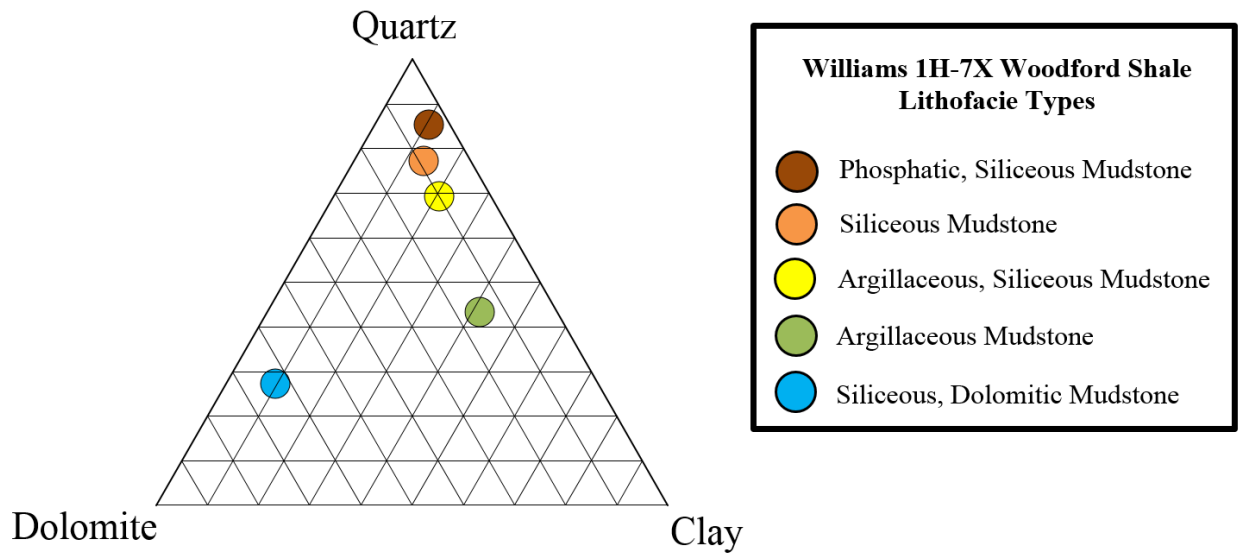


**Figure 9.** Mudstone classification ternary diagram of the Williams 1H-7X (Modified from Caldwell, 2012).

Argillaceous Mudstone (AM)

The thirteen feet thick argillaceous mudstone lithofacies occurs at the base of the Woodford Shale and is predominately silica and clay-rich. XRD analysis indicates an organic-rich interval with silica and clay percentages exceeding 40% due to the high concentrations of illite, mica, and biogenic/detrital quartz. The biogenic quartz appears as chalcedony and chert that replaces radiolarians, and is identifiable in thin section by its fibrous and microcrystalline

form, respectively. Abundant *tasmanites* cysts are apparent in thin section and contribute to the overall organic-richness (9.28%, n=2) of the rock.

The argillaceous mudstone is predominately grayish black with interbedded, parallel medium dark gray (N4) clay-rich bands (Figure 10). The clay-rich bands are fissile and display soft-sediment deformation in the form of disturbed or convoluted bedding and micro-fractures near the Woodford Shale/Hunton Group contact. Abundant burrows occur throughout the interval, mostly within the clay-rich laminations. Phosphate nodules, pyrite and marcasite, clay clasts, and gypsum crystals were observed.

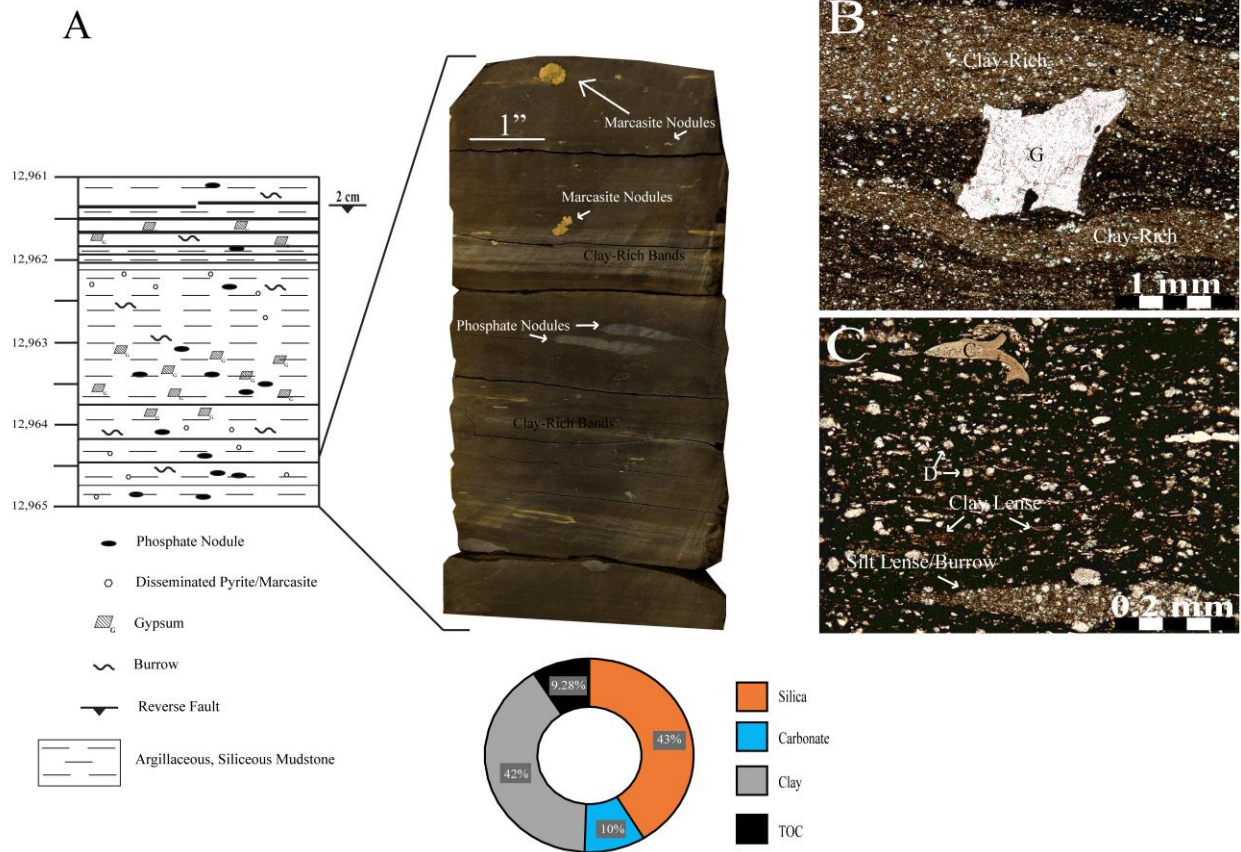


**Figure 10.** Thin section and core photographs of the AM lithofacies of the Woodford Shale, Williams 1H-7X core. A) Core description with associated photograph and graph of constituent percentages for the AM facies. B) Photomicrograph of gypsum crystal (G) deforming clay-rich laminae, plane polarized light (PPL), depth 12,962 feet. C) Conodont (C) with carbonate grains and lenses of silt and clay. Depth 12,963 feet, PPL.

### Argillaceous, Siliceous Mudstone (A-SM)

The argillaceous, siliceous mudstone lithofacies occurs from 12,955 feet to 12,863 feet and is a predominately grayish black mudstone with thin silica-rich laminae. XRD analysis shows high concentrations of silica (69%) combined with lower concentrations of clay (21%) in this interval. The high percentage of silica is mostly attributed to the abundant silica-rich laminae, which are predominately biogenic quartz in the form of chalcedony that precipitated from recrystallized radiolarians. Average total organic carbon (TOC) is higher (5.84%, n=21) within the organic-rich interval, as exemplified by the abundant *tasmanites* cysts evident in thin section.

The argillaceous, siliceous mudstone interval is predominately laminated mudstone containing thin parallel to low-angle laminae of pyrite and silica (Figure 11). The silica-rich laminae, which range from a 1-3 millimeters up to 1.3 cm in thickness, occur, on average, two to three times per foot. The laminae occasionally display normal or inverse grading. Visible calcite cement is evident within these laminae from 12,880 feet to the end of the interval at 12,863 feet. The pyrite-rich laminae are submillimeter-sized in thickness and occur, on average, once every foot (30.48 cm). Fractures are concentrated in the silica- and pyrite-rich laminae. Ptygmatic fractures, vertical fractures, and occasional shear fractures occurring within the laminae are usually mineralized by calcite and in some cases pyrite. Minor burrowing, clay clasts, and marcasite nodules greater than one inch (2.54 cm) in diameter are observed within the argillaceous, siliceous mudstone.



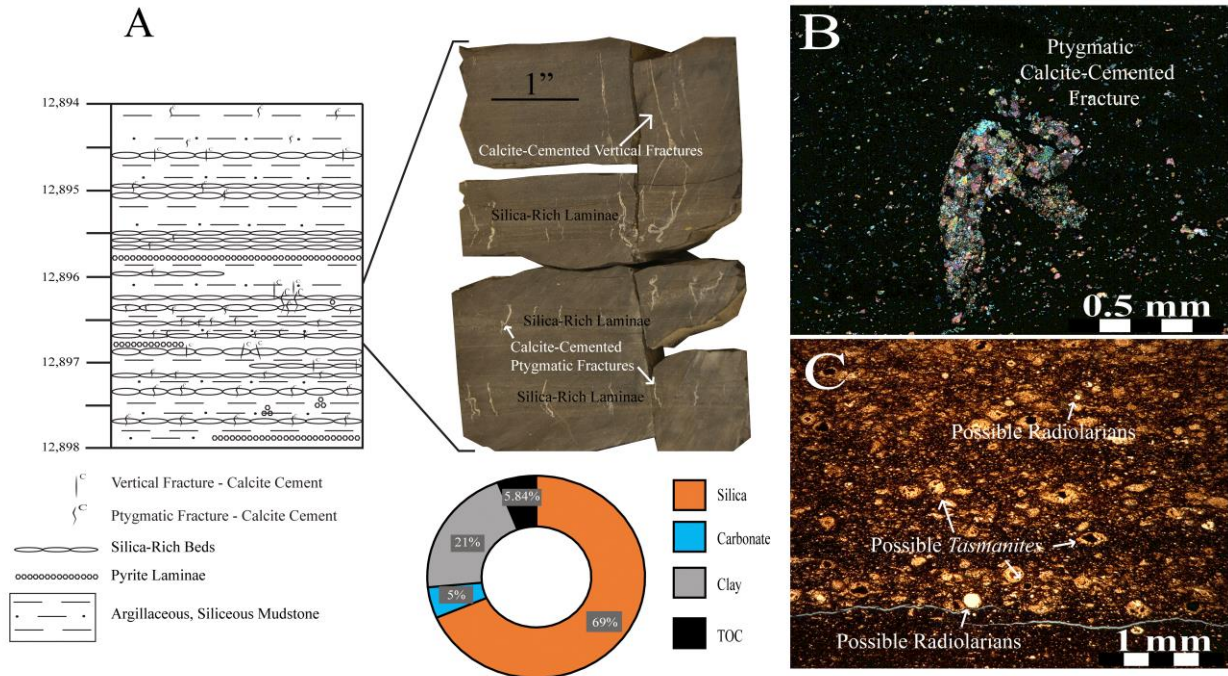


**Figure 11.** Thin section and core photographs of the A-SM lithofacies of the Woodford Shale, Williams 1H-7X core. A) Core description with associated photograph and graph of constituent percentages for A-SM facies. B) Photomicrograph of calcite-cemented pygmatic fracture in cross-polarized light (XPL), depth 12,947.7 feet. C) Contact between clay-rich and silica-rich interval, showing possible radiolarians and *tasmanites*. Depth 12,899.4 feet, PPL.

### Siliceous, Dolomitic Mudstone (S-DM)

Thin intervals of a siliceous, dolomitic mudstone occur within the argillaceous, siliceous lithofacies at depths of 12,915.4 feet and 12,876 feet. XRD analysis of the carbonate-rich mudstone records dolomite concentration of 61% and silica concentration of 27% which based on thin section petrography is mostly attributed to detrital quartz. TOC content decreases from the previous lithofacies as the percentage drops to less than 3%.

The thin siliceous, dolomitic mudstone exhibits an abundance of finely-laminated carbonate-rich laminae that occasionally display normal and inverse grading (Figure 12). The

laminae are submillimeter in thickness and occur throughout the entire lithofacies. A few vertical calcite-cemented fractures are evident at the interval found near 12,876 feet.

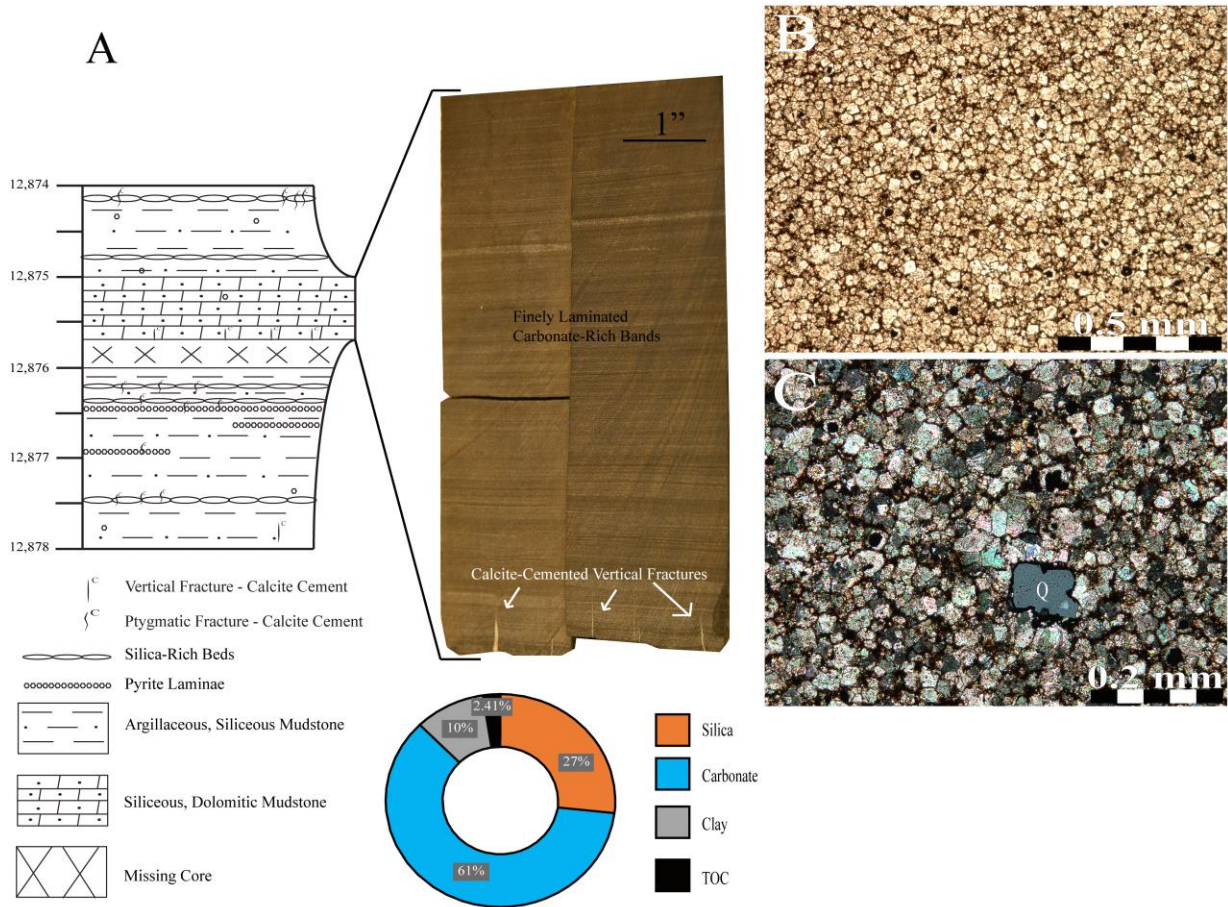


**Figure 12.** Thin section and core photographs of the S-DM lithofacies of the Woodford Shale, Williams 1H-7X core. A) Core description with associated photograph and graph of constituent percentages for the S-DM facies. B) Photomicrograph of dolomite-rich lithology. Depth of 12,915 feet, PPL. C) Subhedral to anhedral abraded dolomite rhombs and a quartz sand grain (Q). Depth 12,915 feet, XPL.



### Siliceous Mudstone (SM)

The siliceous mudstone lithofacies occurs from 12,863 feet to 12,788.5 feet and is distinguishable from the argillaceous, siliceous lithofacies by its thicker silica-rich lamina and subsequently larger fractures. XRD analysis shows an average silica concentration of 77% with clay concentration decreasing to 11%. The silica is a combination of biogenic quartz, in the form of chalcedony and chert that replaces radiolarians, and angular detrital silt- to sand-sized quartz grains. The siliceous mudstone is organic-rich with average TOC content at 6.9%, n=20.

The siliceous mudstone lithofacies is predominately a laminated mudstone with thick laminae of silica and millimeter-thick pyrite as well as silica-cemented bands (Figure 13). The dark gray to black silica-cemented bands range from a few millimeters to a few inches in thickness. The bands commonly contain numerous calcite-cemented vertical and ptigmatic fractures that are limited to the band. The bands occur, on average, one to two times per foot. The silica-rich laminae range from a few millimeters to 2 inches (5 cm) in thickness and occasionally display normal and inverse grading. Some silica-rich laminae are cemented by calcite, which is visible in core and thin section. As a result of the thicker silica banding, fracture height is greater than previously observed in the AM, A-SM, or S-DM. The fractures are mostly vertical and ptigmatic, and are cemented with calcite and dolomite. Micro-faults and horst and graben structures occur near 12,850 feet. Minor burrowing, low angle cross stratification, and phosphate nodules also occur within the siliceous mudstone lithofacies.

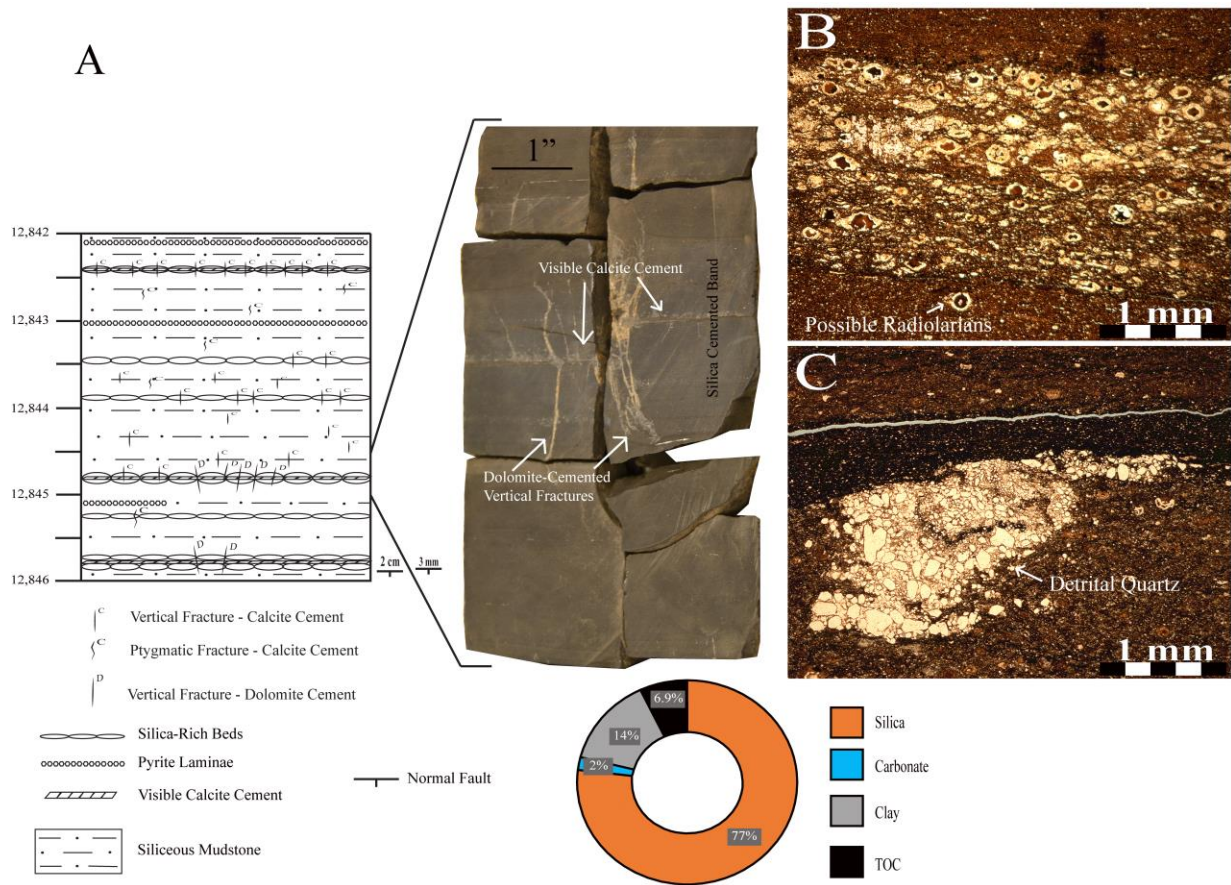


**Figure 13.** Thin section and core photographs of the SM lithofacies of the Woodford Shale, Williams 1H-7X core. A) Core description with associated photograph and graph of constituent percentages for the SM facies. B) Photomicrograph of silica-rich laminae displaying possible radiolarians and *tasmanites*. Depth 12,907.3 feet, PPL. C) Cluster of detrital silt and sand-sized quartz grains. Depth 12,831.35 feet, PPL.

### Phosphatic, Siliceous Mudstone (P-SM)

A phosphatic, siliceous mudstone lithofacies occurs from 12,788.5 feet to the Woodford Shale/Caney Shale contact at 12,744.5 feet. The phosphatic, siliceous lithofacies contains similar XRD characteristics of the siliceous mudstone, with silica concentrations averaging 85% and clay concentrations averaging 11%. However, this interval contains an abundance of phosphate nodules that are absent to rare in the lower siliceous mudstone lithofacies. The high

percentages of silica, similarly, are also attributed to the combination of biogenic and detrital quartz. Measured average TOC within this interval of 5% (n=10) indicates organic-richness.

Similar to the siliceous mudstone, the phosphatic, siliceous mudstone has occasional laminae of silica and millimeter-thick pyrite as well as minor silica cemented bands (Figure 14). The silica-rich laminae range from a 1-3 millimeters to 3 inches (6.6 cm) in thickness and can display normal and inverse grading. Silica-rich laminae commonly contain visible calcite that cements surrounding quartz and feldspar grains. Longer (up to 6.6 cm) extensional vertical fractures and stress-induced ptigmatic fractures are abundant in the silica-rich laminae. The fractures are both open and calcite cemented, and are usually confined within silica-rich laminae. The silica-cemented bands range from a few millimeters to a few inches in thickness. The bands commonly contain numerous open and calcite-cemented vertical and ptigmatic fractures that are limited to the band. The bands occur, on average, one to two times per foot. Phosphate nodules are relatively abundant and occur throughout the interval. The nodules range from 1-3 centimeters to 3 inches (6.6 cm) in diameter. Silicified nodules ( $\text{PO}_4$ ), nodular pyrite and minor burrowing are evident in the phosphatic, siliceous mudstone facies.

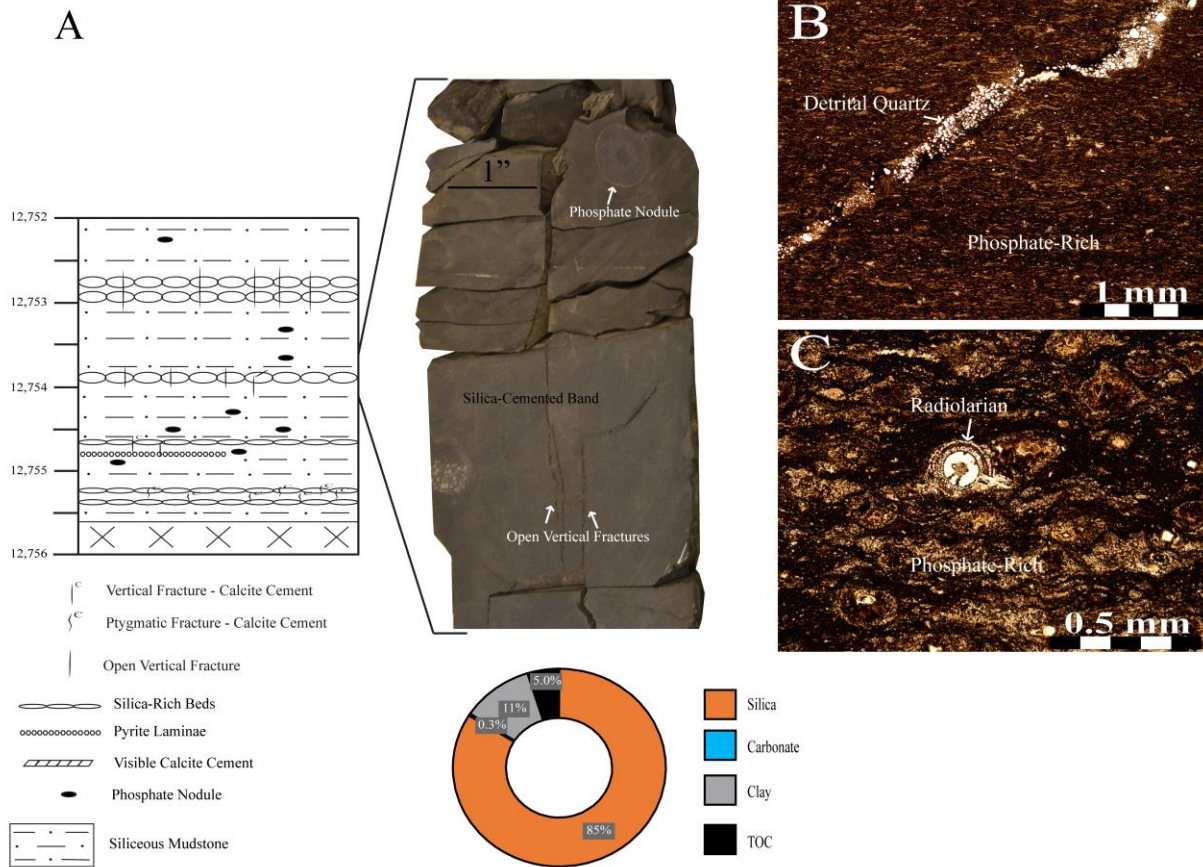


**Figure 14.** Thin section and core photographs of the P-SM lithofacies of the Woodford Shale, Williams 1H-7X core. A) Core description with associated photograph and graph of constituent percentages for the P-SM facies. B) Photomicrograph of a fracture infilled with silt-sized detrital quartz grains and pyrite in a phosphate nodule. Depth 12,771 feet, PPL. C) Radiolarian in a burrowed? phosphate nodule. Depth 12,787.1 feet, PPL.

*McDonald 2H-16E*

The McDonald 2H-16E was cored from 6,232 feet to 6,472.6 feet (core depth) and consists of the lower interval of the Caney Shale (6,232 feet-6,260.9 feet), the Woodford Shale (6,260.9 feet-6,418.8 feet), and the top of the Hunton Group (6,417.8 feet-6,472.6 feet). The underlying 55 feet of Hunton Group is identified as a medium to medium dark gray (N5-N4) limestone with abundant marine invertebrate fossils (ostracods, brachiopods, and crinoids) and calcite cemented fractures. The contact between the Hunton Group and Woodford Shale is absent in core due to 1 foot of missing section (6,418.8 feet-6,417.8 feet). The lowest section of the Woodford Shale starts at 6,417.8 feet and consists of grayish black (N2) mudrock containing clay clasts and burrows, laminae, and disseminated grains. The 157 feet of Woodford Shale is primarily grayish black mudstone with high concentrations of pyrite and marcasite (laminae, nodules, disseminated grains), ptigmatic and vertical fractures, micro-faulting, burrowing, and silt to sand-sized quartz grains and carbonate cement (Figure 15). A phosphatic, glauconitic-rich zone with abundant pyrite and marcasite at 6,260.9 feet indicates the unconformable contact with the overlying Caney Shale, a 55 feet thick medium dark gray to medium gray (N4-N5) mudstone with abundant burrowing, brachiopod fossils, and disseminated pyrite.

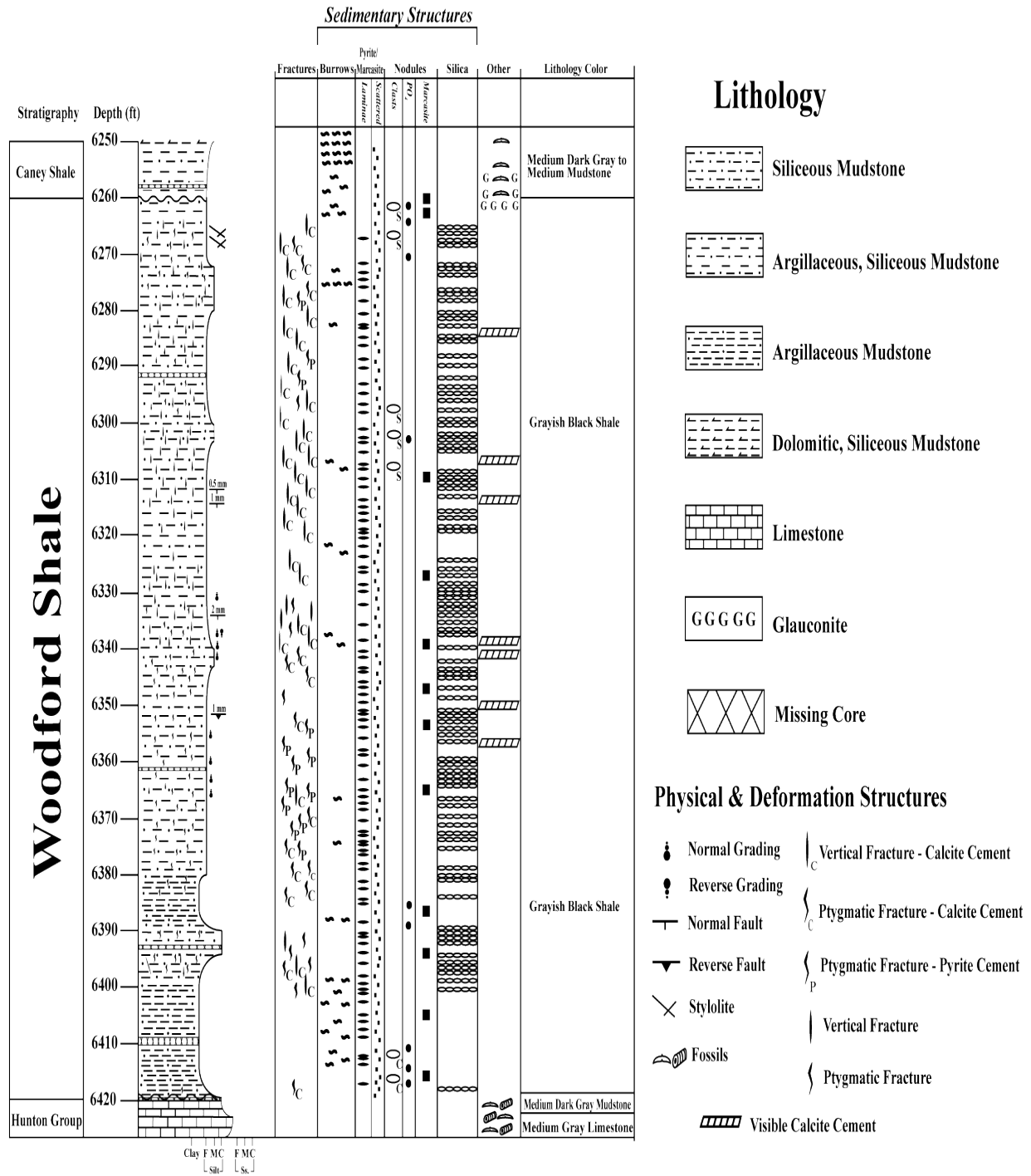


**Figure 15.** Description of the McDonald 2H-16E core with sedimentary, biogenic, and tectonic features.

Based on core description, thin section petrography and XRD, three different lithofacies were recognized for the Woodford Shale interval of the McDonald 2H-16E. The mudstone classification of Caldwell (2012) was used to name these facies: siliceous mudstone, argillaceous, siliceous mudstone, and argillaceous mudstone (Figure 16).

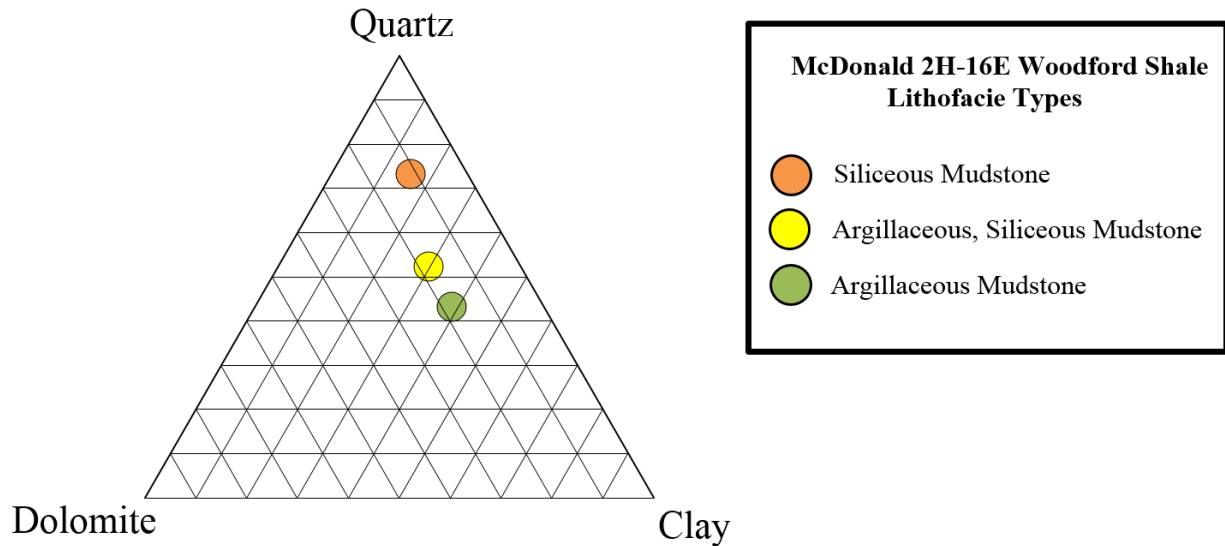


**Figure 16.** Mudstone classification ternary diagram of the McDonald 2H-16E core (Modified from Caldwell, 2012).

Argillaceous Mudstone (AM)

The lower section of the McDonald 2H-16E is dominantly an argillaceous mudstone that is thirty-three feet thick. XRD analysis of this interval shows similar concentrations of silica and clay at around 40%. Based on XRD, the clay minerals are mostly illite with lesser amounts of mixed layer illite-smectite. The silica in this interval is mostly silt-sized detrital quartz grains (Figure 17). The argillaceous mudstone is organic-rich with average TOC content reaching 8.5%, n=5.







### Argillaceous, Siliceous Mudstone (A-SM)

The argillaceous, siliceous mudstone is the most abundant lithofacies in the McDonald 2H-16E. XRD analysis gives high concentrations of silica that reach 52% and clay concentration of about 30%. The silica is a combination of detrital quartz and biogenic silica. Biogenic quartz occurs commonly as chalcedony that replaces and fills radiolarians and is concentrated in silica-rich laminae. The argillaceous, siliceous mudstone is organic-rich with average TOC of 5.5%, n=7.

The argillaceous, siliceous mudstone is commonly laminated and contains thin silica-rich laminae that range from a few millimeters to 1.27 cm in thickness and occasionally exhibit normal and inverse grading (Figure 18). The silica-rich laminae occur, on average, from one to two per foot (30.48 cm). Pyrite- and calcite-cemented ptigmatic and vertical fractures are common and mostly limited to silica-rich laminae. Thinner millimeter-thick pyrite laminae are also abundant within the argillaceous, siliceous mudstone lithofacies. Micro-faulting, minor burrowing and pyrite nodules are observed throughout the interval.

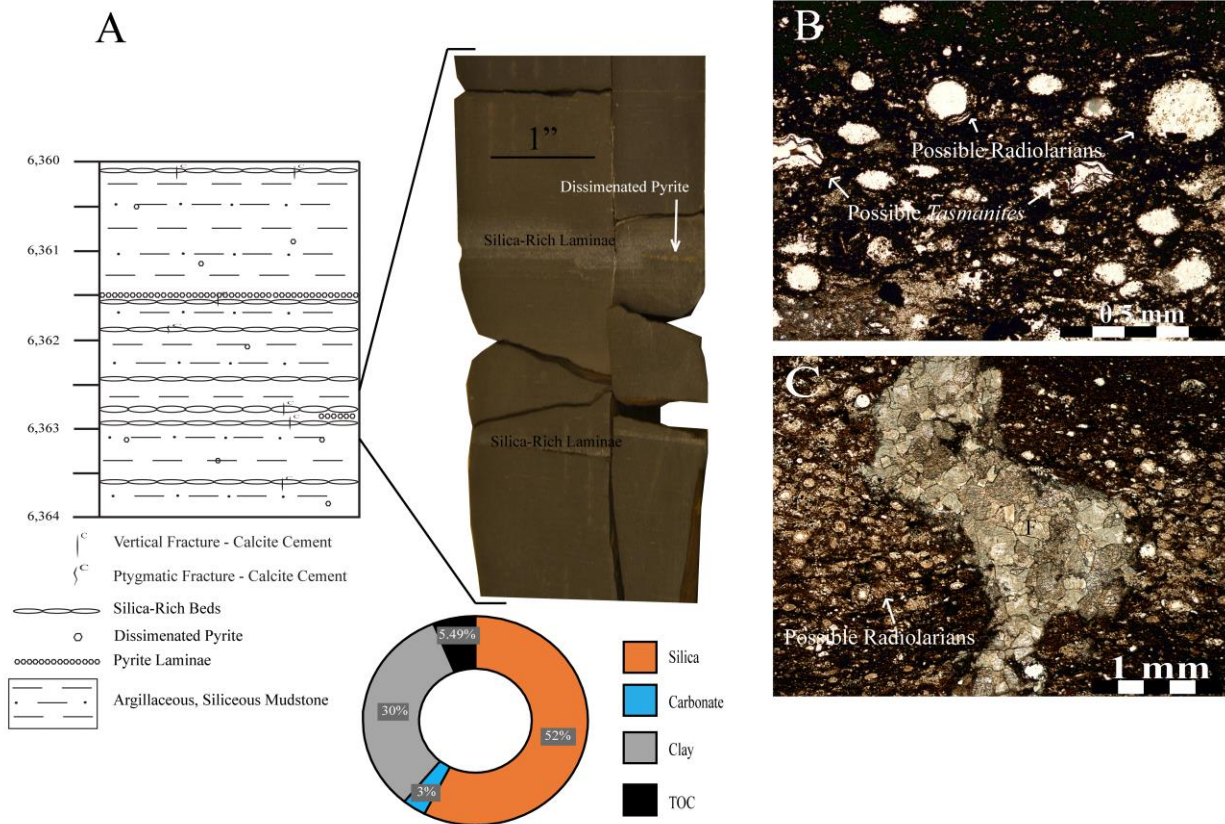


**Figure 18.** Thin section and core photographs of the A-SM lithofacies of the Woodford Shale, McDonald 2H-16E core. A) Core description with associated photograph and graph of constituent percentages for the A-SM facies. B) Photomicrograph of possible *tasmanites* and radiolarians. Depth 6,340 feet, PPL. C) Silica-rich band with possible radiolarians disrupted by a calcite-cemented pygmatic fracture. Depth 6,311 feet, PPL.

### Siliceous Mudstone (SM)

The siliceous mudstone lithofacies within the McDonald 2H-16E core occurs as three irregularly distributed intervals 6,395 feet to 6,391.5 feet, 6,337 feet to 6,325 feet, and 6,306 feet to 6,264 feet. Silica concentrations exceed 70% and clay concentrations average 16% based on XRD analysis. The bulk of the higher silica content occurs as biogenic quartz precipitated from recrystallized radiolarians, with lesser amounts provided by detrital quartz. Average TOC

content decreases slightly within this lithofacies, however, it is still organic-rich with a percentage of 3.8%, n=7.

The siliceous mudstone lithofacies is laminated mudstone with dark gray to black silica-cemented bands, silica-rich laminae, and minor pyrite laminae occurring across the interval (Figure 19). The silica-cemented bands range from a few millimeters to a few inches in thickness. The bands commonly contain numerous open and calcite- and pyrite-cemented vertical and ptigmatic fractures that are limited to the band. The bands occur, on average, three to four times per foot and are cemented with visible calcite that surrounds quartz and feldspar grains. Silica-rich laminae are less common than silica-cemented bands. Silica-rich laminae range from a few millimeters to 3 cm in thickness and contain smaller calcite- and pyrite-cemented vertical and ptigmatic fractures. These laminae exhibit normal and inverse grading along with micro-faulting. Millimeter-thick pyrite laminae occur, on average at a frequency of, one lamina per foot. Minor burrowing, phosphate and marcasite nodules, and silicified nodules are observed in this facies. Stylolites are also present near the top of the siliceous mudstone interval at depth of 6,270 feet.

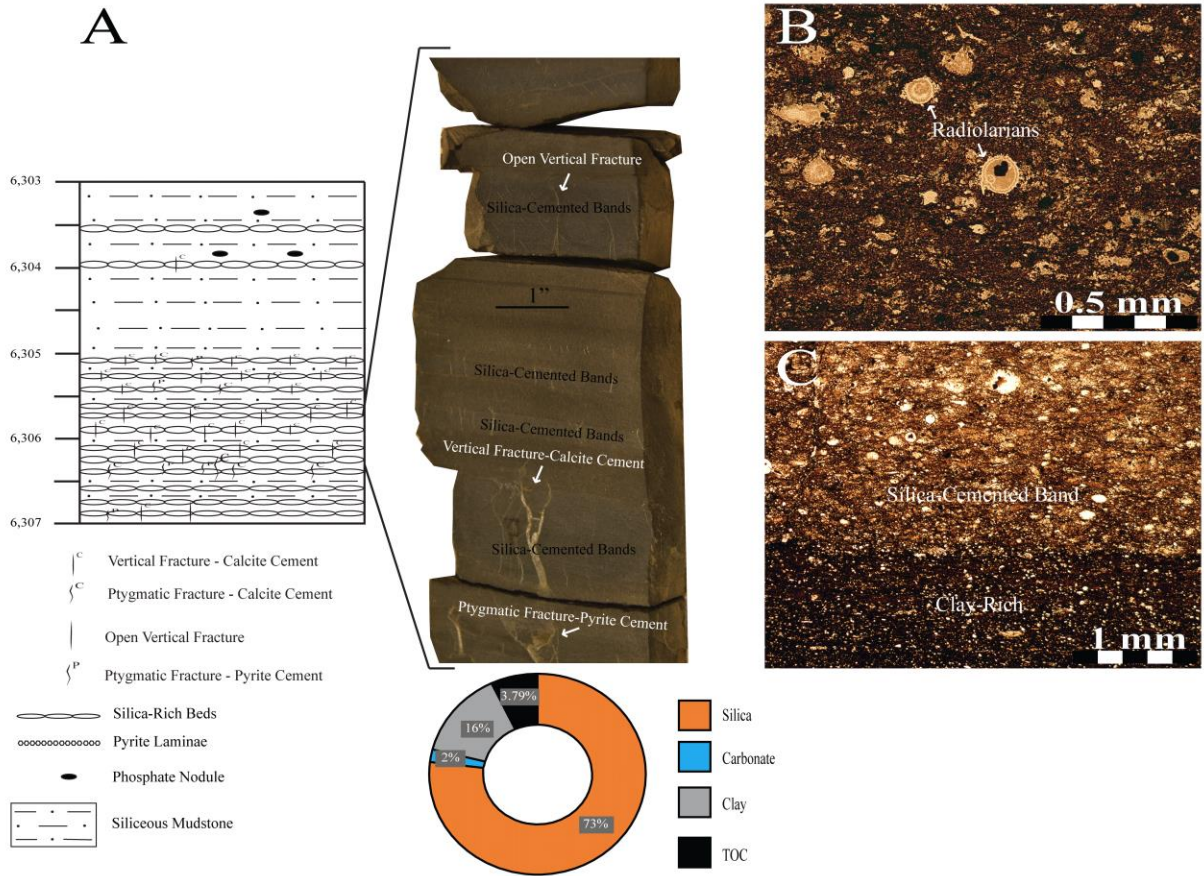







**Figure 19.** Thin section and core photographs of the SM lithofacies of the Woodford Shale, McDonald 2H-16E core. A) Core description with associated photograph and graph of constituent percentages for the SM facies. B) Photomicrograph of radiolarians. Depth 6,330.55 feet, PPL. C) Contact between silica cemented band and clay-rich bed. Depth 6,393 feet, PPL.

### *Chemostratigraphy*

To establish paleo-redox conditions, elemental concentrations of selected elements were measured using x-ray fluorescence (XRF). Approximately 36 elements were measured, but only 10 elements were used: titanium (Ti), zirconium (Zr), silicon (Si), calcium (Ca), strontium (Sr), potassium (K), uranium (U), vanadium (V), chromium (Cr), and aluminum (Al). A chemostratigraphic profile was constructed by plotting these principal elements in conjunction with core depth and gamma-ray readings from the wireline logs (Figures 20 & 21).

Titanium, aluminum, and zirconium are associated with terrestrial input from a continental source (Tribovillard et al., 2006). Intervals showing increase in both titanium and zirconium are interpreted to be sediment derived from a non-marine terrestrial source. Silicon is associated with detrital and biogenic quartz, feldspars, and clay minerals (Pearce and Jarvis, 1992; Pearce et al., 1999). Silicon was normalized with aluminum to reduce the influence of terrestrially derived sediment. Calcium is associated with dolomite, calcite, and aragonite and serves as an indicator of carbonate accumulation (Banner, 1995) as is strontium due to calcium replacement with strontium in aragonite (Tribovillard et al., 2006). Potassium is associated with clays and can be deposited in more distal regions of a basin (Pearce et al., 1999). An increase in potassium concentrations in conjunction with decreased titanium and zirconium concentrations indicates a more distal depositional setting that favors suspended clay deposition (Turner and Slatt, 2015). Uranium and vanadium are useful environmental proxies for bottom water anoxia during deposition (Tribovillard et al., 2006), with higher concentrations indicating more reduced environments (Table 1).

<b>Element</b>	<b>Proxy</b>	<b>Source</b>	<b>Lithofacies Key</b>
Aluminum (Al) Titanium (Ti) Zirconium (Zr)	Continental/Terrestrial	Tribovillard et al. (2006)	 Phosphatic, siliceous mudstone
Silicon/Aluminum (Si/Al)	Biogenic and Detrital Quartz	Tribovillard et al. (2006)	 Siliceous mudstone
Calcium/Aluminum (Ca) Strontium/Aluminum (Sr)	Carbonate and Phosphate	Pearce and Jarvis (1992); Pearce et al. (1999)	 Siliceous, dolomitic mudstone
Potassium/Aluminum (K)	Clay and Feldspar	Tribovillard et al. (2006)	 Argillaceous, siliceous mudstone
Uranium/Aluminum (U) Vanadium/Aluminum (V)	Bottom Water Anoxia	Tribovillard et al. (2006)	 Argillaceous mudstone
Vanadium/Chromium (V/Cr)	Paleoredox Conditions	Rimmer, (2004)	

**Table 1.** Key elements and their associated environmental proxies.

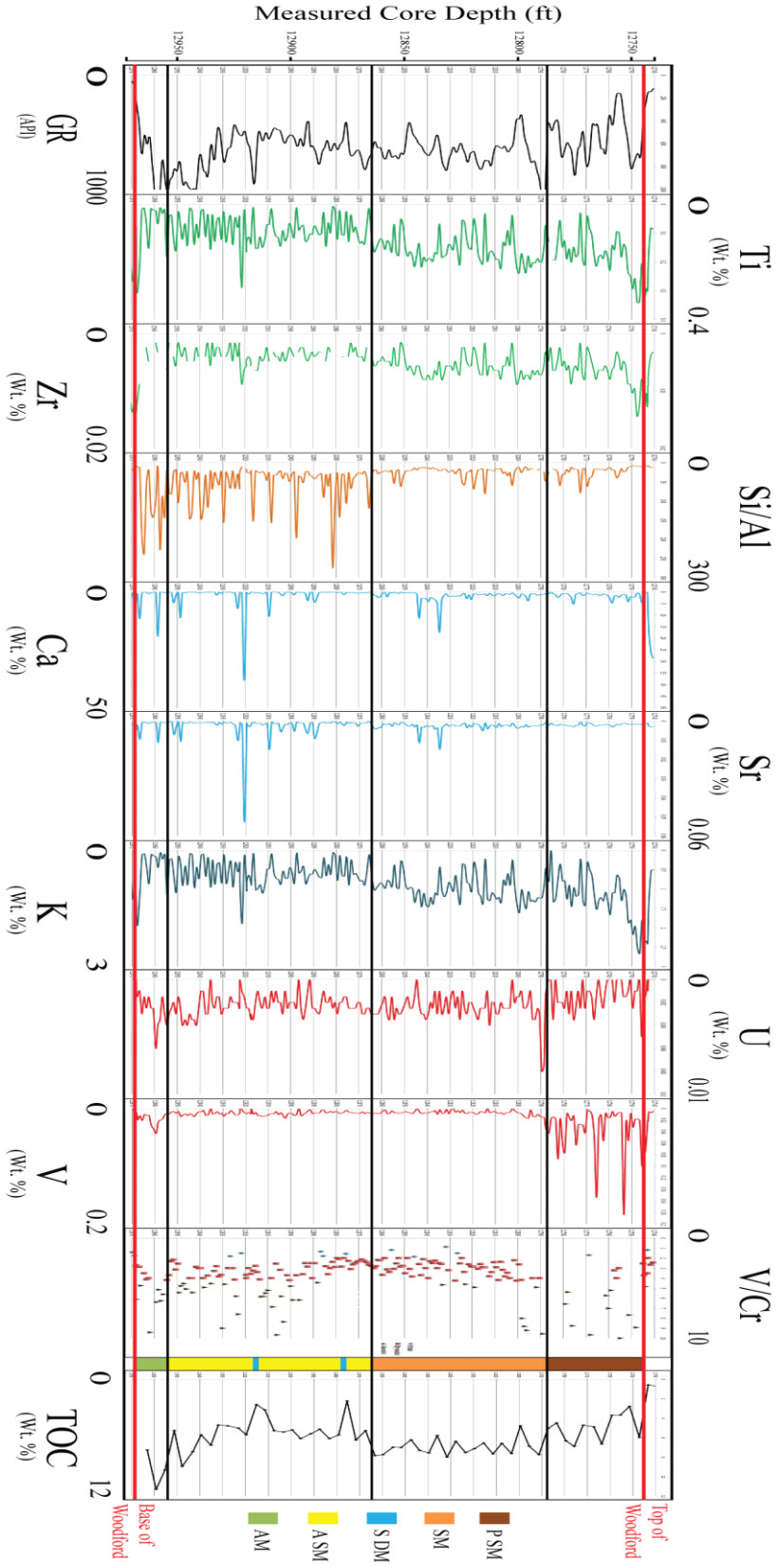


**Figure 20.** Chemostratigraphic profile of the Williams 1H-7X. Noteworthy trends include high silicon, calcium, and strontium concentrations in the lower half of the Woodford interval, with high concentrations of titanium, zirconium, and potassium in the upper half. Vanadium and V/Cr occur in higher concentrations in the lower half and upper quarter of the Woodford interval. Silicon exhibits an inverse relationship to potassium, zirconium, and titanium. After Turner and Slatt (2015).



Argillaceous Mudstone (AM)

Gamma-ray values display relatively low readings near 0 API units near the top of the Hunton Group. Crossing the contact into Woodford Shale, particularly into the argillaceous mudstone lithofacies, gamma-ray increases rapidly with values above 1000 API units (Figure 20). The continental proxies used for terrestrial input (Ti and Zr) show a sharp decrease moving from the Hunton Group to the basal Woodford Shale, where total weight percent approaches 0%. As a comparison, titanium values are around 0.4% in the Hunton Group. Silicon values increase inversely with decreasing concentrations of the terrestrial proxies. As a result, silicon increases from less than 50 in the Hunton Group to greater than 250 in the Woodford Shale with relatively high silicon concentrations maintained across the argillaceous mudstone lithofacies (Figure 20). The carbonate proxies (Ca and Sr) are relatively low within the argillaceous mudstone, in contrast to the two intervals near the base and top of the interval, respectively. The trend of the clay and feldspar proxy (K) is similar to the trend for zirconium and titanium. An initial potassium reading of 2% decreases to 0.1% near the middle of the interval and continues until the top of the argillaceous facies. Uranium and vanadium both show dramatic increases at the base of the Woodford Shale, and display steady relatively high readings of 0.003% and 0.02%, respectively, across the argillaceous mudstone interval (Figure 20). Alternatively, the proxy for paleo-redox environmental conditions (V/Cr) exhibits relatively high values of 5 across the interval, following the same trend as uranium and vanadium. TOC content within the argillaceous mudstone is high with sections displaying weight percentages above 12%.

### Argillaceous, Siliceous Mudstone (A-SM)

Average gamma-ray values decrease across the transition from argillaceous mudstone into argillaceous, siliceous mudstone. The average gamma-ray measurement for the argillaceous, siliceous mudstone facies is greater than 650 API units compared to 1000 API units for the argillaceous mudstone. Titanium and zirconium concentrations increase at 12,920 feet, but overall show relatively low values averaging 0.05% and 0.003%, respectively (Figure 20). Similar to the high concentrations in the argillaceous mudstone, average silicon values range between 50 and 100 across the argillaceous, siliceous mudstone interval. Calcium and strontium both display a generalized blocky trend with fifteen sudden increases across the interval, with relatively low values averaging near 0% and the higher concentrations averaging over 10% and 0.01%, respectively (Figure 20). Potassium increases gradually across the argillaceous, siliceous mudstone interval with values reading 0.2% near the base and increasing to over 0.5% at the top. Vanadium and uranium display numerous positive and negative excursions from the average values. The negative excursions of uranium and vanadium average 0.0015% and 0.005% respectively, whereas concentrations increase in the positive excursions to greater than 0.003% and 0.01%, respectively. The paleo-redox proxy V/Cr shows an overall decreasing trend with values ranging from 5 at the base to less than 2 at the top of the interval (Figure 20). A zone from 12,930 feet to 12,900 feet displays higher values of V/Cr, with numerous readings of over 8. The argillaceous, siliceous mudstone is organic-rich with average values of TOC over 5%.

### Siliceous, Dolomitic Mudstone (S-DM)

The thin interbedded intervals of the siliceous, dolomitic mudstone have decreased gamma-ray values that average about 100 API units less than the values for the argillaceous, siliceous mudstone (Figure 20). The values for titanium and zirconium approach 0 in both of the



carbonate-rich intervals. In the lower interval at 12,915 feet, the terrestrial proxies (Zr and Ti) show values reading 0.025% and 0.003%, respectively. The silicon values correlate inversely with titanium and zirconium as these terrestrial proxies decrease in concentrations to close to 0 at 12,915 feet (Figure 20). In the carbonate interval at 12,875 feet, silicon values average over 100. Calcium and strontium show increases above the average value in both intervals. The lowest siliceous, dolomitic interval contains the highest relative concentrations of calcium and strontium with values of 2% and 0.004%, respectively. The upper interval at 12,875 feet shows only a slight increase above the baseline with average values of 0.8% and 0.003% for calcium and strontium. Potassium concentrations within the siliceous, dolomitic intervals follow the same trend as the terrestrial proxies and show relatively low concentrations in the intervals with values approaching 0%. Uranium and vanadium both exhibit relatively low concentrations of 0.001% and 0.002%, respectively, in both dolomitic intervals. Similarly, the paleo-redox proxy V/Cr reads relatively low with an average of less than 3. The plot of TOC concentrations exhibits a similar trend to the gamma-ray curve, with the average TOC content decreasing more than 3% in the carbonate-rich intervals (Figure 20).

#### Siliceous Mudstone (SM)

The average gamma-ray value of 670 API units for the siliceous mudstone is slightly elevated compared to the siliceous, dolomitic mudstone (555 API units). Titanium and zirconium both show a generalized increasing trend from 12,863 feet to 12,788.5 feet, with values of 0.15% and 0.004% respectively, near the base and values exceeding 2% and 0.08% respectively, near the top (Figure 20). Average silicon values approach the 0 baseline with seven minor increases in concentration that inversely correlate with decreasing values of titanium and zirconium. The calcium and strontium values, similarly, average near 0 and exhibit two minor

positive excursions in concentration that are limited to the bottom half of the siliceous mudstone interval. Potassium increases slightly from 1 to 1.5 across the interval. The uranium and vanadium values are similar to the argillaceous, siliceous mudstone facies, where values average 0.002% uranium and 0.009% vanadium. The paleo-redox proxy V/Cr remains around 4 until near 12,790 feet where values increase over 9. Average TOC increases to 6.9% from 5.8% for the underlying siliceous, dolomitic mudstone lithofacies (Figure 20).

#### Phosphatic, Siliceous Mudstone (P-SM)

Gamma-ray values decrease in the phosphatic, siliceous mudstone to an average value of 550 API units. Titanium and zirconium are highest in this interval with values reaching 0.3% and 0.14% respectively. Silicon displays a baseline value near 0 with five sudden increases that exceed 50 and inversely correlate with titanium and zirconium values (Figure 20). Calcium and strontium increase slightly with numerous zones of increased concentrations scattered across the interval that exceed values of 5% and 0.003%, respectively. Similar to titanium and zirconium, the potassium concentrations are highest and exceed 2.5% in the phosphate-rich interval and display an upward increasing trend. Uranium concentrations decrease from 0.003% at 12,785 feet to less than 0.001% at 12,750 feet. Vanadium displays numerous increases that exhibit higher average values than the previous three lithofacies (Figure 20). The average value of vanadium within the interval is 0.04% with some zones exceeding 0.16%. The paleo-redox proxy V/Cr also has higher values of between 6 and 10 before the contact with the Caney Shale, whose V/Cr values are less than 4. The TOC decreases slightly from the previous silica-rich lithofacies, dropping from 6.9% to 5% in the phosphatic, siliceous mudstone.

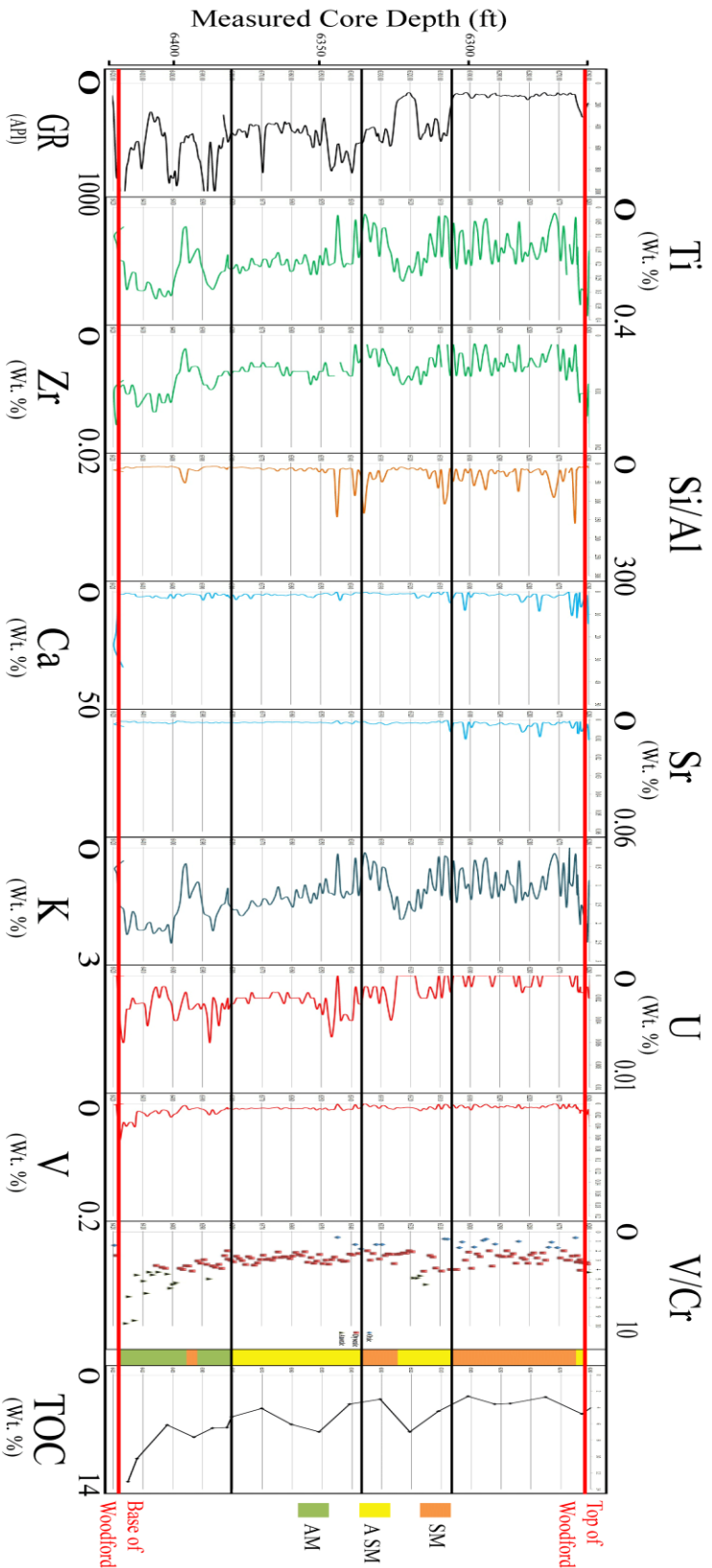


**Figure 21.** Chemostratigraphic profile of the McDonald 2H-16E. Noteworthy trends include higher titanium and zirconium concentrations across the Woodford interval. Silicon, calcium, and strontium concentrations increase in the upper quarter of the Woodford interval. Uranium and vanadium concentrations, as well as V/Cr are relatively low in the upper third of the core. Zirconium, potassium, and titanium vary inversely with silicon. After Turner and Slatt (2015).

## *McDonald 2H-16E Chemostratigraphic Analysis*

### Argillaceous Mudstone (AM)

Gamma-ray values are high (>1000 API units) in the argillaceous mudstone lithofacies of the Woodford Shale compared to values near 0 API units in the Hunton Group (Figure 21). Titanium and zirconium are highest in the argillaceous mudstone lithofacies with values averaging 0.28% and 0.014%, respectively. Silicon exhibits relatively low concentrations that approach 0. Calcium and strontium display values approaching 0. Potassium within the argillaceous mudstone increases from values near 0.25% at the base to an average of 2% across the interval (Figure 21). The highest value occurs near 6,406 feet and exceeds 2.5%. Uranium and vanadium display relatively high concentrations averaging 0.003% and 0.02% respectively. The paleo-redox proxy V/Cr displays high concentrations near 10 at the base before decreasing to average 4 (Figure 21). TOC concentrations are relatively high across the argillaceous mudstone and average 8.5%.

### Argillaceous, Siliceous Mudstone (A-SM)

Average gamma-ray values are less than 364 API units in the argillaceous, siliceous mudstone. The values for titanium and zirconium average 0.2% and 0.007% respectively, before decreasing to near 0% from 6,346 feet to 6,338 feet and 6,310 feet. The silicon concentrations are relatively low, and approach 0 from 6,381 feet to 6,350 feet. Silicon increases from 6,350 feet to 6,337 feet and from 6,320 feet to 6,306 feet, where values exceed 75 (Figure 21). Calcium and strontium concentrations are low (near 0) and increase slightly at 6,345 feet to values exceeding 5% and 0.005%, respectively. Potassium concentrations show two decreasing trends from 6,381 feet to 6,337 feet and from 6,325 feet to 6,306 feet, where values decrease from 1.5% to less than 0.5% and from 1.5% to less than 0.25%. Uranium and vanadium

concentrations are 0.005% and 0.01%, respectively from 6,381 feet to 6,345 feet before increasing to 0.004% and 0.02%, respectively near 6,345 feet to 6,337 feet (Figure 21). The paleo-redox proxy V/Cr is relatively constant and averages 3 from 6,381 feet to 6,350 feet. V/Cr concentrations decrease to less than 2 from 6,350 feet to 6,337 feet and from 6,310 feet to 6,306 feet, before increasing to greater than 5 from 6,325 feet to 6,310 feet. TOC averages 5.5% for the argillaceous, siliceous mudstone.

### Siliceous Mudstone (SM)

Gamma-ray values for the siliceous mudstone average 600 API units across the bottom half of the interval before decreasing to less than 200 API units from 6,306 feet to 6,264 feet (Figure 21). The concentrations of titanium and zirconium are lowest in the siliceous mudstone lithofacies averaging 0.06% and 0.003%, respectively. Silicon is highest in this lithofacies and ranges from 50 to greater than 150 (Figure 21). Calcium and strontium are also highest in the siliceous mudstone facies and range from 3% to 10% and 0.005% to 0.1%, respectively. Potassium concentrations average 1%. Uranium and vanadium in the siliceous mudstone facies average 0.0015% and 0.01%, respectively. The paleo-redox proxy V/Cr ranges from 1 to 4 and averages 2. Average TOC decreases to 3.8% in the siliceous mudstone (Figure 21).

### *Wireline Log Analysis*

Analysis of the digital wireline logs across the Woodford Shale in the Williams 1H-7X and the McDonald 2H-16E was used to establish the petrophysical properties for each lithofacies (Figure 25). The wireline log curves used were: gamma-ray, deep resistivity, neutron porosity, density porosity, photoelectric index (PE), caliper, and spontaneous potential (SP). The gamma-ray curve measures natural radioactivity of minerals containing the radiogenic isotopes

potassium, thorium, and uranium and is reported in API units. The deep resistivity curve records the resistivity of rock and natural fluids contained therein in ohm-meters. The neutron porosity curve is a hydrogen indicator and thus can be used to identify the presence of clay, water, and hydrocarbons. The density porosity curve is a plot of the electron density and reported as bulk density. The photoelectric index (PE) curve is a direct function of the aggregate atomic number of the elements in the formation in barns per electron units and is used to identify specific mineral constituents. The caliper measures the diameter of the borehole in inches and the spontaneous potential (SP) log measures the natural electrical potential in millivolts between rock and fluid contained therein and the drilling fluids.

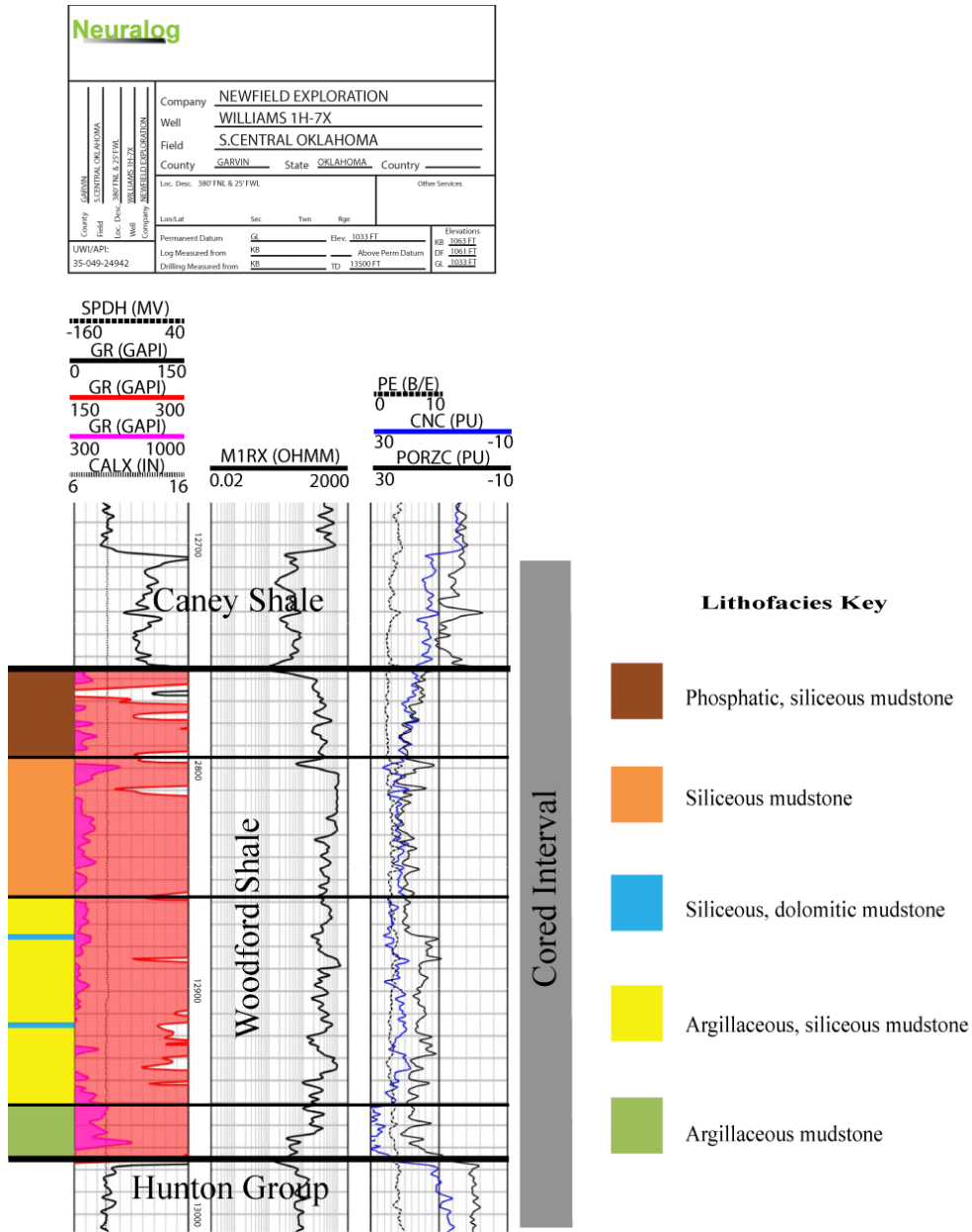


**Figure 22.** Digital wireline logs across the Woodford Shale showing the characteristics of lithofacies in the Williams 1H-7X.

Argillaceous Mudstone (AM)

The argillaceous mudstone contains the highest gamma-ray values with an average of 806 API units. The resistivity curve exhibits relatively low values with an average 144 ohm-m. The large separation between the neutron and density porosity curves is a distinct characteristic of the argillaceous mudstone lithofacies and distinguishes it from the other lithofacies (Figure 22). The neutron porosity within this interval is the highest in the Woodford Shale and averages 27%. The density porosity curve reads much lower than the neutron porosity, but is still relatively high with an average of 10%. The photoelectric index (PE) exhibits values over 3 b/e throughout the interval, with an average of 3.20 b/e. The caliper curve is consistent and averages 8.93 inches. Bit size was 8 7/8 inches.

Argillaceous, Siliceous Mudstone (A-SM)

The average gamma-ray value decreases to 664 API units in the argillaceous, siliceous mudstone interval, but some zones exhibit values less than 150 API units (Figure 22). Resistivity increases throughout the interval with values ranging from 80 ohm-m to over 1000 ohm-m, with an average of 300 ohm-m. The argillaceous, siliceous mudstone lithofacies is characterized by the separation of the neutron and density porosity curves. Average neutron porosity has decreased from 27% in the argillaceous mudstone lithofacies, to 19% in the argillaceous, siliceous mudstone. The average density porosity has decreased to 7%. The PE curve reads slightly above 3 b/e with an average of 3.09 b/e. The caliper stays consistent and averages 8.95 inches.



### Siliceous, Dolomitic Mudstone (S-DM)

Gamma-ray values decline further in the siliceous, dolomitic mudstone and average 555 API units, whereas resistivity increases to an average 533 ohm-m. Neutron and density porosities continue to decrease in the siliceous, dolomitic lithofacies and averages 19% for neutron porosity 4% for density porosity (Figure 22). The PE values are the highest of any lithofacies within the Woodford Shale, displaying an average of 3.50 b/e. The caliper curve is consistent across the zone and averages 8.95 inches.

### Siliceous Mudstone (SM)

In the siliceous mudstone facies, gamma-ray increases to an average value of 672 API units. This facies has the highest average resistivity values that range from 60 ohm-m to over 1000 ohm-m, and average 550 ohm-m. The siliceous mudstone is distinguishable by its similar density and neutron porosities. The neutron porosity in the siliceous mudstone averages 18%, whereas density porosity averages 14% (Figure 22). The PE curve decreases slightly in the siliceous mudstone facies to 3.30 b/e as compared to the value of 3.50 b/e in the underlying siliceous, dolomitic lithofacies. The caliper curve averages 8.96 inches.

### Phosphatic, Siliceous Mudstone (P-SM)

Average gamma-ray values decrease to 550 API units within the phosphate-rich interval compared to 672 API units in the underlying siliceous mudstone. Resistivity also decreases to values with an average 275 ohm-m. The neutron and density porosities are low and display similar trends. Neutron porosity averages 10% and density porosity 3%. The PE curve displays the lowest average values of 2.80 b/e within the phosphate-rich interval (Figure 22). The caliper curve averages 8.97 inches.

<b>Neuralog</b>	
Company	NEWFIELD EXPLORATION
Well	MCDONALD 2H-16E
Field	TUPELO NORTHEAST
County	COAL State OKLAHOMA Country
Loc. Desc.	SHL: 183 FNL & 415 FEL
Other Services	
Lon/Lat	Sec Twp Rge
Permanent Datum	GL Elev. 262 FT
Log Measured from	KB Above Perm Datum DF 266 FT
Drilling Measured from	KB TD 875 FT
Elevations	GL 262 FT
	KB 266 FT
	GL 262 FT

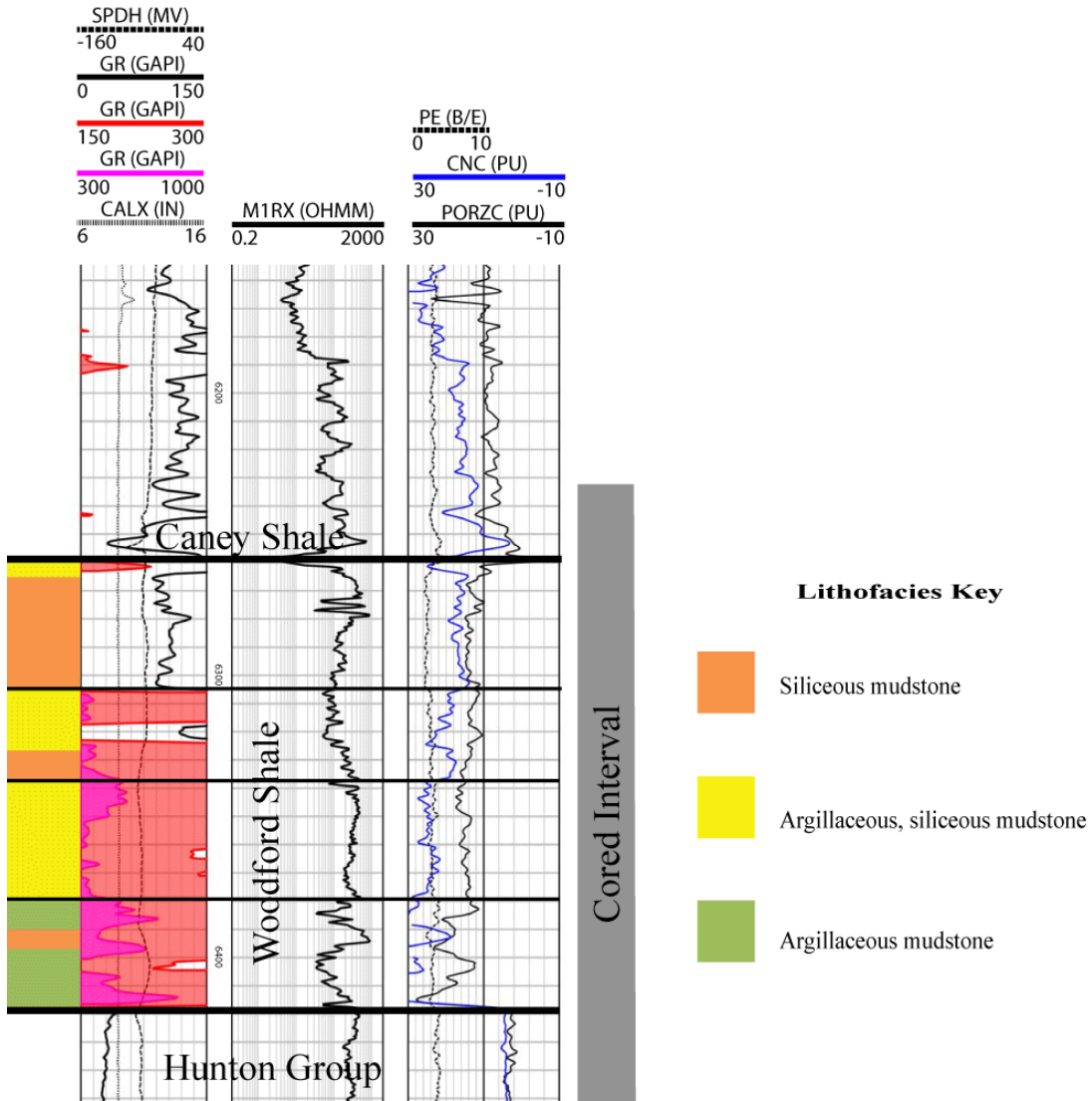


**Figure 23.** Digital wireline logs across the Woodford Shale showing the characteristics of lithofacies in the McDonald 2H-16E.

Argillaceous Mudstone (AM)

The gamma-ray values within the argillaceous mudstone are highest in the Woodford interval and average 675 API units (Figure 23). Alternatively, the resistivity within this interval is the lowest observed within the Woodford Shale and average 80 ohm-m. The neutron and density porosities display large separation with neutron values averaging 29% and density porosity averaging 13%. The PE values are slightly higher than the other lithofacies and average 3.15 b/e. The caliper stays consistent across the interval and averages 9 inches. The spontaneous potential (SP) curve exhibits the lowest negative deflections of all lithofacies with an average of -63 mV.

Argillaceous, Siliceous Mudstone (A-SM)

Gamma-ray values decrease from 675 API units in the argillaceous mudstone to an average of 364 API units across the argillaceous, siliceous mudstone (Figure 23). Average resistivity increases slightly upward to 150 ohm-m. A decrease in both porosity curves is evident with neutron porosity averaging 17% and density porosity averaging 5%. PE measurements drop to an average of 2.90 b/e. The caliper averages 9 inches. The SP curve within the argillaceous, siliceous mudstone averages -60 mV deflection from the shale baseline.

Siliceous Mudstone (SM)

The gamma-ray decreases to an average of 280 API units across the siliceous mudstone facies. The resistivity values are the highest and range from 30 ohm-m to 800 ohm-m, averaging 300 ohm-m. The neutron and density porosity curves display minimal separation and are similar in value. The neutron porosity values are the lowest in the Woodford interval and average 12%,

whereas density porosity increases slightly to an average of 8% (Figure 23). The PE curve exhibits the lowest values of any interval and averages 2.47 b/e. The caliper stays consistent and averages 9 inches. The SP curve exhibits a deflection of -62 mV across the siliceous mudstone facies.

## CHAPTER IV

### DISCUSSION AND CONCLUSIONS

Based on the Upper Devonian regional paleogeography interpreted by Callner (2014), and geochemical data and core observations from this study, the Woodford Shale in the Williams 1H-7X represents deposition on a distal shelf close to the rim of the Southern Oklahoma Aulacogen (Figure 25). The Woodford Shale in the McDonald 2H-16E represents deposition in a shelf environment at a more proximal position to a terrestrial source (Figure 24). The bulk of the Woodford Shale within both cores consists of alternating clay- and silica-rich beds (laminae and bands). The silica-rich beds are predominately novaculitic chert formed from re-precipitated silica derived from radiolarians (Cecil, 2016) and according to Kvale and Bynum (2014), higher concentrations of *tasmanites* and radiolarians occur in the more distal settings close to the zone of upwelling.

#### Williams 1H-7X

The Woodford Shale within the Williams 1H-7X core contains the highest concentrations of TOC, ranging from less than 2% to more than 11%, indicating higher preservation of organic matter or less dilution by detrital sediment. Scarce burrowing limited to the base of the Woodford Shale along with high concentrations of uranium, vanadium, and V/Cr ratio support the dysoxic to anoxic distal shelf depositional environment where an oxygen minimum zone formed in response to organic matter decay.

The lowermost argillaceous mudstone lithofacies represents the initial stage of the Kaskaskia transgression (Lambert, 1993). Abundant burrowing, medium dark clay-rich bands, high concentrations of terrestrial sediment, and low concentrations of uranium, vanadium, and low V/Cr in the basal intervals of the AM lithofacies indicate an initial oxygenated depositional environment. Phosphate occurs throughout the lower half of the interval and was likely the result of upwelling associated with the Ouachita Embayment. The transgression is marked by sudden increases in gamma-ray, vanadium, uranium, V/Cr, TOC, and biogenic silica that occur across the argillaceous mudstone. High clay concentrations in the argillaceous mudstone contribute to low resistivity, high values of gamma-ray and high neutron porosity. The low resistivity is attributed to the conductivity of water-bound clays, which also increase neutron porosity. The high gamma-ray value is likely caused by uranium attached to organic matter and the abundance of potassium-bearing clay minerals. The carbonate cement observed in the argillaceous mudstone could be sourced from the underlying Hunton Group.

The overlying argillaceous, siliceous mudstone lithofacies hosts higher concentrations of biogenic silica in conjunction with decreasing clay contents. The decrease in clay minerals is reflected in lower values of gamma-ray, TOC, and neutron porosity. Abundant biogenic silica contributes to higher resistivity, brittleness, and natural fracturing. These fractures are mostly calcite-cemented and may contribute to the sporadic increase in carbonate detected by XRD. High concentrations of uranium, vanadium, and intermediate to high V/Cr, as well as minor burrowing, ripple marks, and graded bedding indicate the depositional environment for the argillaceous, siliceous mudstone was dominantly dysoxic to anoxic, but occasionally energized by currents, which likely contributed to brief periods of oxygenation.

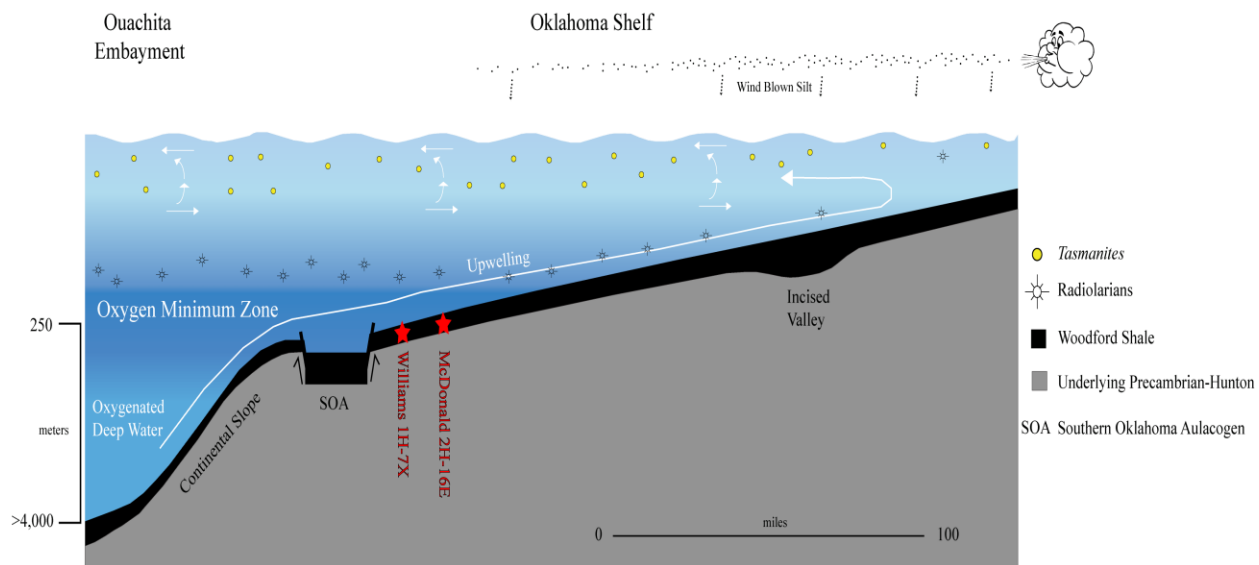


**Figure 24.** Late Devonian schematic depositional model showing cores used in this study. After Callner (2014); Cecil (2016).

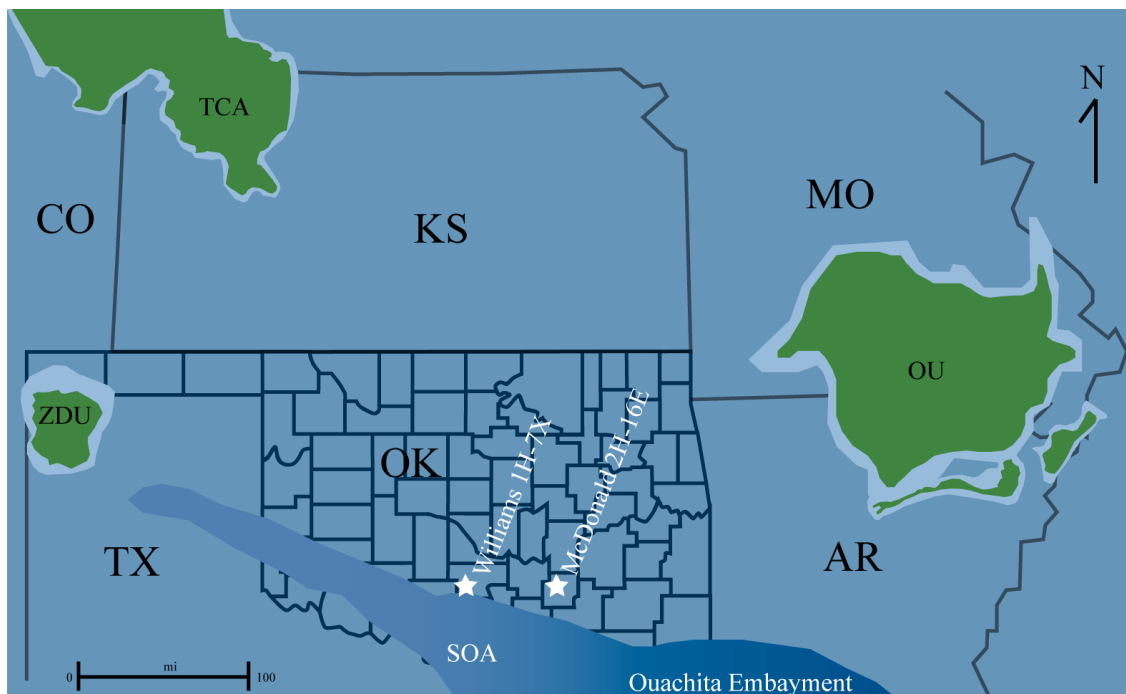


**Figure 25.** Interpretational paleogeographic map with core locations marked by stars. **OU:** Ozark Uplift, **TCA:** Trans-Continental Arch, **ZDU:** Zuni-Defiance Uplift (After Wickham, 1978; Keller, 2012).

Thin intervals of siliceous, dolomitic mudstone are interbedded with the argillaceous, siliceous mudstone. Siliceous, dolomitic mudstone contains a higher percentage of dolomite that contributes to its higher resistivity and PE values. Abraded anhedral and subhedral silt-sized dolomite crystals/grains along with occasional quartz grains in graded layers. These features were likely caused by secondary alteration of calcite that were then altered to dolomite. As a result of the lower clay content in the siliceous, dolomitic mudstone, the gamma-ray values and TOC are low.

The siliceous, dolomitic mudstone is overlain by the siliceous mudstone facies that contains higher concentrations of both biogenic and detrital silica. This increased silica content results in higher resistivity values and the accompanying increased density porosity may be the result of fracturing. Increased bulk density porosity could also be attributed to the high TOC (6.9%) which is lower density material in its own right and to the generation of intraorganic matter porosity during maturation (Milliken, 2013). The neutron and density porosities display similar trends, increasing and decreasing in tandem. Calcite-and dolomite-cemented fractures may contribute to the carbonate concentration. The relative increase in clay percentage from the dolomitic mudstone to the siliceous mudstone is reflected by an increase in gamma-ray values and TOC. Uranium, vanadium, and V/Cr indicate a predominately dysoxic depositional environment interrupted by events that resulted in the input of terrestrially derived sediment, increased burrowing, graded laminae of pyrite, chert, and/or quartz, and slightly oxygenated conditions.

The uppermost lithofacies is a phosphatic, siliceous mudstone that contains similar high concentrations of biogenic and detrital silica. As a result, the PE curve decreases to below 3 b/e. Consequently, the density and neutron porosity curves exhibit decreased, but similar values



and indicate lower concentrations of clay. Abundant phosphate, that is evident in hand sample and by the geochemical concentrations of calcium, occurs across the interval indicating proximity to upwelling of nutrient-rich waters. High concentrations of uranium, vanadium, and V/Cr indicate predominately anoxic depositional conditions. Temporally minor events resulted in the increase in terrestrially derived sediment and graded bedding. These events are reflected by increases in the concentrations of geochemical proxies potassium, aluminum, zirconium, and titanium and their recognition in thin section petrography by well-rounded to angular silt and/or sand-sized grains.

#### McDonald 2H-16E

The Woodford Shale within the McDonald 2H-16E core contains lower concentrations of TOC, ranging from less than 1% to more than 12% with an average of 6-8%. Abundant burrowing and terrestrially derived sediments along with low concentrations of uranium, vanadium, and V/Cr support the interpretation of a shelf depositional environment ranging in oxic to anoxic bottom water conditions.

The lowermost argillaceous mudstone lithofacies marks the initiation of the Kaskaskia transgression. The Woodford Shale has high values of gamma-ray, TOC, and high V/Cr compared to the underlying Hunton Group. Concentrations of uranium, vanadium, and V/Cr indicate dysoxic to anoxic depositional conditions, while hand samples and thin sections reveal abundant burrowing and terrestrially derived clay- to sand-sized quartz and feldspars. The argillaceous mudstone contains the highest percentages of clays resulting in low resistivity, and higher values for gamma-ray and neutron porosity. Abundant phosphate nodules occur across the interval and indicate proximity to upwelling. Frequent burrowing and increased terrestrially derived quartz and feldspars, in conjunction with higher concentrations of uranium, vanadium,

and V/Cr are interpreted to suggest that the argillaceous mudstone was likely deposited on a shelf environment where dysoxic conditions existed and upwelling currents provided nutrients for phosphate precipitation.

The overlying argillaceous, siliceous mudstone contains higher concentrations of silica and when combined with increased concentrations of titanium, aluminum, and zirconium, suggest a detrital quartz source. The increase in silica, along with fractures filled with carbonate cement and pyrite contribute to a lower clay content, higher resistivity, decreased values of PE (<3 b/e), lower gamma-ray readings, reduced TOC, and lower values for neutron porosity. An anomalous interval occurs from 6,325 feet to 6,318 feet where low uranium concentrations coincide with high TOC. This is interpreted as an influx of weathered terrigenous organic matter that increased TOC. Minor burrowing and intermediate values for uranium, vanadium, and V/Cr are interpreted to suggest that the argillaceous, siliceous mudstone was deposited in restricted, dysoxic water.

The siliceous mudstone lithofacies contains the highest concentrations of silica, of mostly biogenic origin. Similar to the previous lithofacies, the high silica content results in high resistivity and a decrease in PE to 2.47 b/e, as well as closer density and neutron porosity values, as a result of reduced clay content and increase in higher density minerals. Aside from suppressing the neutron porosity, the decreased clay concentrations result in relatively low gamma-ray values and TOC measurements. Burrowing and phosphate nodules occur in the upper section of the siliceous mudstone. Most of the upper interval is interpreted as representing deposition in oxic to dysoxic waters in which radiolarian and *tasmanites* debris accumulated. Oxygenation of the upper section, as evidenced by burrowing, may be attributed to regression,

basinward pycnocline retreat, and/or episodic bottom water storm currents such as turbidity flows that oxygenated the water column.

Varying lithofacies, sedimentary and biogenic structures, geochemical data, and paleogeographic reconstruction support diverse paleo-environmental conditions and settings of Woodford Shale deposition in south-central Oklahoma. The Williams 1H-7X core was deposited on a distal outer shelf near the northern rim of the Southern Oklahoma Aulacogen. Alternating beds of argillaceous and siliceous mudstone form the bulk of the Williams 1H-7X. Based on ratios of zirconium, titanium, and aluminum, the silica is predominately biogenic in origin, forming from radiolarian oozes and transforming into novaculitic chert during diagenesis. These silica-rich zones commonly contain ptigmatic and vertical fractures that are mostly calcite-cemented, and do not extend into the overlying or underlying argillaceous beds. Phosphate, found in nodules, is present near the base and top of the Woodford Shale interval, indicating upwelling ocean currents that extended from the Ouachita Embayment to the northwest and the rim of the Southern Oklahoma Aulacogen. The paleo-redox proxy of V/Cr, in conjunction with uranium and vanadium concentrations, show that the Woodford Shale of the Williams 1H-7X core was deposited in predominately dysoxic to anoxic bottom water. Burrowing is evident in hand sample and thin section and correlates with the thin and temporally short oxygenated intervals within the Woodford Shale. Graded silty bedding and occasional ripple marks indicate active bottom water currents on the shelf that may have contributed to oxygenation (Figure 26). TOC concentrations indicate an organic-richness throughout the Woodford Shale due to the combination of dysoxic to anoxic conditions and low input of terrestrially derived sediment.

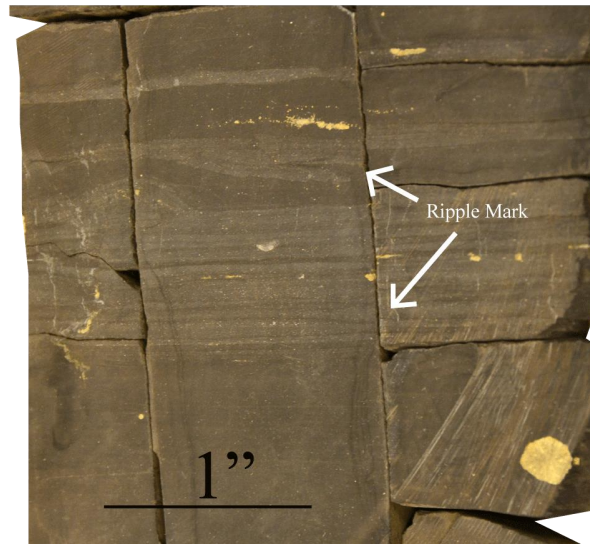


**Figure 26.** Current features and associated oxygenated water indicators. Ripple mark within silica-rich laminae. Depth 12,924 feet, Williams 1H-7X.

The Woodford in the McDonald 2H-16E core was deposited on the shelf more proximal to a source of detrital sediment. Phosphate occurs throughout the Woodford Shale and like the Williams 1H-7X is more abundant at the base and top, indicating upwelling of nutrient-rich water existed along the continental shelf. Similar to the Williams 1H-7X core, the McDonald 2H-16E is predominately alternating argillaceous and siliceous beds. The silica-rich intervals are primarily composed of detrital quartz, which is indicated by the high concentrations of terrestrial proxies (titanium and zirconium) correlating with lower silicon concentrations. These silica-rich zones consist of quartz grains cemented with chert and contain ptigmatic and vertical fractures that are open to calcite-cemented, and confined to the zone. The paleo-redox proxy of V/Cr, in conjunction with uranium and vanadium concentrations, show that the bottom half of the Woodford Shale within the McDonald 2H-16E was deposited in predominately dysoxic bottom water conditions whereas the upper half was deposited in oxic to dysoxic

conditions. Abundant burrowing occurs throughout the Woodford interval and correlates with the oxygenated to dysoxic paleo-redox conditions. Graded bedding and vertical stylolites indicate bottom water currents and tectonic activity, respectively, along the shelf margin. The Woodford Shale within the McDonald 2H-16E contains TOC concentrations that are lower than those for the Williams 1H-7X (McDonald 2H-16E ~5%, Williams 1H-7X ~6%), but enough to be considered organic-rich.

The geographical locations of the Woodford Shale represented by the Williams 1H-7X and McDonald 2H-16E are separated by approximately 70 miles (112 km) and presently located in the southeastern Anadarko Basin and the southwestern Arkoma Basin, respectively. However, both Woodford intervals display similar structures and features due to their deposition in the same paleo-basin and close to the Ouachita Embayment prior to the tectonic activity that formed the Anadarko and Arkoma Basins.

The Woodford Shale of both cores display similar lithofacies that contain high concentrations of silica and clays and lower concentrations of other mineralogical components including pyrite and marcasite, dolomite, and apatite. The silica-rich intervals are more brittle, and as a result, exhibit numerous open and mineralized fractures.

Silica-rich and clay-rich zones are distinguishable on wireline logs and can be used to map the favorable organic-rich siliceous lithofacies. Similar depositional features such as radiolarians, phosphate, and *tasmantites* cysts are observed in the Woodford Shale in both cores and indicate high organic productivity associated with marine upwelling. Geochemical proxies indicate Woodford sediments were deposited in a predominately dysoxic to anoxic setting with oxygenated events supported by burrows, and associated with current features including ripple marks and graded bedding.

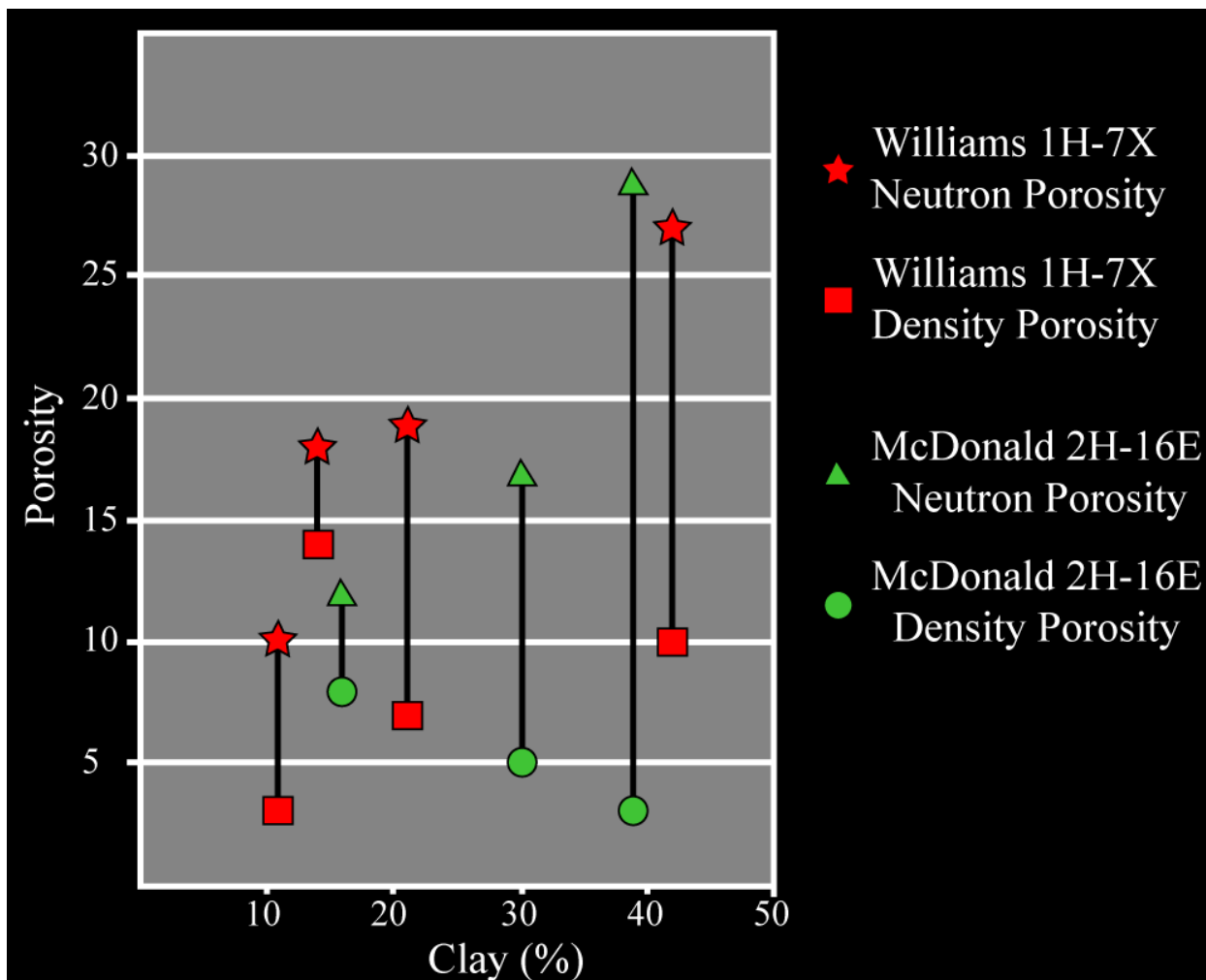


**Figure 27.** Comparison of density and neutron porosity values with increasing clay content in the Williams 1H-7X and McDonald 2H-16E.

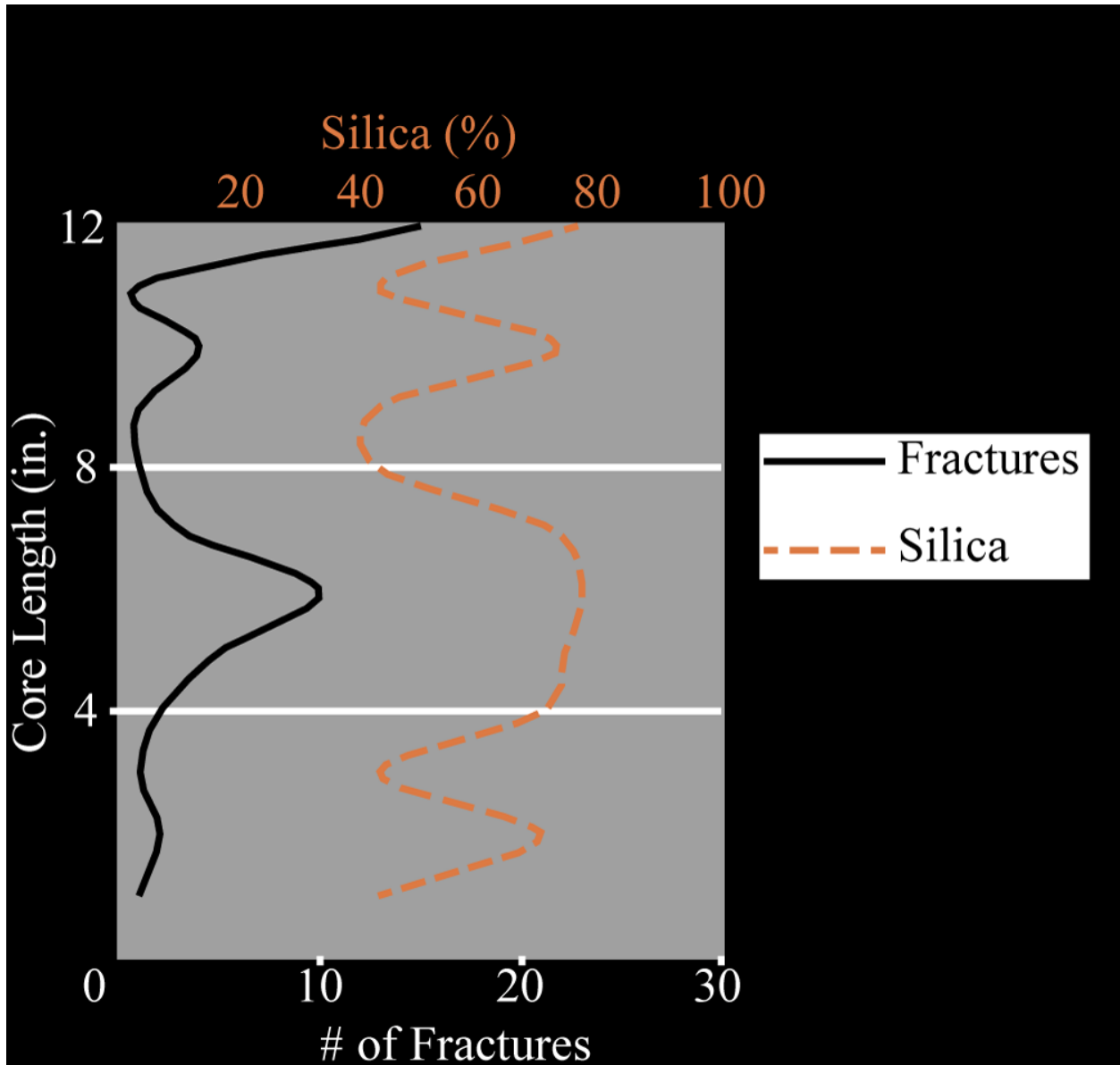


**Figure 28.** Comparison of silica percentage with number of fractures in the SM lithofacies of the Williams 1H-7X.

The attempt to correlate the Williams 1H-7X and the McDonald 2H-16E using chemostratigraphy could not be achieved due to distinct differences between the two cores. For example, the Woodford Shale of the Williams 1H-7X core contains enriched concentrations of Ti, Zr, and K exclusively in the upper section of core (12,850 feet to 12,750 feet) whereas the McDonald 2H-16E core contains high Ti, Zr, and K concentrations across the majority of the Woodford interval. In addition, the biogenic quartz proxy (Si/Al) in the Williams 1H-7X core contains high concentrations across the Woodford interval whereas high concentrations of biogenic quartz are limited to the upper section (6,320 feet to 6,260 feet) in the Woodford interval of the McDonald 2H-16E core. The lack of trace element correlation between the two cores is attributed to the influence of local depositional processes such as upwelling and the influx of eolian or current driven sediment that influenced lithology and bottom water geochemistry.

Correlating lithofacies using wireline logs could not be achieved between the two wells because the Woodford Shale was eroded off of the Late Paleozoic Arbuckle Uplift. Furthermore, the lithologic and chemostratigraphic changes observed in core does not instill confidence in wireline-log correlation. The characteristic wireline signatures of the upper, middle, and lower Woodford Shale members are arguably inapplicable to the Williams 1H-7X and McDonald 2H-16E cores.

These results support the principal hypotheses proposed for this study that 1) because the Woodford sediments were deposited in the same basin, they should contain similar depositional facies, 2) silica-rich beds were expected in both cores and that the biogenic silica resulted from the accumulations of radiolarians tests, and 3) the ability to identify and map silica-, carbonate-, and clay-rich facies can be achieved using wireline logs.



Recommendations for future work include 1) SEM analysis to detect if organic matter is contributing to porosity as well as determining the origin of pyrite (syngenetic or diagenetic), 2) biomarker analysis to reveal more detailed variations in redox conditions and organic matter input, and 3) high-frequency sampling and elemental analysis using inductively coupled plasma mass spectrometry (ICP-MS) to enhance the detection of trace elements concentrations to a level of parts per quadrillion (ppq) and construction of a more redox sensitive geochemical profiles.

The importance of silica banding or chert beds associated with high TOC is reflected in the initial production of Woodford Shale completions. The SM lithofacies of the Williams 1H-7X contains approximately 74.5 feet of organic- and silica-rich bedding. In contrast, the SM lithofacies of the McDonald 2H-16E has approximately 15.5 feet. Both wells were completed in a similar fashion and were treated with greater than 7 million pounds of sand proppant and 200,000 barrels of water with likely lateral zones occurring at the A-SM/SM lithofacies contact interval, this is done in order to preserve the drill bit by drilling in clay as well as the ability to fracture the overlying silica-rich zone. The Williams 1H-7X initially produced 1,059 bbl/day of oil, 3,096 mcf/day of gas, and 900 bbl/day of water, whereas the McDonald 2H-16E produced 51.8 bbl/day of oil, 3,188 mcf/day of gas, and 1,760 bbl/day of water. Cumulative production data is currently not available but the initial production data indicate the importance of identifying and mapping silica-rich intervals in the Woodford Shale.

The distinct petrophysical properties of lithofacies within the Woodford Shale create a possibility of mapping favorable silica-rich intervals using wireline log signatures. The siliceous mudstone lithofacies of the Williams 1H-7X and the McDonald 2H-16E is characterized by the highest concentration of silica and exhibits similar trends of suppressed neutron porosity values and increased density porosity values. These “tracking” porosity curves, along with lower

neutron and gamma-ray values and high resistivity values, indicate a decrease in clay content and increase in the non-clay fraction that contributes to increased resistivity, as well as possible gas-filled fractures contributing to porosity crossovers (Figure 27). The interval is organic-rich based on the TOC and contains abundant natural fracturing due to the silica content (Figure 28).

Organic-rich intervals like the siliceous mudstone lithofacies are potential zones of interest, due to their increased brittleness that enhances natural reservoir properties and potential to propagate hydraulic fractures.

## References

- Algeo, T.J. and Maynard, J.B., 2004, Trace-element behavior and redox facies in core shales of Upper Pennsylvanian Kansas-type cyclothems: *Chemical Geology*, Vol. 206, p. 289-318.
- Algeo, T.J. and Rowe, H., 2011, Paleooceanographic applications of trace-metal concentration data: *Chemical Geology* 324-325, p. 6-18.
- Arthur, M.A., and Sageman, B.B., 1994, Marine Shales: depositional mechanisms and Environments of Ancient Deposits: *Annual Review of Earth and Planetary Sciences*, v.22, p.499-551.
- Ataman, O., 2008, Natural fracture systems in the Woodford Shale, Arbuckle Mountains, Oklahoma: Stillwater, Oklahoma State University, unpublished M.S. thesis, 158 p.
- Banner, J.L. (1995) Application of the trace element and isotope geochemistry of strontium to studies of carbonate diagenesis: *Sedimentology*, 42, p.805-824
- Barron, L.S. and Ettensohn, F.R., 1981, Paleoecology of the Devonian-Mississippian black shale sequence in eastern Kentucky with an atlas of some common fossils: U.S. Department of Energy, p. 1-80.
- Basir, Jasin, 1992. Significance of radiolarian cherts from the Chert-Spilite Formation, Telupid, Sabah. *Bull. Geol. Soc. Malaysia*, 31, 67-83.
- Berner, R.A., 1980, *Early Diagenesis A Theoretical Approach*: Princeton, N.J., Princeton University Press, 241 p.
- Berner, R.A., and Raiswell, R., 1984, C/S method for distinguishing freshwater from marine sedimentary rocks: *Geology*, v. 12, no. 6, p. 365-368.
- Blackford, M.A., 2007, *Electrostratigraphy, thickness, and petrophysical evaluation of the Woodford Shale, Arkoma Basin, Oklahoma*: Ann Arbor, Oklahoma State University, 0372, 94 p.
- Blakey, R.C., 2016, *Global Paleogeographic Views of Earth History - Late Precambrian to Recent*, <http://jan.ucc.nau.edu/rcb7/nam.html>, (accessed November 11, 2016).
- Blueford, J.R., 1989. Radiolarian Evidence: Late Cretaceous through Eocene ocean circulation patterns. In: Hein, J.R. & Obradovic, A. (eds.), *Siliceous deposits of the Tethys and Pacific regions*. Springer-Verlag, New York, pp. 19-29.
- Berryman, R.R., 2012, *Constraints on development of anoxia through geochemical facies mapping of the Devonian black shales in the Midcontinent*: Stillwater, OK, Oklahoma State University, unpublished M.S. thesis.

- Berryman, J.R., 2012, Timing and paragenesis of the calcite fracture fill in the Woodford Shale: Stillwater, Oklahoma State University, unpublished M.S. thesis, 44 p.
- Boardman, D.R., II, J. Puckette, and I. Çemen, 2008, Late Devonian-Early Permian organic-rich gas shales of the North American Midcontinent (abstract): GSA South-Central Section, Abstracts with Programs, p. 5.
- Boardman, D.R., III, 2012, Preliminary analysis of phosphate nodules in the Woodford Shale, Late Devonian-Early Mississippian, southern Oklahoma: Stillwater, Oklahoma State University, unpublished M.S. thesis, 77 p
- Caldwell, C.D., 2011, Lithostratigraphy of the Woodford Shale, Anadarko Basin, West-Central Oklahoma, in Oklahoma Geological Survey Shales Moving Forward Workshop, July, p. 2011.
- Callner, S.A., 2014, An integrated approach to understanding sedimentary structures and depositional processes in Devonian-Mississippian black shale: the Woodford Shale and associated strata in the Southern Midcontinent: Stillwater, Ok, Oklahoma State University, unpublished M.S. thesis.
- Camp, W.K., Diaz, E., Wawak, B., 2013. Electron microscopy of shale hydrocarbon reservoirs. AAPG Mem. 102 (260 p).
- Cardott, B.J., 2008, Overview of Woodford gas-shale play of Oklahoma, U.S.A. (abstract): AAPG 2008 Annual Convention and Exhibition, Abstracts Volume 17, p. 27-28. <http://www.ogs.ou.edu/pdf/AAPG08woodford.pdf>
- Cardott, B.J., 2012, Thermal maturity of Woodford Shale gas and oil plays, Oklahoma, USA: International Journal of Coal Geology, v 103, p. 109-119.
- Cardott, B.J., 2013, Woodford Shale: From hydrocarbon source rock to reservoir: AAPG Search and Discovery Article 50817, 85 p. [http://www.searchanddiscovery.com/documents/2013/50817cardott/ndx\\_cardott](http://www.searchanddiscovery.com/documents/2013/50817cardott/ndx_cardott). Pdf
- Cecil, K.A., 2016, Origin and characterizaiton of Devonian-Mississippian novaculitic chert in Oklahoma; unpublished M.S. thesis, Oklahoma State University, 154 p.
- Comer, J. B., 1991, Stratigraphic analysis of the Upper Devonian Woodford Formation, Permian Basin, West Texas and southeastern New Mexico: Austin, Texas, Bureau of Economic Geology, Report of Investigations 201, 63 p.
- Comer, J.B., 1992, Organic geochemisty and paleogeography of Upper Devonian formations in Oklahoma and western Arkansas, in K.S. Johnson and B.J. Cardott, eds., Source rocks in the southern Midcontinent, 1990 symposium: OGS Circular, no. 93, p. 70-93.

- Comer, J.B., 2007, Reservoir characteristics and gas production potential of Woodford Shale in the Southern Midcontinent [Microsoft PowerPoint presentation]: IUScholarWorks [Indiana University's digital repository], <<http://hdl.handle.net/2022/1826>>, date accessed.
- Comer, J.B., 2008, Reservoir characteristics and production potential of the Woodford Shale: *World Oil*, v. 229, no 8, p.1-7.
- Comer, J.B., 2012, Woodford Shale and the evaporate connection – the significance of aridity and hypersalinity in organic matter productivity and preservation: *Geological Society of America Abstracts with Programs*, v. 44/5, p. 6.
- Einsele, G. (2000) *Sedimentary Basins*. Springer, Berlin, Heidelberg, New York, 792 pp
- Ellison, S. P., 1950, Subsurface Woodford black shale, west Texas and southeast New Mexico: Austin, Texas, Bureau of Economic Geology, Report of Investigations 7, 20 p. Ettensohn, F.R., 1992, Controls on the origin of the Devonian-Mississippian oil and gas shales, east-central United States: *FUEL*, vol. 71, p. 1487-1492.
- Encyclopedia of Tidepools and Rocky Shores*. Edited by Mark W. Denny & Steven D.Gaines. Berkeley, CA: University of California Press, 2007. Pp.735.
- Ettensohn, F.R., Miler, M.L., Dillman, S.B., Elam, T.D., Geller, K.L., Swager, D.R., Markowitz, G., Wook, R., and Brown, L., 1988, Characterization and Implications of the Devonian-Mississippian Black Shale Sequence, Eastern and Central Kentucky, USA: Pycnoclines, Transgression, Regression, and Tectonism: McMillan, N.J., et al., eds., *Devonian of the world*, Volume 2: Canadian Society of Petroleum Geologists Memoir 14, p. 323-345.
- Furmann, A., Mastalerz, M., Brassell, S.C., Schimmelmann, A., Picardal, F., 2013. Extractability of biomarkers from high- and low-vitrinite coals and its effect on the porosity of coal. *International Journal of Coal Geology* 107, 141–151.
- Hardie, W.E., 1990, Subsurface structural study of the buried Ouachita thrust front, southeastern Oklahoma: *Oklahoma City Geological Society, Shale Shaker*, v. 41, p. 32-55.
- Hass, W.H., and Huddle, J.W., 1965, Late Devonian and Early Mississippian age of the Woodford Shale in Oklahoma, as determined from conodonts: US Geological Survey Professional Paper, p. D125-D132.
- Hoffman, P., J.F. Dewey, and K. Burke, 1974, Aulacogens and their genetic relation to geosynclines, with a Proterozoic example from Great Slave Lake, Canada, in R.H. Dott, Jr., and R.H. Shaver, eds., *Modern and ancient geosynclinal sedimentation*: Society of Economic Paleontologists and Mineralogists, Special Publication 19, p. 38-55.
- Johnson, K.S., 1989, Geologic Evolution of the Anadarko Basin: Oklahoma Geological Survey, vol. 90, p. 3-12.

- Jones, B., Manning, D.A.C., 1994. Comparison of geochemical indices used for the interpretation of palaeoredox conditions in ancient mudstones. *Chem. Geol.* 111, 111 – 129.
- Kennedy, M. J., Löhr, S. C., Fraser, S. A., and Baruch, E.T.: Direct evidence for organic carbon preservation as clay-organic nanocomposites in a Devonian black shale; from deposition to diagenesis, *Earth Planet. Sc. Lett.*, 388, 59–70, doi:10.1016/j.epsl.2013.11.044, 2014
- Kirkland, D.W., Denison, R.E., Summers, D.M., Gormly, J.R., 1992, *Geology and organic geochemistry of the Woodford Shale in the Criner Hills and Western Arbuckle Mountains: Oklahoma Geological Survey, Vol. 93, p. 38-69.*
- Kvale, E and Bynum, J., (2014), *Regional Upwelling During Late Devonian Woodford Deposition in Oklahoma and Its Influence on Hydrocarbon Production and Well Completion. Woodford Shale Forum: Lecture conducted from AAPG.*
- Lambert, M., 1993, *Internal Stratigraphy and Organic Facies of the Devonian-Mississippian Chattanooga (Woodford) Shale in Oklahoma and Kansas, in Source Rocks in a Sequence Stratigraphic Framework, Studies in Geology 37, p. 163-176.*
- Lisitzin, A.P., 1972. *Sedimentation in the world ocean. Society of economic paleontologist and mineralogists. Special publication no. 17, 218 pp.*
- Lüning, S. and Kolonic, S., 2003, Uranium spectral gamma-ray response as a proxy for organic richness in black shales: applicability and limitations: *Journal of Petroleum Geology*, vol. 26, p. 153-174.
- McCarthy, K., Rojas, K., Niemann, M., Palmowsky, D., Peters, K., Stankiewicz, A. (2011): *Basic Petroleum Geochemistry for Source Rock Evaluation. Oilfield Review*, 23, no. 2. p. 32-43
- McCullough, B and Slatt, R., (2014), *Stratigraphic Variability of the Woodford Shale across Oklahoma Woodford Shale Forum: Lecture conducted from AAPG.*
- Meyers P. A. and Mitterer R. M. (1986) *Introduction and Overview: Deep ocean black shales: Organic geochemistry and palaeoceanographic setting. Mar. Geol.* **70**, 1-8.
- Milliken KL, Rudnicki M, Awwiller DN, Zhang T. *Organic matter-hosted pore system, Marcellus Formation (Devonian), Pennsylvania. Am Assoc Pet Geol Bull* 2013;97:177–200.
- Morford J. L. and Emerson S. (1999) *The geochemistry of redox sensitive trace metals in sediments. Geochim. Cosmochim. Acta* 63, 1735–1750.

- Northcutt, R. A., Johnson, K. S., and Hinshaw, G. C. (2001) Geology and petroleum reservoirs in Silurian, Devonian, and Mississippian rocks in Oklahoma: In Johnson K. S. (ed.) Silurian, Devonian, and Mississippian geology and petroleum in the southern Midcontinent, 1999 symposium. *Oklahoma Geological Survey Circular* **105**, 1-29.
- O'Brien, N.R., Slatt, R.M., and Senftle, J., 1994, The significance of oil shale fabric in primary hydrocarbon migration: *Fuel*, v. 73, no. 9, p. 1518-1522.
- OGS, 2016. <http://www.ogs.ou.edu/MapsBasic/Provinces.jpg>
- Pashin, Jack and Callner, Sara. (2014), Paleooceanographic and Estuarine Influences on Sedimentation in an Unconventional Source Rock-Reservoir System: Devonian Shale in the Southern Midcontinent, USA. 2014 Eastern Unconventional Oil and Gas Symposium- November 5-7, 2014 in Lexington, Kentucky, USA.
- Pearce, T.J. and Jarvis, I. (1992) Applications of geochemical data to modelling sediment dispersal patterns in distal turbidites: Late Quaternary of the Madeira Abyssal Plain: *Journal of Sedimentary Petrology*, 62, p.1112-1129
- Pearce, T.J., Besly, B.M., Wray, D.S., Wright, D.K. (1999) Chemostratigraphy: a method to improve interwell correlation in barren sequences – a case study using onshore Duckmantian/Stephanian sequences (West Midlands, U.K.): *Sedimentary Geology*, 124, p.197-220
- Peters-Kottig, W., Strauss, H., Kerp, H., 2006. The land plant  $\delta^{13}\text{C}$  record and plant evolution in the Late Palaeozoic. *Palaeogeography, Palaeoclimatology, Palaeoecology* 240, 237–252.
- Pettijohn, F. J., 1957. *Sedimentary Rocks*. New York: Harper and Row, 718p.
- Puckette, J., Boardman, D.R., and Cemen, I., 2008, Shelf to basin transect of Middle Paleozoic organic-rich shales of North America Mid-continent (Chattanooga, Woodford, Arkansas Novaculite): Oklahoma Geological Survey, Oklahoma Gas Shales Conference, October 22, 2008.
- Puckette, J., Boardman, D.R., and Watney, W.L., 2013, Woodford Shale: Correlating rock properties in outcrop and core with wireline log characteristics: Search and Discovery, AAPG/Datapages electronic journal # 50885.
- Raiswell, R., and Berner, R. A., 1985, Pyrite formation in euxinic and semi-euxinic environments: *American Journal of Science*, v. 285, p. 710–724.
- Rezaee R (eds) (2015) *Fundamental of gas shale reservoirs*. Wiley, New Jersey
- Rimmer, S.M., 2004, Geochemical paleoredox indicators in Devonian–Mississippian black shales, central Appalachian Basin (USA): *Chemical Geology*, v. 206, no. 3, p. 373-391.

- Schieber, J., 1994, Evidence for high-energy events and shallow-water deposition in the Chattanooga Shale, Devonian, central Tennessee, USA: *Sedimentary Geology*, v. 93, no. 3, p. 193-208.
- Sloss, L. L., and Speed, R. C., 1974, Relationships of Cratonic and Continental-Margin Tectonic Episodes; in Dickenson, W. R., (ed.), *Tectonics and Sedimentation*, SOC. Econ. Paleontologists and Mineralogists Spec. Pub. 22, pp. 98-119
- Snider, A.L., 2014, Characterization of the Woodford Shale in Southern Noble and Northern Payne Counties Oklahoma: Stillwater, OK, Oklahoma State University, unpublished M.S. thesis.
- Suits, N.S., and Wilkin, R.T., 1998, Pyrite formation in the water column and sediments of a meromictic lake: *Geology*, v. 26, p. 1099-1102.
- Suneson, N.H., 1995, Structural interpretations of the Arkoma Basin – Ouachita Mountains transition zone, southeastern Oklahoma: a review, in Johnson, K.S., ed., *Structural styles in the southern Midcontinent, 1992 symposium: Oklahoma Geological Survey Circular 97*, p. 259-263.
- Taff, J.A., 1902, Description of the Atoka quadrangle [Indian Territory]: US Geological Survey Atlas Folio, v.79, p.8.
- Tourtelot, H.A., 1979, Black shale – its deposition and diagenesis: *Clays and Clay Minerals*, vol. 27, No. 5, p. 313-321.
- Trask, P.D., and Patnode, H.W., 1942, Source beds of petroleum: *American Association of Petroleum Geologists*, 566 p.
- Tribovillard, N., A. Trentesaux, A. Ramdani, F. Baudin, and A. Biboulleau (2004b), Controls on organic accumulation in late Jurassic shales of northwestern Europe as inferred from trace metal geochemistry, *Bull. Soc. Geol. Fr.*, 175, 491–506, doi:10.2113/175.5.491
- Tribovillard, N., Ramdani, A., Trentesaux, A., 2005. Controls on organic accumulation in Late Jurassic shales of Northwestern Europe as inferred from trace-metal geochemistry. In: Harris, N. (Ed.), *The Deposition of Organic-Carbon-Rich Sediments: Models, Mechanisms, and Consequences: SEPM Special Publication*, No. 82, pp. 145–164.
- Tribovillard, N., Algeo, T.J., Lyons, T., Riboulleau, A., 2006, Trace metal as paleoredox and paleoproductivity proxies: An update: *Chemical Geology*, vol. 232, p. 12-32.
- Turner, B.W., Molinares-Blanco, C.E., and Slatt, R.M. (2015) Chemostratigraphic, palynostratigraphic, and sequence stratigraphic analysis of the Woodford Shale, Wyche Farm Quarry, Pontotoc County, Oklahoma: *Interpretation*, 3, p.SH1-SH9



Ulmishek, G.F. and Klemme, H.D., 1990, Effective petroleum source rocks of the world: Stratigraphic distribution and controlling depositional factors: AAPG Bulletin, vol.75, p. 1809-1851.

USGS, 2012, Map of Assessed Shale Gas in the United States: U.S. Department of the Interior and U.S. Geological Survey, 16 p.

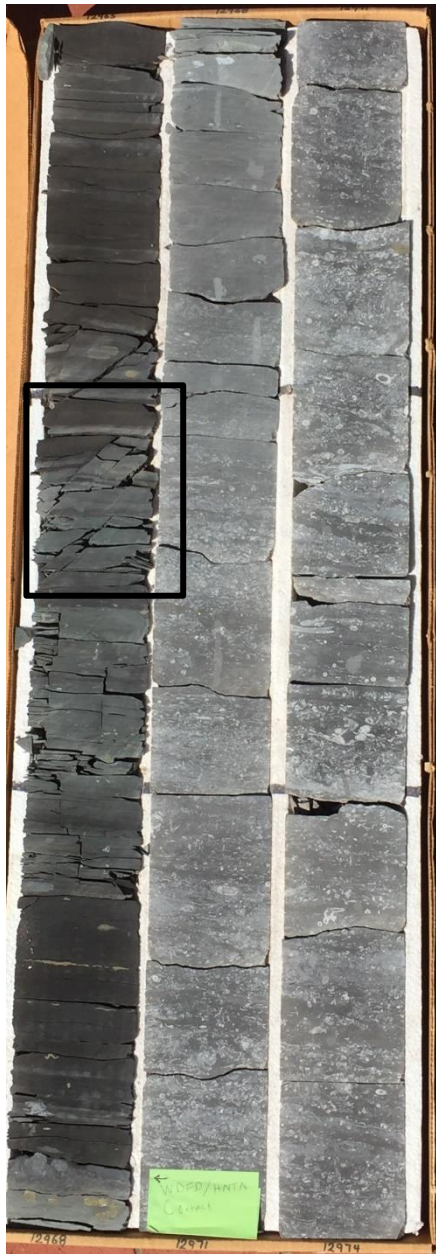
Vine, J. D. and Tourtelot, E. B. (1970) Geochemistry of black shale deposits---a summary report: Econ. Geol. 65, 253-272.

Weissert, H., 1981. The environment of deposition of black shales in the early Cretaceous An ongoing controversy. In: J.E. Warme, R.G. Douglas and E.L. Winterer (Editor., The Deep Sea Drilling Project: A Decade of Progress. Soc. Econ. Paleontol. Minera Spec. Publ., 32: 547--560.

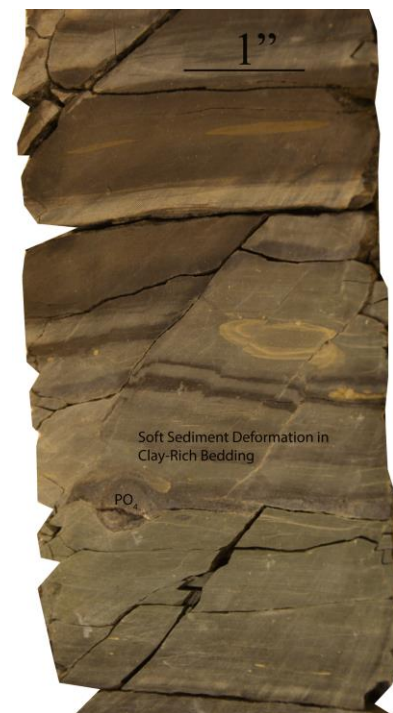
Appendix A

Williams 1H-7X

Core and Thin Section Photographs



**Appendix A.** Williams 1H-7X core photographs of subsea depths 12,974 feet to 12,965 feet (left figure). Depth shallows from bottom right corner to top left corner at a thickness of 3 feet per column in core box. Right figure shows SSD, phosphate nodules, and pyrite in the AM lithofacies. Depth of 12,966.5 feet to 12,966 feet.

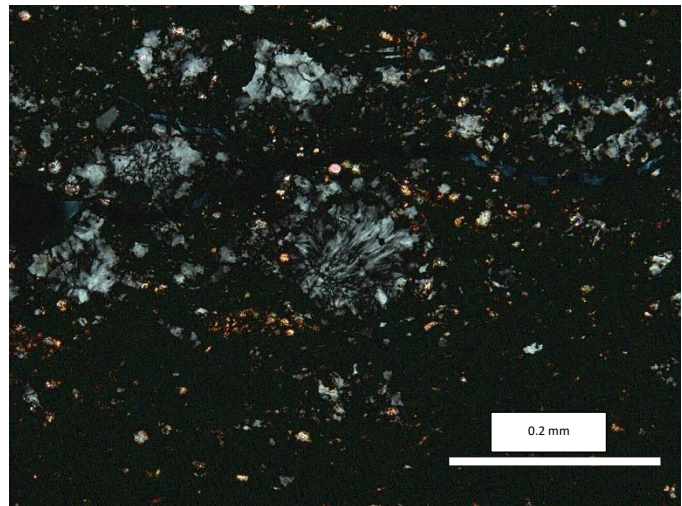
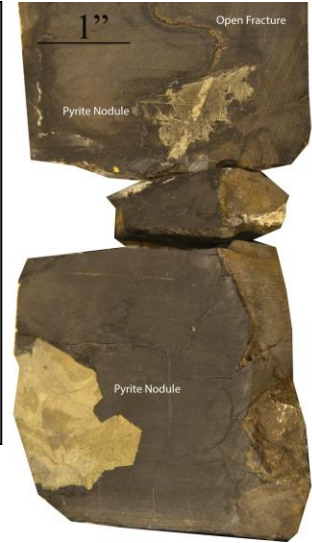




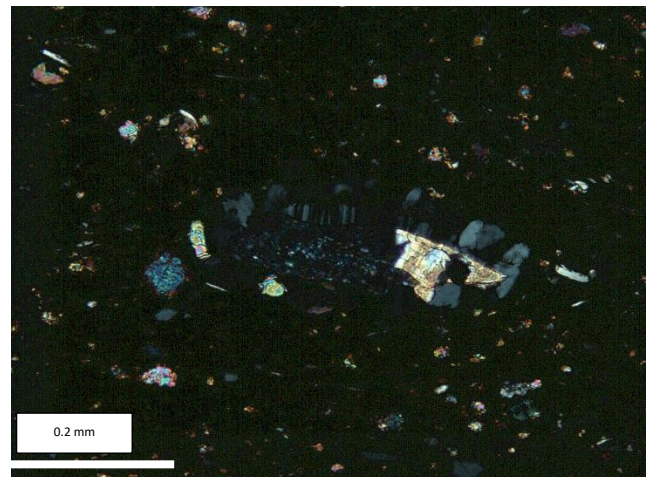
**Appendix A.** Williams 1H-7X core photographs of subsea depths 12,965 feet to 12,956 feet. Depth shallows from bottom right corner to top left corner at a thickness of 3 feet per column in core box. Light gray clay-rich bands, gypsum crystals, and marcasite nodules and nodule are evident.



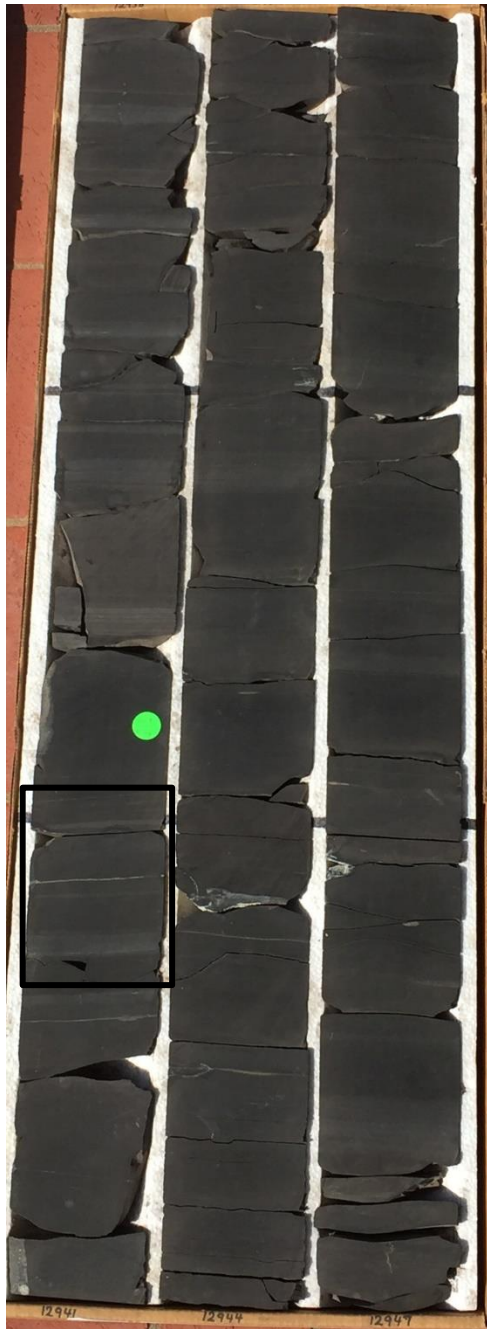
**Appendix A.** Williams 1H-7X core photographs of subsea depths 12,956 feet to 12,947 feet (left figure). Depth shallows from bottom right corner to top left corner at a thickness of 3 feet per column in core box. Upper right figure shows pyrite nodules and open fractures in the A-SM lithofacies. Depth of 12,951.5 feet to 12,951 feet.



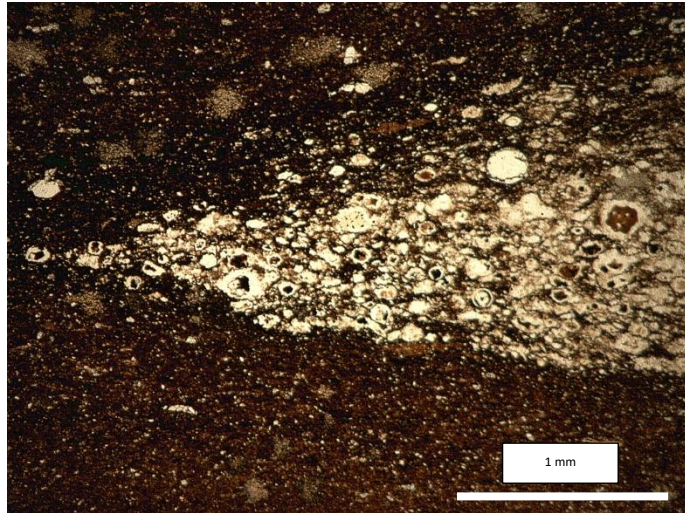
**Appendix A.** Possible radiolarians displaying undulatory chalcedony ranging in size from silt to very fine sand in XPL (middle right). Depth at 12,955.35 feet. Fine sand grain with surrounding silt size detrital quartz and plagioclase grains, also minor dolomite replacement occurs on fine sand grain (bottom right). Depth at 12,947.7 feet, XPL.







**Appendix A.** Williams 1H-7X core photographs of subsea depths 12,947 feet to 12,938 feet (left figure). Depth shallows from bottom right corner to top left corner at a thickness of 3 feet per column in core box. Upper right figure shows silica- and pyrite-rich laminae as well as a possible scour surface in the A-SM lithofacies. Depth of 12,940.5 feet to 12,940 feet.

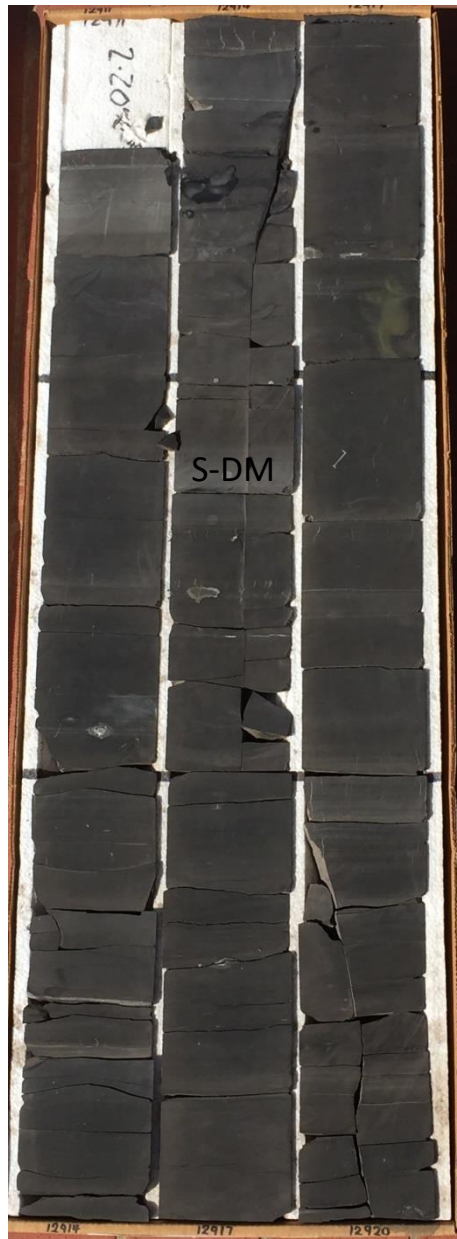


**Appendix A.** Williams 1H-7X core photographs of subsea depths 12,938 feet to 12,929 feet (left figure). Depth shallows from bottom right corner to top left corner at a thickness of 3 feet per column in core box. A cluster of silt to very fine sand-sized possible radiolarians surrounded in a clay-rich lithology in the A-SM lithofacies. Depth at 12,935 feet, PPL.



**Appendix A.** Williams 1H-7X core photographs of subsea depths 12,929 feet to 12,920 feet (middle figure). Depth shallows from bottom right corner to top left corner at a thickness of 3 feet per column in core box. Ripple mark near 12,924 feet.





**Appendix A.** Williams 1H-7X core photographs of subsea depths 12,920 feet to 12,911 feet (middle figure). Depth shallows from bottom right corner to top left corner at a thickness of 3 feet per column in core box. Thin interval of S-DM lithofacies occurs from 12,915.6 feet to 12,915.4 feet.



**Appendix A.** Williams 1H-7X core photographs of subsea depths 12,911 feet to 12,902 feet (middle figure). Depth shallows from bottom right corner to top left corner at a thickness of 3 feet per column in core box.



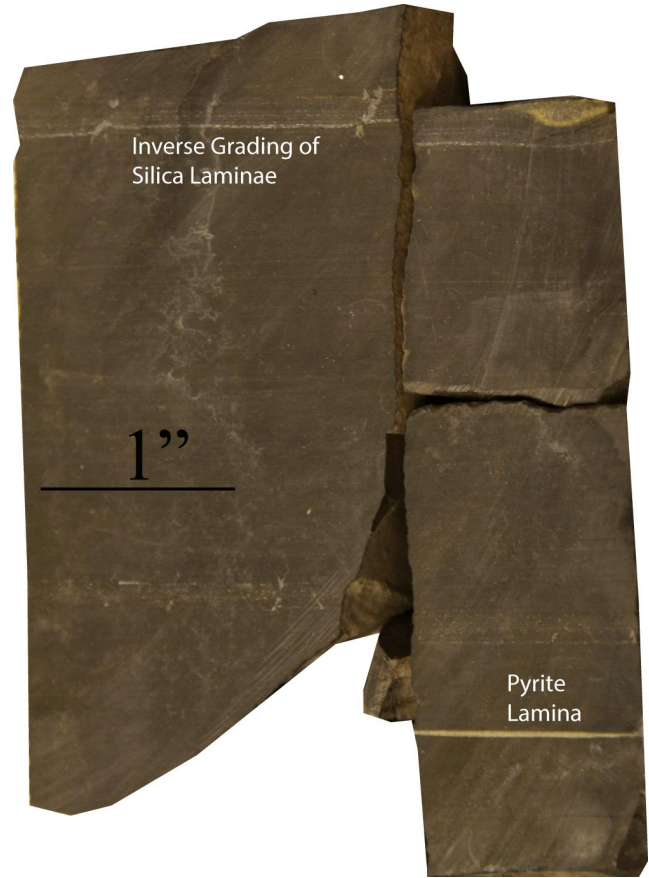
**Appendix A.** Williams 1H-7X core photographs of subsea depths 12,902 feet to 12,893 feet (middle figure). Depth shallows from bottom right corner to top left corner at a thickness of 3 feet per column in core box.



**Appendix A.** Williams 1H-7X core photographs of subsea depths 12,893 feet to 12,887 feet (left figure). Depth shallows from bottom right corner to top left corner at a thickness of 3 feet per column in core box. Inverse grading within silica-rich laminae in the A-SM lithofacies (upper right). Depth of 12,890.3 feet to 12,890 feet.

\*Only photograph available





**Appendix A.** Williams 1H-7X core photographs of subsea depths 12,887 feet to 12,878 feet (left figure). Depth shallows from bottom right corner to top left corner at a thickness of 3 feet per column in core box. Inverse grading within silica-rich laminae in the A-SM lithofacies (upper right). Depth of 12,884.3 feet to 12,884 feet.

\*Only photograph available



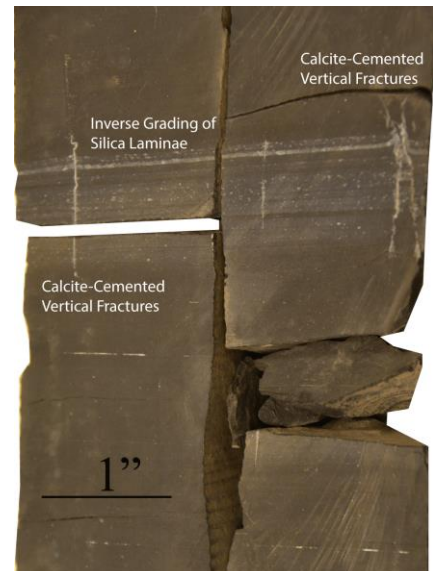
\*Only photograph available

**Appendix A.** Williams 1H-7X core photographs of subsea depths 12,878 feet to 12,869 feet (middle figure). Depth shallows from bottom right corner to top left corner at a thickness of 3 feet per column in core box. Thin S-DM lithofacies occurs from 12,876 feet 12,875 feet.



**Appendix A.** Williams 1H-7X core photographs of subsea depths 12,869 feet to 12,860 feet (left figure). Depth shallows from bottom right corner to top left corner at a thickness of 3 feet per column in core box. Pyrite laminae and inverse grading of silica-rich laminae occur from 12,865.8 feet to 12,865.4 feet in the A-SM lithofacies (upper right). Multiple silica-rich laminae containing calcite-cemented vertical fractures and inverse grading occurs from 12,862 feet to 12,861.7 feet in the SM lithofacies (bottom right).

**\*Only photograph available**



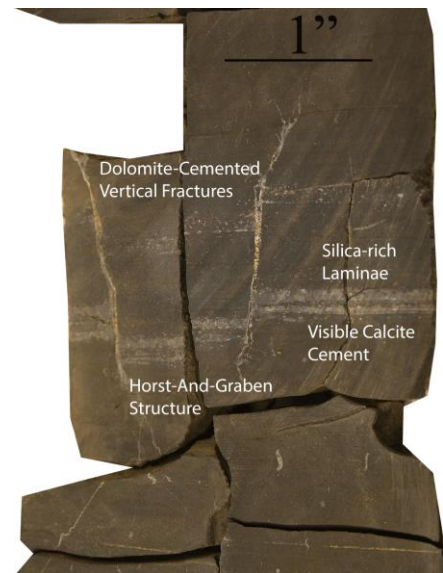
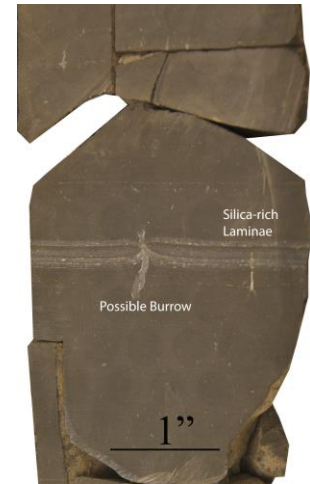




\*Only photograph available

**Appendix A.** Williams 1H-7X core photographs of subsea depths 12,860 feet to 12,851 feet (middle figure). Depth shallows from bottom right corner to top left corner at a thickness of 3 feet per column in core box.

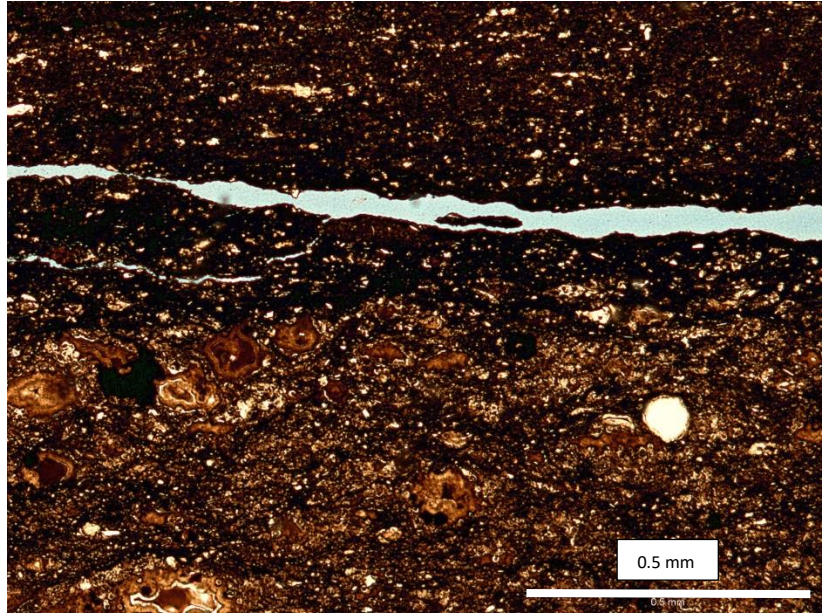




**Appendix A.** Williams 1H-7X core photographs of subsea depths 12,851 feet to 12,842 feet (left figure). Depth shallows from bottom right corner to top left corner at a thickness of 3 feet per column in core box. Possible burrow disrupting silica-rich laminae occurs from 12,849.6 feet to 12,849.4 feet in SM lithofacies (upper right). Two dolomite-cemented vertical fractures cause a horst and graben structure with silica-rich laminae. The silica-rich laminae also displays visible calcite cement. Image occurs from 12,846 feet to 12,845.7 feet (middle right).

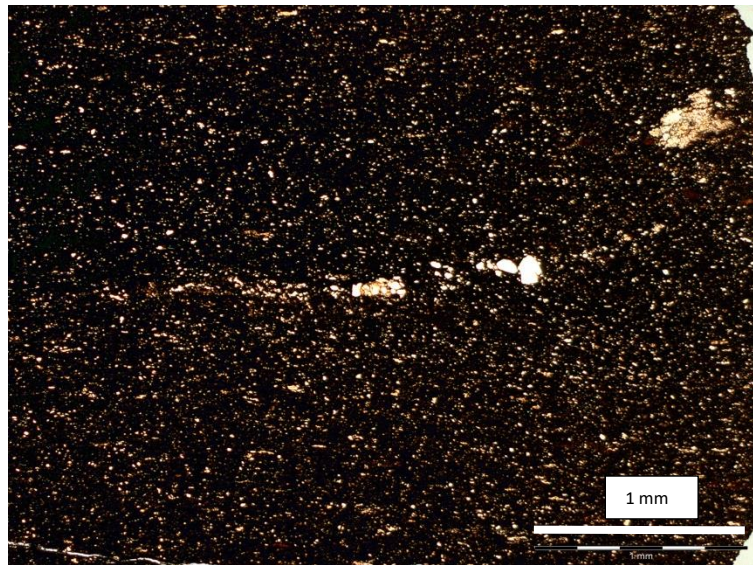


**Appendix A.** Williams 1H-7X core photographs of subsea depths 12,842 feet to 12,833 feet (middle figure). Depth shallows from bottom right corner to top left corner at a thickness of 3 feet per column in core box.

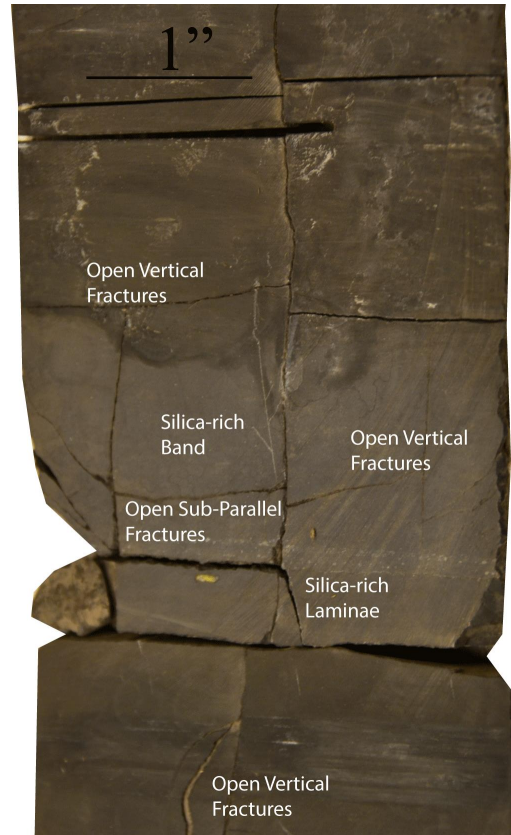


**Appendix A.** Williams 1H-7X core photographs of subsea depths 12,833 feet to 12,824 feet (left figure). Depth shallows from bottom right corner to top left corner at a thickness of 3 feet per column in core box. Possible silt-sized white radiolarian surrounded by tasmanites cysts that have been mineralized by phosphate occurs at 12,831.35 feet, PPL (upper right).





**Appendix A.** Williams 1H-7X core photographs of subsea depths 12,824 feet to 12,815 feet (left figure). Depth shallows from bottom right corner to top left corner at a thickness of 3 feet per column in core box. Detrital silt to sand-sized quartz grains with associated calcite cement in the upper right corner occurs at 12,815.3 feet, PPL (upper right).

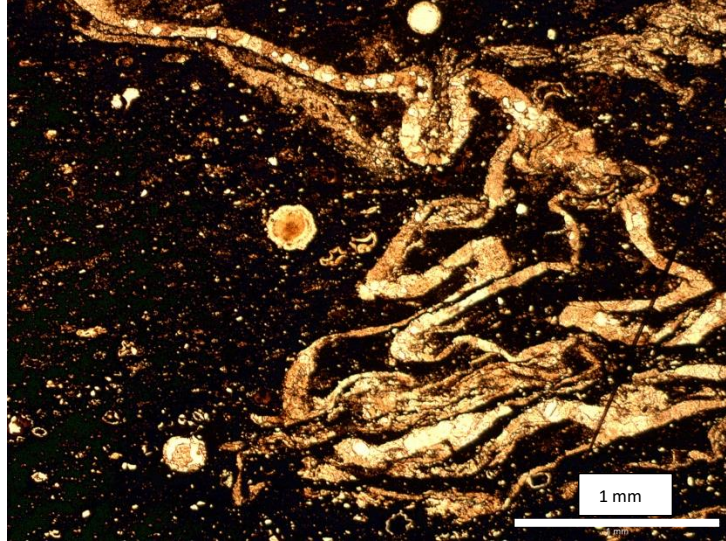


**Appendix A.** Williams 1H-7X core photographs of subsea depths 12,815 feet to 12,806 feet (left figure). Depth shallows from bottom right corner to top left corner at a thickness of 3 feet per column in core box. Silica-cemented band containing open vertical and sub-parallel fractures as well as silica-rich laminae occurs from 12,813.6 feet to 12,813.4 feet (upper right).



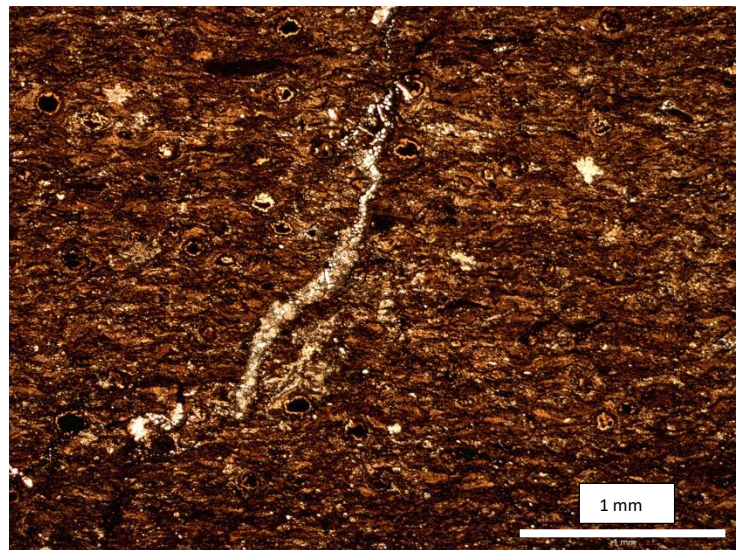
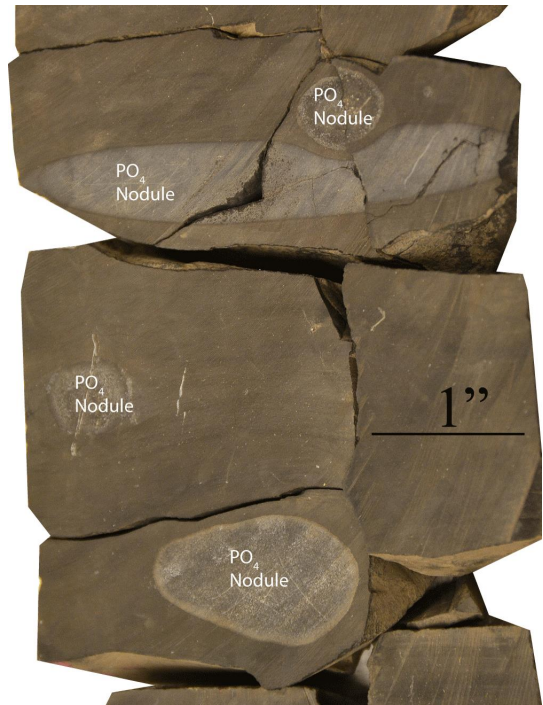
**Appendix A.** Williams 1H-7X core photographs of subsea depths 12,806 feet to 12,797 feet (middle figure). Depth shallows from bottom right corner to top left corner at a thickness of 3 feet per column in core box.





**Appendix A.** Williams 1H-7X core photographs of subsea depths 12,797 feet to 12,788 feet (left figure). Depth shallows from bottom right corner to top left corner at a thickness of 3 feet per column in core box. Calcite-cemented pygmatic fracture surrounded by very fine sand-sized possible radiolarians occurs at 12,791.1 feet, PPL (upper right).





**Appendix A.** Williams 1H-7X core photographs of subsea depths 12,797 feet to 12,788 feet (left figure). Depth shallows from bottom right corner to top left corner at a thickness of 3 feet per column in core box. Abundant phosphate nodules occurring from 12,785.6 feet to 12,785.4 feet (upper right). Calcite-cemented pygmatic fracture within phosphate nodule occurring at 12,783.35 feet, PPL (bottom right).





**Appendix A.** Williams 1H-7X core photographs of subsea depths 12,779 feet to 12,770 feet (middle figure). Depth shallows from bottom right corner to top left corner at a thickness of 3 feet per column in core box.



**Appendix A.** Williams 1H-7X core photographs of subsea depths 12,770 feet to 12,761 feet (middle figure). Depth shallows from bottom right corner to top left corner at a thickness of 3 feet per column in core box.



**Appendix A.** Williams 1H-7X core photographs of subsea depths 12,761 feet to 12,752 feet (middle figure). Depth shallows from bottom right corner to top left corner at a thickness of 3 feet per column in core box.



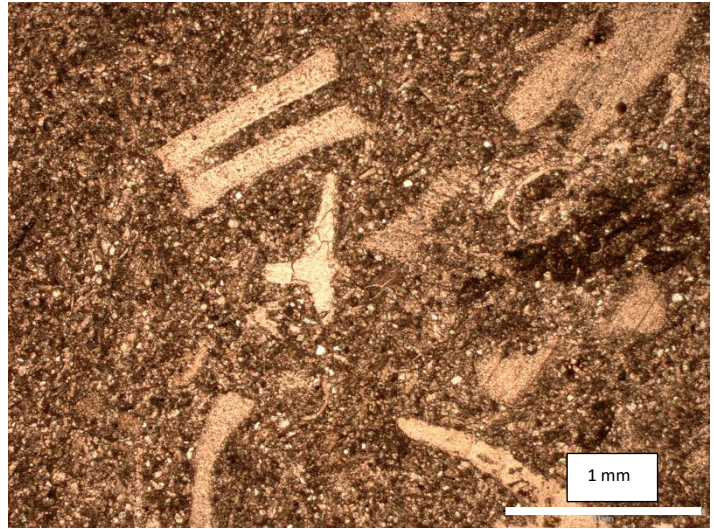
**Appendix A.** Williams 1H-7X core photographs of subsea depths 12,752 feet to 12,743 feet (middle figure). Depth shallows from bottom right corner to top left corner at a thickness of 3 feet per column in core box. Woodford/Caney contact occurs at 12,744.5 feet.



**Appendix A.** Williams 1H-7X core photographs of subsea depths 12,743 feet to 12,734 feet (left figure). Depth shallows from bottom right corner to top left corner at a thickness of 3 feet per column in core box. Caney Shale with bottom right corner consisting of a glauconitic zone.

Appendix B  
McDonald 2H-16E  
Core and Thin Section Photographs



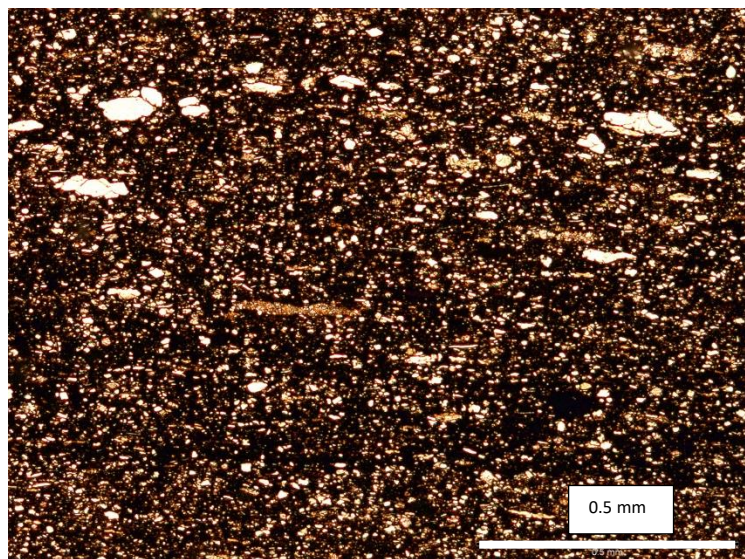
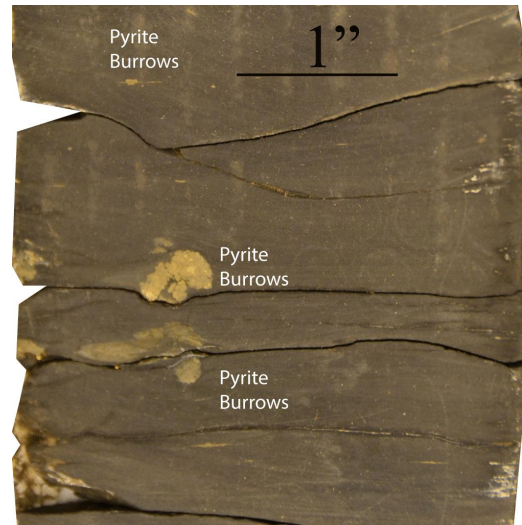


**Appendix B.** McDonald 2H-16E core photographs of subsea depths 6,427 feet to 6,418 feet (left figure). Depth shallows from bottom right corner to top left corner at a thickness of 3 feet per column in core box. Varying macrofossils such as ostracods and brachiopods occur at 6,428.55 feet, PPL (upper right).



**Appendix B.** McDonald 2H-16E core photographs of subsea depths 6,417.8 feet to 6,409 feet (middle figure). Depth shallows from bottom right corner to top left corner at a thickness of 3 feet per column in core box. Base of Woodford and AM lithofacies occurs at 6,417.8 feet.





**Appendix B.** McDonald 2H-16E core photographs of subsea depths 6,409 feet to 6,400 feet (left figure). Depth shallows from bottom right corner to top left corner at a thickness of 3 feet per column in core box. Abundant burrows mineralized by pyrite occur from 6,404.3 feet to 6,404 feet (upper right). Silt to sand-sized detrital quartz as well as clay-rich lenses occur at 6,401.85 feet, PPL (middle right).



**Appendix B.** McDonald 2H-16E core photographs of subsea depths 6,400 feet to 6,391 feet (middle figure). Depth shallows from bottom right corner to top left corner at a thickness of 3 feet per column in core box. SM lithofacies occurs from 6,395 feet to 6,391.5 feet and contains abundant silica-cemented bands.

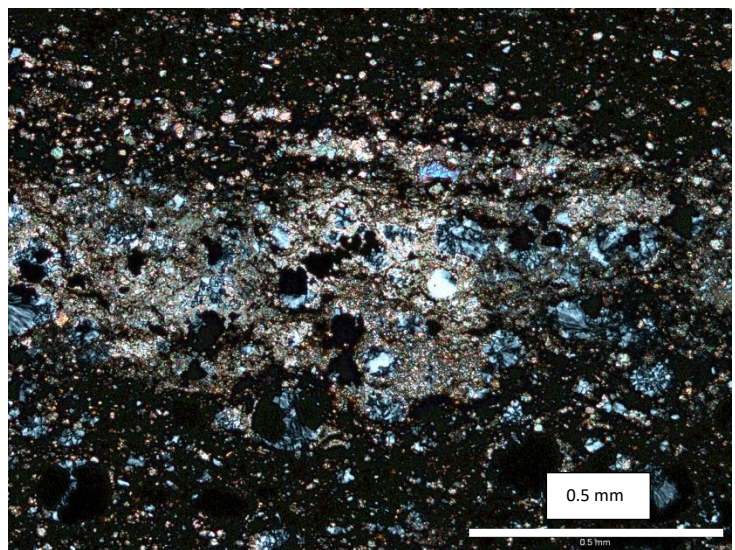
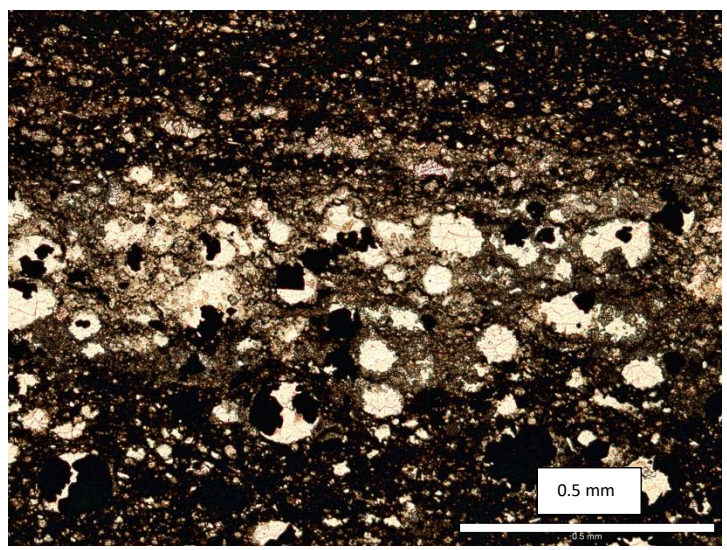


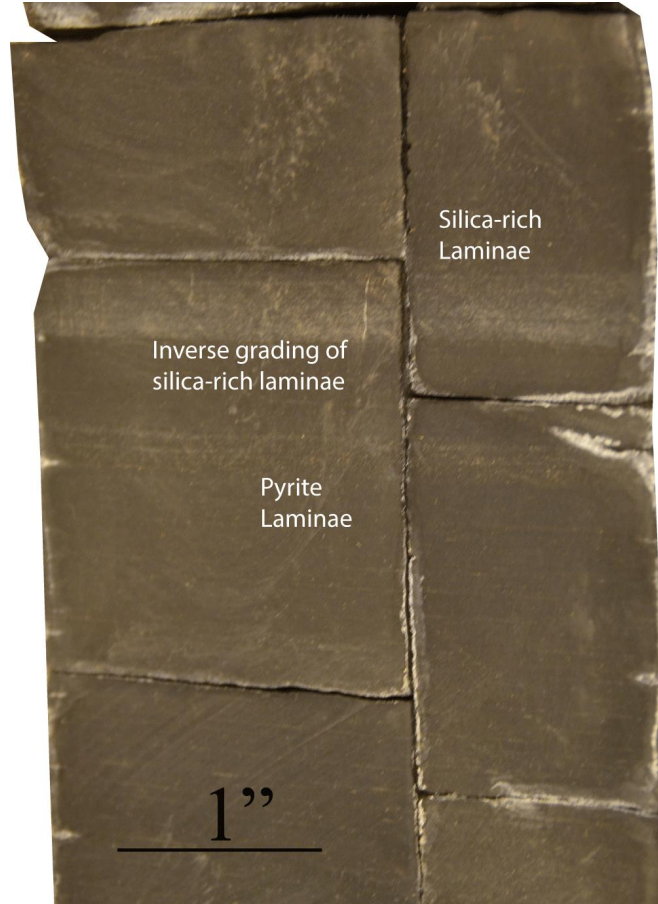
**Appendix B.** McDonald 2H-16E core photographs of subsea depths 6,391 feet to 6,382 feet (middle figure). Depth shallows from bottom right corner to top left corner at a thickness of 3 feet per column in core box. Base of A-SM lithofacies occurs at 6,381.9 feet.





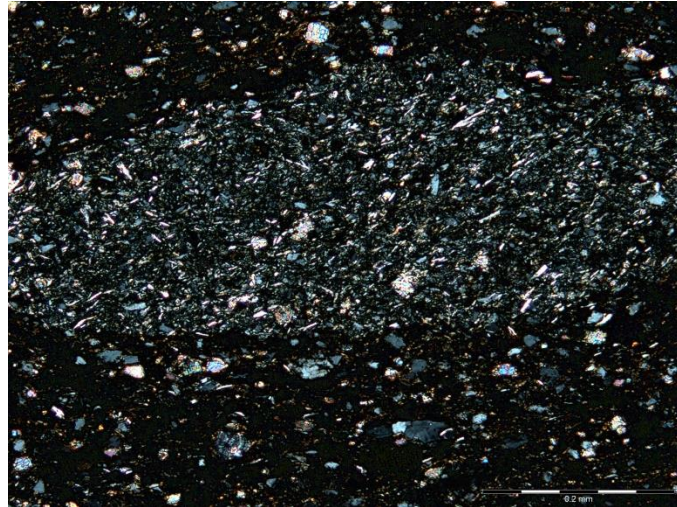
**Appendix B.** McDonald 2H-16E core photographs of subsea depths 6,381.9 feet to 6,373 feet (far left figure). Depth shallows from bottom right corner to top left corner at a thickness of 3 feet per column in core box. Pyrite burrows occur from 6,374.1 feet to 6,373.9 feet (left figure). PPL and XPL of silt to sand-sized possible radiolarians displaying undulatory chalcedony at 6,380.35 feet (bottom right).





**Appendix B.** McDonald 2H-16E core photographs of subsea depths 6,373 feet to 6,364 feet (left figure). Depth shallows from bottom right corner to top left corner at a thickness of 3 feet per column in core box. Evident inverse grading in silica-rich laminae and pyrite laminae occur from 6,364.6 to 6,364.4 feet (upper right).

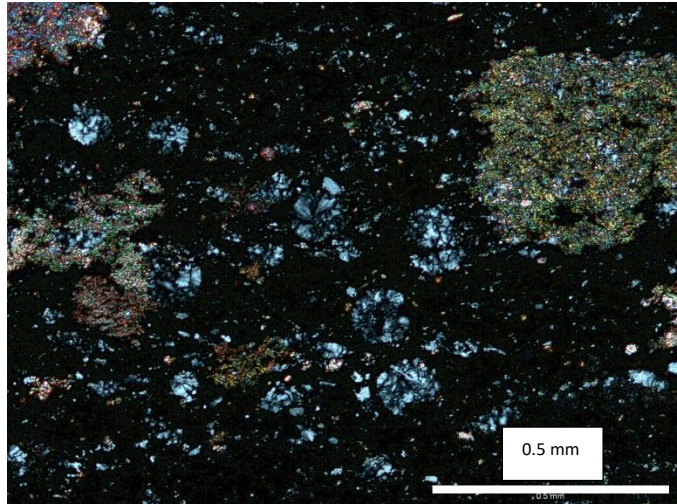




**Appendix B.** McDonald 2H-16E core photographs of subsea depths 6,364 feet to 6,355 feet (left figure). Depth shallows from bottom right corner to top left corner at a thickness of 3 feet per column in core box. Silt-sized detrital quartz lense surrounded by silt-sized detrital quartz and dolomite rhombs occurs at 6,360.2 feet, XPL (upper right).

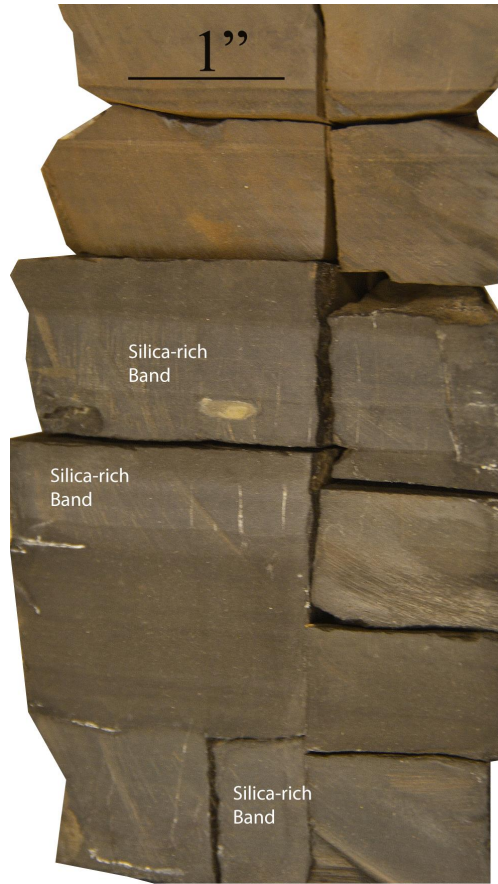


**Appendix B.** McDonald 2H-16E core photographs of subsea depths 6,355 feet to 6,346 feet (middle figure). Depth shallows from bottom right corner to top left corner at a thickness of 3 feet per column in core box.



**Appendix B.** McDonald 2H-16E core photographs of subsea depths 6,346 feet to 6,337 feet (left figure). Depth shallows from bottom right corner to top left corner at a thickness of 3 feet per column in core box. Silt to sand-sized possible radiolarians exhibiting chalcedony chert with associated calcite cement occurs at 6,340.65 feet, XPL (upper right).



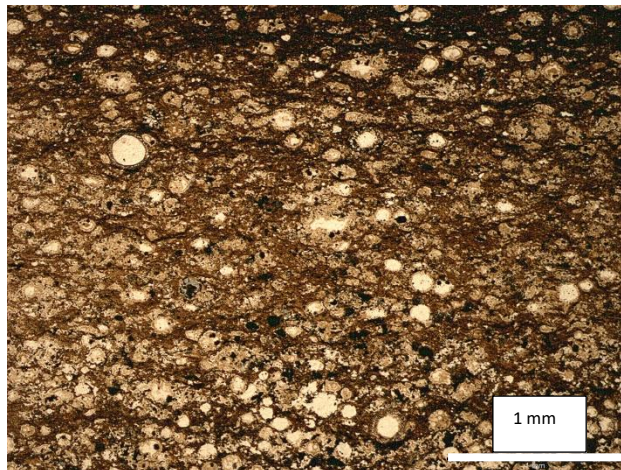


**Appendix B.** McDonald 2H-16E core photographs of subsea depths 6,337 feet to 6,328 feet (left figure). Base of SM lithofacies occurs at 6,337 feet. Depth shallows from bottom right corner to top left corner at a thickness of 3 feet per column in core box. Abundant silica-cemented bands containing numerous calcite-cemented ptymatic fractures occur from 6,331.8 feet to 6,331.5 feet (upper right).



**Appendix B.** McDonald 2H-16E core photographs of subsea depths 6,328 feet to 6,319 feet (middle figure). Depth shallows from bottom right corner to top left corner at a thickness of 3 feet per column in core box. Base of A-SM occurs at 6,325 feet.





**Appendix B.** McDonald 2H-16E core photographs of subsea depths 6,319 feet to 6,310 feet (left figure). Depth shallows from bottom right corner to top left corner at a thickness of 3 feet per column in core box. Silica-rich laminae containing a micro fault occurs from 6,312.5 feet to 6,312.4 feet (upper right). Abundant silt to sand-sized possible radiolarians occur at 6,311 feet, PPL (middle right).



**Appendix B.** McDonald 2H-16E core photographs of subsea depths 6,310 feet to 6,301 feet (left figure). Base of SM lithofacies occurs at 6,306 feet. Depth shallows from bottom right corner to top left corner at a thickness of 3 feet per column in core box. Silica-cemented bands containing calcite-cemented vertical fractures and visible calcite cement and a pyrite nodule occur from 6,312.6 feet to 6,312.4 feet (upper right).





**Appendix B.** McDonald 2H-16E core photographs of subsea depths 6,301 feet to 6,292 feet (middle figure). Depth shallows from bottom right corner to top left corner at a thickness of 3 feet per column in core box.



**Appendix B.** McDonald 2H-16E core photographs of subsea depths 6,291.4 feet to 6,286 feet (middle figure). Depth shallows from bottom right corner to top left corner at a thickness of 3 feet per column in core box.

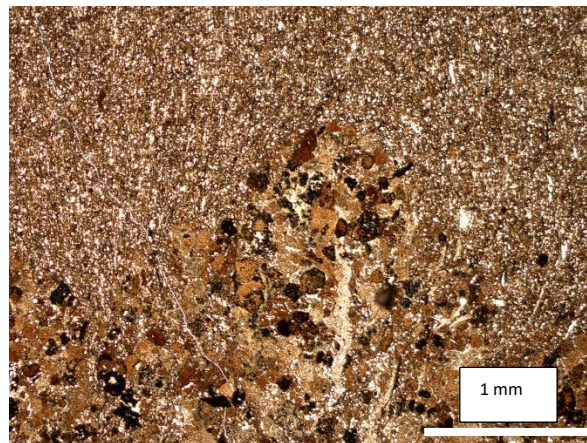




**Appendix B.** McDonald 2H-16E core photographs of subsea depths 6,286 feet to 6,277 feet (middle figure). Depth shallows from bottom right corner to top left corner at a thickness of 3 feet per column in core box.



**Appendix B.** McDonald 2H-16E core photographs of subsea depths 6,277 feet to 6,268 feet (left figure). Depth shallows from bottom right corner to top left corner at a thickness of 3 feet per column in core box. Evident burrowing occurs within silica- and pyrite-rich laminae from 6,274.4 feet to 6,274 feet (upper right).



**Appendix B.** McDonald 2H-16E core photographs of subsea depths 6,268 feet to 6,259 feet (left figure). Depth shallows from bottom right corner to top left corner at a thickness of 3 feet per column in core box. The base of the A-SM lithofacies occurs at 6,264 feet and the Woodford/Caney contact occurs at 6,260.9 feet. Silica clasts containing open and calcite-cemented fractures occur from 6,266 feet to 6,265.7 feet (upper right). A contact between a clay-rich interval and a phosphate-rich interval occurs at 6,262.95 feet, PPL (middle right).





**Appendix B.** McDonald 2H-16E core photographs of subsea depths 6,259 feet to 6,250 feet (middle figure). Depth shallows from bottom right corner to top left corner at a thickness of 3 feet per column in core box. A burrowed, glauconitic zone occurs in the lower third of the core box within the Caney Shale.

## Williams 1H-7X Core Descriptions

### *Box 4 of 21*

**12,734-12,743:** Bioturbated massive, medium gray (N5) mudstone transitioning to medium dark gray (N4) mudstone with deeper depths. At 12,742.8 ft, a 4 cm dark gray glauconitic zone exists; beneath the glauconitic zone is a light gray (N7) fissile 4 cm interval (12,742.9-12,743 ft).

### *Box 5 of 21*

**12,743-12,744:** Massive, poorly-laminated phosphate-rich interval in light gray (N7) mudstone. Bottom 2/3 of interval is missing

**12,744-12,745:** 3" of light gray (N7) phosphatic-rich interval at 12,744. **WDFD/Caney Contact at 12,744.25** with massive grayish black (N2) naturally fractured (3") interval beneath. Fine grained disseminated pyrite grains and laminae are visible as well as a 3mm medium grained carbonate band at 12,745.

**12,745-12,746:** Thin 1" laminated grayish black interval at 12,745 ft. Interval is mostly massive, grayish black with natural fractures splaying from a silica-cemented zone at 12,745.6 ft. 1" pyrite nodule is present at 12,745.5 ft.

**12,746-12,747:** Massive, grayish black with two pyrite nodules at base (12,747). Small (5mm) ptygmatic calcite-filled fractures exist at the top of interval (12,746).

**12,747-12,748:** Broken up grayish black mudstone

**12,748-12,749:** Broken-up, laminated grayish black mudstone from 12,748 to 12,748.8 ft. Coarse 5mm laminations are common in top interval. Massive silica-cemented zone from 12,748.8 to 12,749 feet

**12,749-12,750:** Grayish black somewhat laminated mudstone with thin (3 mm) carbonate-rich laminae near 12,749. Calcite filled fractures splay from the carbonate-rich zone. Coarse 1" laminations are found throughout this interval.

**12,750-12,751:** Grayish black massive mudstone exists from 12,750-12,750.8 feet. Large silica-cemented zones (4-5") occur at 12,750.2 & 12,750.6 containing natural and calcite filled fractures. The bottom interval is a laminated grayish black mudstone (12,750.8-12,751).

**12,751-12,752:** Grayish black somewhat laminated mudstone exists from 12,751 to 12,751.3 & 12,751.8 to 12,752 feet. A large silica cemented zone is present from 12,751.3-12,751.8 containing 1" vertical calcite fractures.

***Box 6 of 21***

**12,752-12,753:** Grayish black massive mudstone with 1" phosphate nodule at 12,752 feet. Large silica cemented zone from 12,752.6-12,753 contains 5" long natural fractures.

**12,753-12,754:** Grayish black massive mudstone contains phosphate nodules at 12,753.3 (0.5"x2") and 12,753.6 feet (2 cm x 2 cm). Silica cemented zone at 12,753.7 to 12,754 contains three 2.5" long natural fractures.

**12,754-12,755:** Grayish black massive mudstone with phosphate nodules at 12,754.7, 12,754.9, and 12,755.

**12,755-12,756:** Grayish black massive mudstone from top of interval to 12,755.4 feet. Thin, faint 1 to 6 mm silica laminations occur from 12,755.4-12,755.6 feet.

**12,756-12,757:** Grayish black massive mudstone with silica-cemented zone from 12,756.2-12,756.5 containing a 0.5"x2" phosphate nodule. A 1" very finely laminated interval with calcareous laminations occurs from 12,756.5-12,756.6 feet. Mudstone becomes massive with 2" long calcite fracture within silica cemented zone at 12,756.6-12,756.8 feet. Thin silica-rich laminations occur after massive interval until 12,757 feet.

**12,757-12,758:** Grayish black massive mudstone containing four phosphate nodules at 12,757.3 (1x1 cm), 12,757.6 (1x1 cm), 12,757.7 (1x1 cm), and 12,757.8 (2.5x2 cm).

**12,758-12,759:** Grayish black somewhat laminated mudstone with laminations occurring greater than or equal to 3 cm apart.

**12,759-12,760:** Grayish black massive mudstone with phosphate nodules at 12,759.4 (1x5 cm), 12,759.5 (1x4 cm), and 12,759.8 (1x4 cm). Silica clasts are present at 12,759.4 (1x4 cm) and 12,759.9 (1x2 cm) feet. Thick carbonate lamina (1 cm) is present at 12,759.5 feet and contains numerous calcite-filled ptigmatic and vertical fractures (5 mm).

**12,760-12,761:** Grayish black massive mudstone (12,760-12,760.6) containing phosphate nodules (5x1 & 5x2 cm) at 12,760.5 feet. A carbonate rich band at 12,760 contains two ptigmatic calcite fractures (1 cm). Thin 1 mm pyrite laminations occur from 12,760.6-12,761 and are separated by at least three inches between each lamination and contains numerous vertical (1.5") calcite filled fractures splaying off the laminations.

***Box 7 of 21***

**12,761-12,762:** Grayish black poorly laminated mudstone from 12,761-12,761.5 containing one 2mm silica-rich laminae at 12,761.1 with small laminae bound calcite ptigmatic fractures.

Grayish black mudstone with silica-rich laminations (~2-5 mm) usually separated by ~1/2" occur



from 12,761.5-12,762 containing vertical calcite filled fractures (2 mm to 1"); a possible silica clast with recrystallized pyrite around the edges occurs at 12,761.9 feet.

**12,762-12,763:** A large silica clast occurs from 12,762-12,762.4 feet containing pygmatic and vertical calcite filled fractures ranging from a few millimeters to 2" long. Grayish black mudstone with 1 mm laminations of pyrite and silica separated by ~1/2" occur from 12,762-12,763. A possible nodule with recrystallized pyrite surrounding the edges occurs at 12,762.9 feet.

**12,763-12,764:** A silica cemented zone occurs from 12,763-12,763.3 feet containing small very fine grained disseminated pyrite and minor vertical calcite filled fractures (<5 mm). Grayish black mudstone with pyrite (~1 mm) and silica (1-7 mm) laminations occur from 12,763.3-12,764 containing small (<3 mm) calcite filled fractures and separated by ~1/2". Small disseminated pyrite grains (<1 mm) are evident in the laminated mudstone interval.

**12,764-12,765:** Grayish black mudstone with pyrite (1 mm) and silica (1 mm) rich laminations occur from 12,764-12,764.4 containing vertical calcite fractures (4 mm to 1") and separated usually by ~1". A silica cemented zone occurs from 12,764.4 to 12,764.6 feet and contains small disseminated pyrite grains and vertical calcite fractures (~1 mm). Silica (3 mm) and pyrite (1 mm) laminations occur in the grayish black mudstone from 12,764.6-12,765 feet and contain small calcite fractures that are bounded by the silica-rich laminated intervals.

**12,765-12,766:** Grayish black somewhat laminated mudstone with 1 cm fine-grained quartz rich interval at 12,765.1 feet. Pyrite (1 mm) and silica (2-3 mm) laminations occur throughout the interval with 1/2-1" of separation between the laminations. A small nodule with recrystallized pyrite around the edges occurs at 12,765.9 feet and has a small pyrite filled fracture (3 mm) splaying off the edge of the pyrite ring.

**12,766-12,767:** A silica cemented zone occurs from 12,766-12,766.2 containing 2" vertical calcite fractures. Grayish black mudstone with 1 mm pyrite laminations separated by an average of 1/2" occurs from 12,766.2-12,766.6. A highly fractured silica cemented zone occurs from 12,766.6-12,766.9 feet and contains calcite filled fractures ranging in size from a few millimeters to 2". A bundle of silt-sized carbonate grains occurs at the top of the silica cemented zone at 12,766.6 feet. Grayish black mudstone with 1 mm pyrite laminations with an average separation of 1" occur from 12,766.6-12,767.

**12,767-12,768:** Grayish black mudstone with silica (1-3 mm) and pyrite (1 mm) laminations separated by ~1/2". Silica-rich laminations commonly have vertical and pygmatic calcite fractures (1 mm to 2") that either are limited to the silica cemented lamination or splay from the silica-rich interval.

**12,768-12,769:** Grayish black mudstone with low angle silica (5 mm to 1 cm) and pyrite (1 mm) somewhat laminations separated by ~1/2". The dark silica cemented laminations near the top of

the interval contain numerous vertical and ptymatic calcite fractures (5 mm to 1 cm) are limited to the silica cemented laminated zones. Silica-rich laminations (1-2 mm) commonly experience longer vertical calcite fractures (1-4") that splay from the thinner laminations. Marcasite nodules occur at the top of the interval (12,768-12,768.1). A phosphate nodule (1"x1") occurs at 12,768.6 feet and has carbonate grains encrusted around the edges of the nodule.

**12,769-12,770:** Grayish black somewhat laminated mudstone containing pyrite (1 mm), silica (2 mm), and carbonate (3 mm) laminations. Calcite fractures (1-3 mm) are limited to the silica and carbonate-rich laminations that occur within this interval.

### *Box 8 of 21*

**12,770-12,771:** Grayish black somewhat laminated mudstone containing numerous pyrite (1 mm) laminations that occur throughout the interval and separated by ~1/2". Silica-cemented laminations (1-3 mm) occur near 12,770.7 feet and contain small vertical calcite fractures bound within the cemented laminations. Carbonate-rich laminations (2 mm) and disseminated silt-sized grains occur near the top of the interval from 12,770-12,770.3 feet.

**12,771-12,772:** Grayish black somewhat laminated mudstone with minor, thin pyrite laminations (1 mm) from 12,771-12,771.4. A poorly-laminated grayish black mudstone exists from 12,771.4-12,771.6. Minor pyrite laminations (1 mm) exist from 12,771.6-12,772 with at least 1" separation between laminations.

**12,772-12,773:** Grayish black somewhat laminated mudstone with laminations of pyrite (1 mm) and carbonates (4 mm to 1") that are separated by an average of 1" between laminations. A coarsening upward 1" carbonate laminations is present at 12,772.1 and contains a 4" calcite filled fracture splaying from the lamination. The silt-sized carbonate laminations also occur at 12,772.7 and 12,772.9, with the latter lamination showing a fining upward sequence.

**12,773-12,774:** A grayish black somewhat laminated mudstone with thin 1/2" separated laminations of pyrite (1 mm) and carbonate (1") occurs from 12,773-12,773.2 feet. A massive, poorly-laminated mudstone exists from 12,773.2-12,773.4 feet. The mudstone interval becomes laminated from 12,773.4-12,774 feet containing thin pyrite laminations (1 mm) that are separated by at least 1" and a coarsening upward 1/2" carbonate lamination at the base of the interval.

**12,774-12,775:** Grayish black somewhat laminated mudstone with thin pyrite laminations (1 mm), separated by at least 1" between laminations. Two silica cemented laminated zones (2 mm) occur at 12,774.9 feet that are separated by 1/2" and contain vertical calcite fractures limited to the height of the silica cemented zone.

**12,775-12,776:** Grayish black somewhat laminated mudstone with laminations of pyrite (1 mm), silica cements (2-7 mm), and carbonate (1 mm to 1"). A pyrite lamination (1 mm) at the top of the interval contains a 1" calcite filled fracture that splays from the pyritic laminae. Silica

cemented laminations at 12,775.2, 12,775.4, 12,775.5, 12,775.6, and 12,775.7 contain pygmatic and vertical calcite fractures limited to the extent of the cemented zones. Carbonate laminations at 12,775.8 and 12,775.9 contains long vertical calcite fractures (1"-2") that splay from the laminated intervals. The lowest carbonate lamination at 12,775.9 also shows a coarsening and fining upward sequence.

**12,776-12,777:** Grayish black somewhat laminated mudstone with laminations of pyrite (1 mm) that are separated by at least 2".

**12,777-12,778:** Grayish black somewhat laminated mudstone with laminations of silica cemented bands (1/2") and carbonate-rich laminae (4-5 mm). The carbonate-rich laminae occur at 12,777.3 and 12,777.4 containing vertical millimeter-sized calcite fractures that splay off the laminae. The silica cemented bands occur at 12,777.5 and 12,777.9 feet and contain fractures bound to the height of the cemented zones. A fractured zone at 12,777.5-12,777.7 contains long vertical calcite fractures that are 1.5" in length.

**12,778-12,779:** Grayish black somewhat laminated mudstone with laminations of carbonate (1/2") occurring at 12,778.2 feet. A fractures zone at the base of the interval contains 1" vertical calcite fractures.

### ***Box 9 of 21***

**12,779-12780:** Grayish black somewhat laminated mudstone

**12,780-12,781:** Grayish black somewhat laminated mudstone with a calcite fracture at 12,780.1 feet and a 1"x1" circular phosphate nodule at 12,780.8 feet.

**12,781-12,782:** Grayish black somewhat laminated mudstone with a fractured zone at 12,781.6 feet containing 1" calcite filled vertical fractures. The lower interval from 12,781.7-12,782 feet contains silt-sized carbonate laminae (1.5") and long vertical and horizontal calcite fractures ranging from a few millimeters to 4".

**12,782-12,783:** Grayish black somewhat laminated mudstone with silica clasts (1/2"x1") at 12,782.6 feet containing long vertical calcite fractures (2") that at times fracture through the silica clasts.

**12,783-12,784:** Grayish black somewhat laminated mudstone with phosphate nodules (1/2"x1") at 12,783.6, 12,783.8, and 12,783.9 feet. The phosphate nodules are commonly surrounded by intervals that are highly fractured with vertical calcite fractures ranging from a few millimeters long to an inch.

**12,784-12,785:** Grayish black somewhat laminated mudstone with silica cemented bands at 12,784.5 and 12,784.6 feet. The bands contain vertical and pygmatic calcite fractures that are usually bound to the cemented zone.

**12,785-12,786:** Grayish black somewhat laminated mudstone containing phosphate nodules at 12,785.5, 12,785.6, and 12,785.8 feet that ranges from ½” to 2”. Phosphate lamina is also present at 12,785.5 that is 1/2”x3”.

**12,786-12,787:** Grayish black somewhat laminated mudstone with silica clasts (1/2”x1”) at 12,786.1 feet. Phosphate nodule is present at 12,786.2 feet and is 1”x1”.

**12,787-12,788:** Grayish black somewhat laminated mudstone with a silica-rich laminated (1/2”) at 12,787.1 feet. Two phosphate nodules (1/4” & ½”) occur at 12,787.6 feet. A light gray fissile shale interval is present from 12,787.7-12,787.9 feet.

### ***Box 10 of 21***

**12,788-12,789:** Grayish black somewhat laminated mudstone two large phosphate nodules at 12,788.4-12,788.6 feet. The upper nodule is 1”x1” and contains small vertical millimeter-sized calcite fractures on the bottom edge of the nodule. The lower nodule is ½” x 3” and is reverse faulted with a 3 mm displacement. Two carbonate-rich laminae are present at 12,788.9 feet.

**12,789-12,790:** Grayish black somewhat laminated mudstone with laminations of silica-rich and carbonate-rich laminae. Silica-rich lamina (3 mm) exists at 12,789.7 feet and contains small 3 mm sized vertical calcite fractures. Pyrite laminations occur throughout the interval as well and laminations are separated by ½”. A carbonate-rich lamina (1 mm) exists at 12,789.9 feet and contains small 1 mm sized calcite vertical fractures.

**12,790-12,791:** Grayish black somewhat laminated mudstone with laminations of carbonate-rich intervals present at 12,790.1, 12,790.2, 12790.4, 12,790.6, and 12,790.9 feet and ranges in size from 1 to 3 mm. Small vertical calcite fractures (1-3 mm) commonly splay from the carbonate-rich intervals. The carbonate-rich lamina at 12,790.9 exhibits a fining upward sequence.

**12,791-12,792:** Grayish black somewhat laminated mudstone with carbonate-rich intervals (1-3 mm) separated by 6 mm between laminations. The carbonate-rich intervals are highly fractured containing numerous small pygmatic calcite fractures (2-4 mm) splaying off the carbonate intervals.

**12,792-12,793:** Grayish black somewhat laminated mudstone with pyrite (1 mm) and carbonate-rich laminations. Carbonate-rich lamina (2 mm) at 12,792.1 contains 5 mm vertical calcite fractures that splay off the carbonate-rich interval. Carbonate rich intervals at 12,792.8 and 12,792.9 feet also contain millimeter-sized vertical calcite fractures.

**12,793-12,794:** Grayish black somewhat laminated mudstone with pyrite (1 mm) and carbonate-rich laminations (2-4 mm). Carbonate-rich interval (4 mm) at 12,793.4 feet shows a fining upward sequence and contains a ½” vertical calcite fracture splaying off the interval.

**12,794-12,795:** Grayish black somewhat laminated mudstone with minor pyrite (1 mm) and carbonate-rich laminations (3 mm). Silt-sized carbonate lamination is present at 12,794.6 feet.

**12,795-12,796:** Grayish black somewhat laminated mudstone with minor carbonate-rich laminations (3-5 mm). Laminations are separated by an average of 2”.

**12,796-12,797:** Grayish black somewhat laminated mudstone with carbonate-rich laminations (1-5 mm) separated by at least 4”. Carbonate-rich interval at 12,796.3 feet shows silt-sized grains exhibiting a fining upward sequence.

### ***Box 11 of 21***

**12,797-12,798:** Grayish black somewhat laminated mudstone with two carbonate-rich lamina intervals at 12,797.8 (3 mm) and 12,797.9 (3 mm) feet.

**12,798-12,799:** Grayish black laminated mudstone with a 1 mm pyrite lamina at 12,798.6 feet and a 3 mm carbonate-rich interval at 12,798.7 feet containing small millimeter-sized vertical calcite fractures splaying off the interval. A finely laminated interval exists from 12,798.7-12,799 feet.

**12,799-12,800:** Grayish black somewhat laminated mudstone with a very fine laminated interval from 12,799-12,799.1 feet. A 4 mm carbonate-rich interval is present at 12,799.2 feet and a 1 mm pyrite lamina exists at 12,799.9 feet.

**12,800-12,801:** Grayish black somewhat laminated mudstone with a 1 mm pyrite lamina at 12,800.1 feet and two carbonate-rich laminations at 12,800.2 and 12,800.3 that are 1-3 mm and contain two ½” vertical calcite fractures.

**12,801-12,802:** Grayish black laminated mudstone with silica cemented bands and silica-rich laminae separated by at least 2”. A 3 mm silica cemented band at 12,801.7 feet contains numerous vertical and pygmatic calcite fractures limited to the cemented interval. A 1” silica-rich lamination at 12,801.9 feet contains very fine grains with vertical calcite fractures (1”).

**12,802-12,803:** Grayish black somewhat laminated mudstone with pyrite (1 mm) and carbonate-rich laminae from 12,802-12,802.5 feet. Carbonate-rich interval (2 mm) at 12,802 feet shows a fining upward sequence with silt-sized grains and contains a 4 mm vertical calcite fracture. A silica cemented zone at 12,802.5 exhibits a possible ripple mark and contains minor millimeter-sized vertical calcite fractures.

**12,803-12,804:** Grayish black somewhat laminated mudstone with two 1 mm pyrite laminations at 12,803.1 feet.

**12,804-12,805:** Grayish black somewhat laminated mudstone with 1 mm pyrite laminations separated by 2” throughout interval.

**12,805-12,806:** Grayish black somewhat laminated mudstone with 1 mm pyrite lamina present at 12,805.5 feet.

***Box 12 of 21***

**12,806-12,807:** Grayish black somewhat laminated mudstone with laminations of pyrite (1 mm) and carbonate-rich (1 mm-1/2") laminae. Carbonate-rich intervals at 12,806.1 and 12806.2 contain 3 mm to 1" vertical calcite fractures that splay off the carbonate-rich intervals.

**12,807-12,808:** Grayish black somewhat laminated mudstone with silica-rich (1 mm) and carbonate-rich (2 mm) intervals. A carbonate-rich interval exists at the top of the section with three 3 mm vertical calcite fractures underlying the carbonate interval. Three silica-rich 1 mm laminations occur at 12,807.4 feet.

**12,808-12,809:** Grayish black somewhat laminated mudstone contains carbonate-rich (1-3 mm), silica-rich (1 mm), and pyrite (1 mm) laminations. Disseminated pyrite grains occur at 12,808.7 feet. Fractured intervals associated with the carbonate-rich zones occur near the top of the interval from 12,808-12,808.4 feet and show ptymatic to vertical calcite fractures (2 mm-1/2"). A silica-rich lamina at 12,808.8 feet contains small 1 mm vertical calcite fractures. A finely laminated zone occurs at 12,808.9 feet and then transitions into a bottom 1" of disseminated carbonate grains that exhibit fining upward sequences as well as calcite filled fractures.

**12,809-12,810:** Grayish black somewhat laminated mudstone containing pyrite (1 mm) and carbonate-rich laminae. A carbonate-rich interval at 12,809.3 feet exhibits a coarsening and fining upward sequence. A silica cemented zone at 12,809.9 feet is massive and contains one 3 mm vertical calcite filled fracture.

**12,810-12,811:** Grayish black somewhat laminated mudstone containing 1/2" separated laminations of 1 mm pyrite, as well as two 7 mm carbonate-rich intervals at 12,810.9 feet that are separated by 1/2".

**12,811-12,812:** Grayish black somewhat laminated mudstone containing pyrite (1 mm) and carbonate-rich (1 mm-5 mm) laminations. Carbonate-rich intervals at 12,811, 12,811.7, and 12,811.9 feet contain millimeter-sized vertical calcite filled fractures.

**12,812-12,813:** Grayish black somewhat laminated mudstone containing disseminated carbonate and pyrite grains near the top of the interval. Disseminated carbonate grains are also present at 12,812.6 and 12,812.9 feet and contain ptymatic (1-3 mm) calcite fractures.

**12,813-12,814:** Grayish black somewhat laminated mudstone from 12,813-12,813.5 feet containing carbonate-rich (1 mm) and pyrite (1 mm) laminae. A massive silica cemented zone occurs from 12,813.5-12,813.7 and contains a 1/2" vertical calcite fracture as well as a 2 mm carbonate-rich lamina at the base of the cemented zone. A somewhat laminated mudstone is present from 12,813.7-12,814 feet with 1 mm pyrite laminae.



**12,814-12,815:** Grayish black somewhat laminated mudstone with 1 mm pyrite laminae and disseminated pyrite grains. Vertical calcite fractures (1 mm-1/2") exist between pyrite laminations at 12,814.1 and 12,814.9 feet.

***Box 13 of 21***

**12,815-12,816:** Grayish black somewhat laminated mudstone with 1 mm pyrite laminae at the top and base of the interval, with the latter containing one 3 mm vertical calcite fracture.

**12,816-12,817:** Grayish black somewhat laminated mudstone with disseminated pyrite grains near the top of the interval and vertical calcite fractures splaying off a carbonate-rich interval at 12,816.5 feet.

**12,817-12,818:** Grayish black somewhat laminated mudstone containing a carbonate-rich interval at 12,817 with three vertical 3 mm calcite fractures and 1 mm pyrite laminae near the base of the interval.

**12,818-12,819:** Grayish black somewhat laminated mudstone with disseminated pyrite grains, pyrite laminations (1 mm), and a 2 mm carbonate-rich lamina at 12,818.6 feet containing small 2 mm vertical calcite fractures.

**12,819-12,820:** Grayish black massive fractured mudstone from 12,819-12,819.2 feet containing a 2" dolomite-filled fracture. A somewhat laminated mudstone with disseminated pyrite grains and 1 mm pyrite laminae occurs from 12,819.2-12,820.

**12,820-12,821:** Grayish black somewhat laminated and blocky mudstone with 1 mm pyrite laminations and disseminated pyrite grains. A fractured zone at 12,820.5 feet contains four 1 cm calcite filled vertical fractures.

**12,821-12,822:** Grayish black laminated mudstone with silica-rich (1-5 mm), carbonate-rich (1-3 mm), and pyrite (1 mm) laminae. Silica-rich laminae occur near the top of the interval from 12,821-12,821.4 feet and contain vertical calcite fractures (3 mm-1/2"). Two carbonate-rich laminae occur at 12,821.9 feet.

**12,822-12,823:** Grayish black somewhat laminated mudstone with disseminated pyrite grains, pyrite laminae (1 mm) and a carbonate-rich interval at 12,822.9 feet containing one 1/2" vertical calcite fracture.

**12,823-12,824:** Grayish black somewhat laminated mudstone with 1 mm pyrite laminations and a carbonate-rich interval near the base containing small millimeter-sized vertical calcite fractures.

***Box 14 of 21***

**12,824-12,825:** Grayish black massive silica cemented zone from 12,824-12,824.2 feet containing vertical 3 mm to ½” calcite fractures. A somewhat laminated mudstone occurs from 12,824.2-12,825 containing 1 mm pyrite laminations and disseminated pyrite grains.

**12,825-12,826:** Grayish black somewhat laminated mudstone occurs from 12,825-12,825.3 feet containing 1 mm pyrite laminations and four 3 mm vertical calcite fractures at 12,825.3 feet. A massive silica cemented zone at 12,825.3 contains two vertical ½” calcite fractures. A finely laminated mudstone occurs from 12,825.4-12,826 feet and contains silica-rich and carbonate-rich intervals with numerous vertical calcite fractures (1 mm-7 mm).

**12,826-12,827:** Grayish black finely laminated mudstone occurs from 12,826-12,826.4 feet with minor 1 mm pyrite laminations. A somewhat laminated silica cemented zone occurs at 12,826.4 feet and contains four 5 mm to ½” vertical calcite filled fractures. A somewhat laminated mudstone occurs from 12,826.6-12,827 feet with minor 1 mm pyrite laminations.

**12,827-12,828:** Grayish black somewhat laminated mudstone occurs from 12,827.33-12,827.5 containing a fractured zone at 12,827.5 feet with multiple 5 mm vertical calcite fractures. A finely laminated interval exists from 12,827.5-12,827.6 feet and contains three disseminated pyrite grains. A silica cemented zone exists from 12,827.6-12,828 feet and contains two vertical ½” calcite fractures.

**12,828-12,829:** Grayish black somewhat laminated mudstone with disseminated pyrite grains, 1 mm pyrite laminations, and two carbonate-rich intervals at 12,828.2 and 12,828.4 feet containing vertical calcite fractures (3 mm to 7 mm).

**12,829-12,830:** Grayish black finely laminated mudstone containing minor disseminated pyrite and 1 mm pyrite laminations.

**12,830-12,831:** Grayish black somewhat laminated mudstone containing a 2 mm carbonate-rich lamina at 12,830.1 with splaying vertical calcite fractures (1/2”). Minor 1 mm pyrite laminations occur throughout the interval.

**12,831-12,832:** Grayish black somewhat laminated mudstone with silica cemented bands occurring from 12,831, 12,831.5, and 12,831.9 feet containing millimeter-sized vertical calcite fractures.

**12,832-12,833:** Grayish black laminated mudstone with minor 1 mm pyrite laminations throughout interval.

***Box 15 of 21***

**12,833-12,834:** Grayish black somewhat laminated mudstone with minor disseminated pyrite grains and 1 mm pyrite laminations. Sporadic ptigmatic millimeter-sized calcite fractures occur

throughout the interval. At 12,833.9-12,834 feet a finely laminated interval with two ½” vertical calcite fractures occurs.

**12,834-12,835:** Grayish black somewhat laminated mudstone with carbonate-rich intervals at 12,834.1 (7 mm), 12,834.6 (1 mm), and 12,834.9 (2 mm) containing millimeter-sized vertical calcite fractures. Pyrite laminations (1 mm) do occur throughout the interval as well.

**12,835-12,836:** Grayish black somewhat laminated mudstone with carbonate-rich (2 mm) and pyrite (1 mm) laminae. Carbonate-rich lamina at 12,835 contains 5 mm vertical calcite fractures splaying off the carbonate-rich interval.

**12,836-12,837:** Grayish black somewhat laminated and blocky mudstone with sporadic millimeter-sized ptigmatic and vertical calcite fractures occurring throughout the interval.

**12,837-12,838:** Grayish black somewhat laminated mudstone containing carbonate-rich lamina at 12,837.3 and 12,837.9 feet with vertical calcite fracturing (3 mm-1/2”). A 2 mm x ½” pyrite nodule occurs at 12,827.8 feet.

**12,838-12,839:** Grayish black somewhat laminated mudstone with minor 1 mm pyrite laminations.

**12,839-12,840:** Grayish black laminated mudstone with silica-rich (1 mm) and pyrite (1 mm) laminations. Silica-rich (1 mm) laminations occur at 12,839.9 feet and contain numerous vertical calcite fractures (3 mm-1/2”).

**12,840-12,841:** Grayish black somewhat laminated mudstone with carbonate-rich lamina at the top and base of interval contain ½-1” vertical calcite fractures.

**12,841-12,842:** Grayish black somewhat laminated mudstone with minor 1 mm pyrite laminations and a carbonate-rich interval (1/2”) at 12,841.6 feet exhibiting a fining upward sequence.

### ***Box 16 of 21***

**12,842-12,843:** Grayish black somewhat laminated mudstone with minor 1 mm pyrite laminations and a carbonate-rich interval (1/2”) at 12,842.6 feet containing numerous vertical calcite fractures (1 mm-1/2”).

**12,843-12,844:** Grayish black somewhat laminated mudstone with 1 mm pyrite laminations, silica-rich (1/2”), and carbonate-rich laminae (5 mm). A silica-rich lamina at 12,843.4 feet contains ½” vertical calcite fractures. A carbonate-rich lamina at 12,843.9 contains numerous 5 mm vertical calcite fractures. Sporadic millimeter-sized ptigmatic calcite fractures occur throughout the interval as well.

**12,844-12,845:** Grayish black somewhat laminated mudstone with a carbonate-rich lamina at 12,844.8 feet containing two 1” dolomite filled vertical fractures cutting through the lamina to create a reverse fault with 3 mm displacement.

**12,845-12,846:** Grayish black somewhat laminated mudstone with minor 1 mm pyrite laminae and two carbonate-rich laminae at 12,845.9 feet containing two 1” dolomite filled vertical fractures that create a horst and graben structure with 1 mm of displacement.

**12,846-12,847:** Grayish black somewhat laminated mudstone containing sporadic millimeter-sized ptigmatic calcite fractures and a carbonate-rich interval (3 mm) at 12,846.1 feet consisting of numerous vertical (1/2”) and ptigmatic (1 mm-3 mm) calcite fractures.

**12,847-12,848:** Grayish black somewhat laminated mudstone with two carbonate-rich (1 mm) intervals at 12,847.1 and 12,847.2 containing vertical (1”) and ptigmatic (1-2 mm) calcite fractures. A silica-rich lamina (7 mm) at 12,847.9 feet contains one 1/2” vertical calcite fracture.

**12,848-12,849:** Grayish black somewhat laminated mudstone with three thin (1 mm) carbonate-rich laminae at the top of the interval containing numerous vertical (2-7 mm) and ptigmatic (1-3 mm) calcite fractures. A silica-rich lamina (7 mm) at 12,848.9 feet consists of two vertical calcite filled fractures (1/2”).

**12,849-12,850:** Grayish black somewhat laminated mudstone with a silica-rich lamina at 12,849.1 feet consisting of three 5mm to 1/2” vertical calcite fractures. Underlying the silica-rich interval is a 3 mm solid pyrite lamina. Finely laminated 5 mm of carbonate lamina exist at 12,849.5 feet with a burrow creating a pinch and swell structure through the laminae. Finely laminated 1/2” of carbonate laminae exists at 12,849.9 feet.

**12,850-12,851:** Grayish black somewhat laminated mudstone with minor 1 mm of pyrite and carbonate-rich laminae near the bottom of the interval. Carbonate-rich lamina at 12,850.8 and 12,850.9 feet contain vertical calcite fractures ranging in size from a few millimeters to 1/2”.

#### ***Box 17 of 21***

**12,851-12,852:** Grayish black somewhat laminated mudstone with 3 mm carbonate-rich lamina at 12,851.9 feet containing two 3 mm vertical calcite fractures.

**12,852-12,853:** Grayish black somewhat laminated mudstone with finely laminated 1 mm carbonate-rich laminae in a 5 mm interval consisting of one 1/2” vertical calcite fracture. A pyrite nodule (1 mm x 2”) exists at 12,852.2 feet. A 3 mm carbonate-rich interval at 12,852.8 feet consists of three 3 mm vertical calcite fractures.

**12,853-12,854:** Grayish black somewhat laminated mudstone with 1 mm pyrite laminations throughout the interval.

**12,854-12,855:** Grayish black somewhat laminated mudstone with pyrite laminations (1 mm) and carbonate-rich laminae occurring at 12,854.2 and 12,854.9 feet containing vertical calcite fractures (3 mm-1/2”).

**12,855-12,856:** Grayish black somewhat laminated mudstone with minor pyrite laminations (1 mm) and carbonate-rich laminae occurring at 12,855.9 feet containing millimeter-sized vertical calcite fractures.

**12,856-12,857:** Grayish black somewhat laminated mudstone with carbonate-rich lamina (5 mm) at 12,856.4 feet consisting of three 5mm to 1/2” vertical calcite fractures. A 1 mm x 2” pyrite nodule occurs at 12,856.9 feet.

**12,857-12,858:** Grayish black somewhat laminated mudstone with three 1 mm carbonate-rich laminae at 12,857.5 feet containing two long 1” pygmatic calcite fractures that cut through all three carbonate laminae. 4 mm carbonate-rich laminae at 12,857.8 feet contain two 3 mm vertical calcite fractures.

**12,858-12,859:** Grayish black somewhat laminated mudstone with 1 mm laminations of pyrite throughout the interval.

**12,859-12,860:** Grayish black somewhat laminated mudstone with 1 mm laminations of pyrite throughout the interval.

### ***Box 18 of 21***

**12,860-12,861:** Grayish black somewhat laminated mudstone with three 2 mm laminations of carbonate-rich intervals near the top of the section containing numerous millimeter-sized calcite vertical fractures. A 1” fracture occurs at 12,860.8 feet as well.

**12,861-12,862:** Grayish black somewhat laminated mudstone with three carbonate-rich laminae at 12,861.1 (7 mm), 12,861.2 (5 mm), and 12,861.9 (1/2”) feet. The 7 mm carbonate interval contains numerous vertical 5 to 7 mm calcite fractures. The 5 mm carbonate interval is thick and consists of silt-sized grains and two 7 mm vertical calcite fractures. The bottom 1/2” carbonate interval exhibits a fining upward sequence and contains four 1/2” vertical calcite fractures.

**12,862-12,863:** Grayish black somewhat laminated mudstone with four thin (2-4 mm) carbonate-rich laminae occurring throughout the interval. The carbonate-rich laminae commonly have numerous pygmatic and vertical millimeter-sized calcite fractures.

**12,863-12,864:** Grayish black somewhat laminated mudstone with two thin 1 mm carbonate-rich laminae at the top of the interval.

**12,864-12,865:** Grayish black laminated mudstone with many 1 mm pyrite laminations and a 5 mm carbonate-rich lamina occurring at 12,864.9 feet containing three millimeter-sized vertical calcite fractures.

**12,865-12,866:** Grayish black somewhat laminated mudstone with 1 mm pyrite laminations, a 1 mm carbonate-rich lamination at 12,865.2 feet, and a large pyrite nodule (7 mm x 3") at 12,865.9 feet.

**12,866-12,869:** Grayish black finely laminated mudstone from 12,866-12,866.4 consisting of 1 mm carbonate-rich laminae. Blocky, broken-up grayish black mudstone occurs from 12,866.4-12,869.

### ***Box 19 of 21***

**12,869-12,870:** Grayish black blocky, broken-up mudstone with minor disseminated pyrite grains.

**12,870-12,871:** Grayish black blocky, broken-up mudstone with minor disseminated pyrite grains.

**12,871-12,872:** Grayish black blocky, broken-up mudstone with minor disseminated pyrite grains. A 1 mm carbonate-rich lamina at 12,871.1 consists of numerous 3 to 7 mm pygmatic calcite fractures.

**12,872-12,873:** Grayish black blocky, broken-up mudstone with minor disseminated pyrite and silica grains.

**12,873-12,874:** Grayish black blocky, broken-up mudstone with minor disseminated pyrite grains. A 4 mm pyrite lamina at 12,873.9 feet consists of numerous 4 mm to 1" pygmatic calcite fractures.

**12,874-12,875:** Grayish black blocky, broken-up mudstone with minor disseminated pyrite grains.

**12,875-12,876:** Grayish black finely laminated mudstone from 12,875-12,875.55 consisting of 1 mm carbonate-rich laminae with six millimeter-sized calcite vertical fractures at 12,875.55.

**12,876-12,877:** Grayish black finely laminated mudstone from 12,876-12,876.1 feet consisting of 1 mm carbonate-rich laminae. A grayish black laminated mudstone occurs from 12,876.1-12,877 containing minor thin pyrite (1 mm) and carbonate-rich (1 mm) laminae.

**12,877-12,878:** Grayish black somewhat laminated mudstone with a 4 mm carbonate-rich lamina at 12,877.3 consisting of two 3 mm to 4 mm pygmatic calcite fractures.

### ***Box 20 of 21***

**12,878-12,879:** Grayish black laminated mudstone with silica-rich laminae present at the top and base of the interval. The silica-rich lamina (1/2") at 12,878 consists of numerous millimeter-



sized ptygmatic calcite fractures. The silica-rich lamina (1") at 12,878.9 feet consists of numerous vertical calcite fractures that range from 4 mm to 1" in size.

**12,879-12,880:** Grayish black somewhat laminated mudstone with two carbonates laminae occurring at 12,879.8 and 12,879.9 feet containing numerous millimeter-sized vertical calcite fractures. Numerous millimeter-sized ptygmatic calcite fractures also occur at 12,879.85 feet.

**12,880-12,881:** Grayish black somewhat laminated mudstone consisting of two laminations of carbonate-rich intervals at 12,880.1 (1 mm) and 12,880.8 (2 mm). Both carbonate-rich laminae consist of vertical calcite fractures ranging from 3 mm to 1" in size.

**12,881-12,882:** Grayish black somewhat laminated mudstone consisting of two carbonate-rich intervals at the top of the section and a silica-rich interval in between the two carbonate-rich intervals. The second carbonate interval at 12,881.3 feet consists of numerous millimeter-sized vertical calcite fractures. The silica-rich lamina at 12,881.2 feet consists of numerous millimeter-sized ptygmatic and vertical fractures. A pyrite nodule (3 mm x 2") occurs at 12,881.9 feet and has numerous vertical calcite fractures (3 mm-1/2") splaying from it.

**12,882-12,883:** Grayish black laminated mudstone consisting of a silica-rich laminated interval at 12,882.5 feet that consists of numerous vertical and ptygmatic calcite filled fractures ranging from a few millimeters to 1" in size.

**12,883-12,884:** Grayish black laminated mudstone consisting of a large pyrite nodule (1"x1/2") at 12,883.9 feet. The nodule has numerous calcite and pyrite vertical and ptygmatic fractures ranging from a few millimeters to 1" in size.

**12,884-12,885:** Grayish black laminated mudstone consisting of 1 mm pyrite laminations and a 3 mm carbonate-rich lamination at the top of the interval.

**12,885-12,886:** Grayish black laminated mudstone consisting of carbonate-rich (2 mm) and silica-rich (3-7 mm) laminae. Silica-rich laminae are present from 12,885.4 and 12,885.7 feet and consists of numerous millimeter-sized vertical and ptygmatic calcite fractures. A carbonate-rich interval exists at 12,885.5 feet and contains small 1 mm vertical calcite fractures.

**12,886-12,887:** Grayish black laminated mudstone with two pyrite nodules (2 mm x 1/2")(1 mm x 4 mm) separated by a long 2" vertical calcite fracture at 12,886.5 feet.

### ***Box 21 of 21***

**12,887-12,888:** Grayish black blocky mudstone from 12,887-12,887.8 feet. A laminated mudstone consisting of two disseminated pyrite grains occurs from 12,887.8-12,888 feet.

**12,888-12,889:** Missing core

**12,889-12,890:** Grayish black laminated mudstone with minor sporadic millimeter-sized ptygmatic calcite fractures and disseminated pyrite grains.

**12,890-12,891:** Grayish black low angle laminated mudstone with 2 mm carbonate-rich lamina at the top of the interval exhibiting a fining upward sequence.

**12,891-12,892:** Grayish black low angle laminated mudstone with two 1 mm carbonate laminations at the top of the interval consisting of vertical calcite fractures (1 mm-1/2"). A silica-rich laminated interval at 12,891.5 feet consists of numerous vertical calcite fractures (3 mm-1"). A pyrite nodule (1 mm x 1") is present at 12,891.4 feet and disseminated pyrite grains are present throughout the interval.

**12,892-12,893:** Grayish black low angled silica-rich laminated mudstone occurs from 12,892-12,892.4 feet. Two 1/2" vertical calcite fractures occur at the top of the interval. Grayish black blocky mudstone occurs from 12,892.4-12,893 feet.

### ***Box 1 of 13***

**12,893-12,894:** Grayish black laminated mudstone with silica-rich laminae intervals at 12,893 (1 mm) and 12,893.9 (1") feet containing vertical calcite fractures ranging from 4 mm to 1/2" long. A compacted pyrite nodule (3 mm x 3") is present at 12,893.5 feet.

**12,894-12,895:** Grayish black laminated mudstone with silica-rich (3-7 mm) and pyrite (2 mm) laminae. Silica-rich intervals at 12,894.3 and 12,894.9 feet consist of ptygmatic and vertical calcite fractures ranging from 3 mm to 7 mm in length. Pyrite lamina (2 mm) at 12,894.2 feet consists of two ptygmatic 2 mm calcite fractures.

**12,895-12,896:** Grayish black laminated mudstone with silica-rich (3-5 mm) and pyrite (2 mm) laminae intervals. Silica-rich intervals occur at 12,895 (5 mm), 12,895.5 (3 mm), and 12,895.9 (4 mm) feet. The silica-rich intervals consist of millimeter-sized vertical calcite fractures.

**12,896-12,897:** Grayish black silica laminated mudstone that is highly fractured. A finely laminated interval from 12,896-12,896.7 consists of 1-2 mm laminations of silica with high concentrations of vertical and ptygmatic calcite fractures (2 mm to 2"). A lesser laminated mudstone interval occurs from 12,896.7-12,897.

**12,897-12,898:** Grayish black laminated mudstone with silica-rich laminae occurring from 12,897 (7 mm), 12,897.2 (7 mm), and 12,897.7 (4 mm) feet. The silica-rich intervals consist of ptygmatic and vertical calcite fractures ranging from 3 mm to 7 mm in length. A pyrite nodule (2 mm x 4 mm) is present at 12,897.6 feet.

**12,898-12,899:** Grayish black laminated mudstone with a silica-rich interval (5 mm) at 12,898.9 feet containing three vertical calcite fractures (3-7 mm).

**12,899-12,900:** Grayish black laminated mudstone with two silica-rich laminae intervals occurring at 12,899.5 (3 mm) and 12,899.9 (1/2") feet. Vertical calcite fractures occur within these silica-rich intervals and are commonly limited to the height of the silica-rich interval.

**12,900-12,901:** Grayish black laminated mudstone that transitions into a finely laminated mudstone where silica-rich laminae occur. The silica-rich laminae occur at 12,900 (3 mm), 12,900.1 (6 mm), 12,900.2 (1"), and 12,900.6 (2") feet. The silica-rich laminae intervals contain numerous vertical and ptygmatic calcite fractures that are commonly restricted to the silica-rich height.

**12,901-12,902:** Grayish black low angle laminated mudstone that transitions into a finely laminated mudstone where silica-rich laminae occur. The silica-rich laminae occur at 12,901.1 (4 mm), 12,901.7 (7 mm), and 12,901.9 (1 mm) feet. Vertical and ptygmatic calcite fractures (1 mm-1") are numerous throughout these silica-rich intervals.

### *Box 2 of 13*

**12,902-12,903:** Grayish black laminated mudstone consisting of silica-rich (3 mm-1/2") and pyrite (1 mm) laminations. A silica-rich lamina (5 mm) at 12,902.4 feet consists of numerous ptygmatic calcite fractures (1 mm-5 mm). A silica-rich lamina (1/2") at 12,902.9 feet contains numerous ptygmatic and vertical calcite fractures (3 mm-7 mm).

**12,903-12,904:** Grayish black laminated mudstone with two silica-rich laminae intervals at 12,903.8 (7 mm) and 12,903.9 (1/2") feet. The silica-rich intervals contain millimeter-sized vertical and ptygmatic calcite fractures.

**12,904-12,905:** Grayish black laminated mudstone consisting of two 1/2" vertical calcite filled fractures in a silica-rich zone at the top of the interval.

**12,905-12,906:** Grayish black laminated mudstone with numerous silica-rich intervals throughout the section. The top of the interval contains silica-rich intervals containing small millimeter-sized calcite fractures. A pyrite nodule (2 mm x 4 mm) is present at 12,905.3 feet.

**12,906-12,907:** Grayish black laminated mudstone with numerous silica-rich intervals throughout the section. Ptygmatic and vertical calcite fractures (1-5 mm) are present within the silica-rich intervals at 12,906 and 12,906.7 feet.

**12,907-12,908:** Grayish black laminated mudstone with numerous silica-rich intervals throughout the section. A 1" silica-rich finely laminated interval at 12,907.9 feet consists of numerous ptygmatic calcite fractures (1 mm-4 mm).

**12,908-12,909:** Grayish black laminated mudstone with numerous silica-rich intervals throughout the section. Silica-rich intervals at the top of the section contain millimeter-sized vertical calcite fractures as well as recrystallized disseminated silt-sized pyrite grains. A 1.5"

vertical pyrite fracture exists at 12,908.6 feet within a silica-rich lamina. A possible current mark exists at 12,908.8 feet.

**12,909-12,910:** Grayish black laminated mudstone with numerous silica-rich intervals throughout the section. Silica-rich laminae (4 mm) at 12,909.4 feet exhibits micro (0.5 mm) reverse faulting. Pyrite- (5 mm) and calcite (1/2") filled fractures are present at 12,909.7 and 12,909.8 feet. A clay clast (1 mm x 1mm) occurs at 12,909.1 feet.

**12,910-12,911:** Grayish black laminated mudstone with numerous silica-rich intervals throughout the section.

### ***Box 3 of 13***

**12,911-12,912:** Grayish black laminated mudstone with a 2 mm silica-rich lamina at 12,911.5 feet containing four pygmatic calcite fractures ranging from 1 mm to 7 mm long. A clay clast (1 mm x 1 mm) is present at 12,911.7 feet.

**12,912-12,913:** Grayish black laminated mudstone with silica-rich intervals throughout the section. A silica-rich (4 mm) interval containing one vertical calcite fracture (6 mm). A pyrite- and silica-rich interval (7 mm) at 12,912.9 feet containing a pyrite nodule (3 mm x 3 mm) and a 7 mm vertical calcite fracture.

**12,913-12,914:** Grayish black laminated mudstone with two silica- and pyrite-rich laminae intervals at 12,913.8 (4 mm and 2 mm) containing small millimeter-sized pygmatic calcite fractures.

**12,914-12,915:** Grayish black laminated mudstone with pyrite (5 mm) and silica-rich (1-7 mm) laminations. A 7 mm silica-rich lamination at the top of the interval contains numerous pygmatic calcite fractures (2 mm-1/2").

**12,915-12,916:** Grayish black laminated mudstone with a finely carbonate laminated interval between 12,915.4-12,915.6 feet containing small millimeter-sized vertical calcite fracture underlying the interval. A pyrite rich lamina (3 mm) at 12,915.8 consists of numerous small millimeter-sized pygmatic calcite fractures and a pyrite nodule (3 mm x 5 mm).

**12,916-12,917:** Grayish black laminated mudstone consisting of high concentrations of disseminated pyrite grains and laminae. A pyrite nodule (2 mm x 3 mm) exists at 12,916.7 feet.

**12,917-12,918:** Grayish black laminated mudstone consisting of numerous pyrite- and silica-rich laminae intervals. A 7 mm lamina of pyrite consists of a 7 mm pyrite filled vertical fracture at 12,917.6 feet. Silica-rich intervals at 12,917.8 feet consist of numerous pygmatic calcite fractures (1-4 mm).

**12,918-12,919:** Grayish black laminated mudstone with silica rich intervals (1 mm) throughout the interval. Finely laminated silica-rich intervals at 12,918.6 contain numerous millimeter-sized ptymatic calcite filled fractures.

**12,919-12,920:** Finely laminated silica-rich mudstone from 12,919-12,919.5 feet containing numerous ptymatic and vertical (1 mm-1/2") calcite fractures. A lesser laminated mudstone occurs from 12,919.5-12,920.

#### ***Box 4 of 13***

**12,920-12,921:** Grayish black laminated mudstone with finely laminated silica-rich intervals near the top of the section. 1 mm pyrite laminae exist at 12,920.4 and 12,920.6 feet.

**12,921-12,922:** Grayish black laminated mudstone with silica- and pyrite-rich laminae throughout the interval.

**12,922-12,923:** Grayish black laminated mudstone with silica- and pyrite-rich laminae throughout the interval. Vertical calcite fractures (4 mm) occur in silica-rich laminae at the top of the interval (12,922). A pyrite filled fracture (2 mm) occurs at the base of the interval within silica-rich laminae.

**12,923-12,924:** Grayish black laminated mudstone with silica-rich laminae throughout the interval.

**12,924-12,925:** Grayish black laminated mudstone with silica-rich laminae occurring from 12,924 (5 mm), 12,924.3 (2 mm), 12,924.4 (1/2"), 12,924.9 (7 mm) feet. Possible current ripple mark occurring in silica-rich laminae at 12,924.4 feet. Disseminated pyrite grains occur throughout interval. Marcasite nodules occur at 12,924.3-12,924.6 feet.

**12,925-12,926:** Grayish black finely laminated mudstone with millimeter-sized silica-rich laminae. Vertical calcite fractures (4 mm-1") occur in silica-rich laminae at 12,925.2 feet.

**12,926-12,927:** Grayish black laminated mudstone with silica- and pyrite-rich laminae occurring throughout the interval.

**12,927-12,928:** Grayish black laminated, blocky mudstone with fine silica-rich and pyrite laminae occurring throughout the interval. Large 1" vertical pyrite filled burrow at 12,927.2 feet.

**12,928-12,929:** Grayish black laminated mudstone with silica- and pyrite-rich laminae occurring throughout the interval. Possible pyrite filled burrow at the top of the interval (12,928).

#### ***Box 5 of 13***

**12,929-12,930:** Grayish black laminated mudstone with silica- and pyrite-rich laminae occurring throughout the interval.

**12,930-12,931:** Grayish black laminated mudstone with silica- and pyrite laminae occurring throughout the interval. A 1" finely silica-rich laminated interval occurs at 12,930.9 feet containing numerous 1 mm silica-rich laminae.

**12,931-12,932:** Grayish black laminated mudstone with intervals of silica-rich and pyrite laminae that occur at times throughout the interval. Disseminated pyrite grains also occur throughout the interval.

**12,932-12,933:** Grayish black laminated mudstone with intervals of silica-rich and pyrite laminae that occur at times throughout the interval. Silica-rich intervals at the top and base of the interval contain vertical and pygmatic (1-4 mm) calcite fractures.

**12,933-12,934:** Grayish black laminated mudstone with intervals of silica-rich and pyrite laminae that occur at times throughout the interval. Two vertical (5 mm) calcite filled fractures occur within a silica-rich lamina (5 mm) at the top of the interval.

**12,934-12,935:** Grayish black laminated mudstone with intervals of silica-rich and pyrite laminae that occur at times throughout the interval. Numerous disseminated pyrite grains occur throughout the interval.

**12,935-12,936:** Grayish black laminated mudstone with intervals of silica-rich and pyrite laminae that occur at times throughout the interval. Disseminated pyrite grains also occur at 12,935.5 feet.

**12,936-12,937:** Grayish black laminated mudstone with numerous concentrations of pyrite in the forms of disseminated grains and laminae. Minor silica-rich lamina also occurs throughout the interval. A large pyrite filled shear fracture (1/2") occurs at 12,936.1 feet.

**12,937-12,938:** Grayish black laminated mudstone with numerous concentrations of pyrite in the forms of disseminated grains and laminae. Minor silica-rich lamina also occurs throughout the interval. Small pygmatic calcite fractures (1 mm) occur in pyrite-rich laminae from 12,937-12,937.1 feet. A thick 2 mm pyrite lamina occurs at 12,937.6 feet.

***Box 6 of 13***

**12,938-12,939:** Grayish black laminated mudstone with numerous silica-rich laminations that occur throughout the interval. A possible burrow cuts through a 5 mm silica-rich lamina at 12,938.1 feet. Small vertical 2 mm vertical fractures are present within a silica-rich lamina (2 mm) at 12,938.9 feet.

**12,939-12,940:** Grayish black low angle laminated mudstone with intervals of finely laminated 1 mm silica-rich laminations occurring at the top, middle, and base of the section.



**12,940-12,941:** Grayish black low angle laminated mudstone with silica- and pyrite-rich laminations occurring throughout the interval. A thin 1 mm silica-rich lamina exhibits a possible scour mark at 12,940.4 feet.

**12,941-12,942:** Grayish black laminated mudstone with laminations of pyrite and silica, as well as disseminated pyrite grains throughout the interval.

**12,942-12,943:** Grayish black laminated mudstone with laminations of pyrite and silica, as well as disseminated pyrite grains throughout the interval.

**12,943-12,944:** Grayish black laminated mudstone with laminations of pyrite and minor silica, as well as disseminated pyrite grains throughout the interval.

**12,944-12,945:** Grayish black laminated mudstone with laminations of pyrite and minor silica, as well as disseminated pyrite grains throughout the interval. Pyrite filled pygmatic fractures occur at 12,944.7 feet. Millimeter-sized calcite pygmatic fractures (7 mm) occur within a 7 mm silica-rich interval at 12,944.9 feet.

**12,945-12,946:** Grayish black laminated mudstone with laminations of pyrite and minor silica, as well as disseminated pyrite grains throughout the interval. A possible burrow within a 3 mm pyrite lamina at 12,945.9 feet is present.

**12,946-12,947:** Grayish black laminated mudstone with laminations of pyrite and minor silica, as well as disseminated pyrite grains throughout the interval. A pyrite filled pygmatic fracture (4 mm) is found within a 3 mm pyrite lamina.

***Box 7 of 13***

**12,947-12,948:** Grayish black laminated mudstone with laminations of pyrite throughout the interval.

**12,948-12,949:** Grayish black laminated mudstone with laminations of pyrite and numerous disseminated pyrite grains throughout the interval.

**12,949-12,950:** Grayish black laminated mudstone with laminations of pyrite and numerous disseminated pyrite grains throughout the interval. A silica-rich lamina occurs at 12,949.3 feet. A pyrite nodule (2 mm x 4 mm) occurs at 12,949.4 feet.

**12,950-12,951:** Grayish black laminated mudstone with laminations of pyrite and minor silica, as well as disseminated pyrite grains throughout the interval.

**12,951-12,952:** Grayish black poorly laminated mudstone with high concentrations of pyrite throughout the interval. Two large pyrite nodules (1/2"x1" & 1/2"x1/2") occur at 12,951.1 and 12,951.2 feet. A pygmatic natural fracture occurs at the top of the interval and fractures the first pyrite nodule.

**12,952-12,953:** Grayish black laminated mudstone with laminations of pyrite and minor silica, as well as disseminated pyrite grains throughout the interval. A pyrite nodule (7 mm x 3 mm) occurs at 12,952.1 feet.

**12,953-12,954:** Grayish black laminated mudstone with laminations of pyrite and minor silica, as well as disseminated pyrite grains throughout the interval. Ptygmatic calcite fractures occur at the top of the interval in silica-rich laminae ranging from a few millimeters to ½” long.

**12,954-12,955:** Grayish black laminated mudstone with laminations of pyrite and minor silica, as well as disseminated pyrite grains throughout the interval.

**12,955-12,956:** Grayish black laminated mudstone with laminations of pyrite and disseminated pyrite grains throughout the interval.

### ***Box 8 of 13***

**12,956-12,957:** Grayish black laminated mudstone with laminations of pyrite and minor silica, as well as disseminated pyrite grains throughout the interval. Small phosphate nodules (1 mm x 1 mm & 2 mm x 3 mm) occur at 12,956 and 12,956.6 feet. A phosphate nodule at 12,956.6 feet deforms silica laminae surrounding it.

**12,957-12,958:** Grayish black laminated mudstone with laminations of pyrite and disseminated pyrite grains throughout the interval. A large pyrite nodule (1”x1/2”) occurs at 12,957.1 feet. Abundant marcasite nodules occur from 12,957.6-12,958 feet.

**12,958-12,959:** Grayish black laminated mudstone with laminations of pyrite and marcasite nodules throughout the interval. Marcasite nodules occur from 12,958.4-12,958.6 feet. A medium dark gray (N4) argillaceous band (2 mm) occurs at 12,958.9 feet.

**12,959-12,960:** Grayish black laminated mudstone with disseminated pyrite grains occurring throughout the interval.

**12,960-12,961:** Grayish black laminated mudstone with laminations of medium dark gray (N4) argillaceous bands and marcasite nodules throughout the interval. Marcasite nodules occur at 12,960 and 12,960.9 feet. Cyclic gray argillaceous bands (~4 mm) occur throughout the interval with average separation of ½”. Two phosphate nodules (1 mm x 1 mm) occur at the top and base of the interval.

**12,961-12,962:** Grayish black laminated mudstone with laminations of medium dark gray (N4) argillaceous bands and marcasite nodules throughout the interval. Marcasite nodules occur near the bottom of the interval. Gray cyclic argillaceous bands occur throughout the interval with a reverse fault at 12,961.3 feet showing 3 mm of displacement. Small gypsum fragments (1 mm x 1 mm) occur from 12,961.6-12,961.8 feet.

**12,962-12,963:** Grayish black laminated mudstone with laminations of medium dark gray (N4) argillaceous bands and marcasite nodules throughout the interval. Gray argillaceous bands (4 mm) occur at the top of the interval. Marcasite nodules occur throughout the interval. A small phosphate nodule (2 mm x 2 mm) occurs at 12,962.2 feet.

**12,963-12,964:** Grayish black laminated mudstone with laminations of medium dark gray (N4) argillaceous bands and marcasite nodules throughout the interval. Gray argillaceous bands (4 mm) occur throughout the interval as well as small gypsum fragments (1 mm x 1 mm). Clay clasts occur at 12,963.1 and 12,963.7 feet.

**12,964-12,965:** Grayish black laminated mudstone with laminations of medium dark gray (N4) argillaceous bands and marcasite nodules throughout the interval. Marcasite nodules and clay clasts occur throughout the interval, as well as gray argillaceous bands.

### ***Box 9 of 13***

**12,965-12,966:** Grayish black laminated mudstone with laminations of medium dark gray (N4) argillaceous bands, marcasite nodules, and clay clasts occur throughout the interval.

12,966-12,967: Grayish black laminated mudstone with laminations of medium dark gray (N4) argillaceous bands and marcasite nodules throughout the interval. The gray argillaceous bands exhibit soft sediment deformation. Mostly a gray argillaceous interval with grayish black interbedded intervals at 12,966.1 and 12,966.7 feet. High concentrations of marcasite nodules occur throughout the interval.

12,967-12,968: Grayish black laminated mudstone with laminations of medium dark gray (N4) argillaceous bands and marcasite nodules throughout the interval. Gray argillaceous band occurs from 12,967-12,967.1 feet. Grayish black massive mudstone with minor argillaceous bands (1 mm) and high concentrations of marcasite nodules occurs from 12,967.1-12,967.9 feet. **The Woodford/Hunton contact** occurs at 12,967.9 feet with a sharp contact between grayish black mudstone and medium light gray (N5) limestone with abundant pyrite nodules and phosphate nodules.

## McDonald 2H-16E Core Descriptions

### *Box 3 of 7*

**6,250-6,259:** Medium to medium dark gray (N5-N4) massive mudstone with bioturbated intervals and abundant skeletal fossils. A glauconitic rich zone containing large marcasite nodules and minor fossils is present from 6,257.05-6,259 feet.

### *Box 4 of 7*

**6,259-6,260:** Medium dark gray (N4) massive mudstone containing abundant glauconite marcasite nodules throughout interval. Minor phosphate nodules at the base of the interval and range in size from 1 mm x 1mm and ½”x 2 mm.

**6,260-6,261:** Medium dark gray (N4) fissile mudstone from 6,260-6,260.4 feet containing tabular phosphate nodules at the top of the interval. Medium dark gray massive mudstone occurs from 6,260.4-6,260.9 feet. **Woodford/Caney contact** occurs at 6,260.9 feet with a sharp erosional contact transitioning from a medium dark gray to grayish black (N7) massive mudstone.

**6,261-6,262:** Grayish black massive mudstone containing micro- and millimeter-sized disseminated pyrite grains.

**6,262-6,263:** Grayish black massive mudstone containing phosphate nodules and marcasite nodules. Two laminations of dark homogenized sediment (possibly silica?) occur at 6,262.2 and 6,262.3 feet. Small millimeter-sized marcasite nodules occur at the top of the interval. Three small phosphate nodules (1 mm x 2 mm) occur at 6,262.8 feet.

**6,263-6,264:** Grayish black massive mudstone containing phosphate nodules and burrows. A 2” long burrow occurs from 6,263.4-6,263.6 feet. Phosphate nodules occur at 6,263.5 feet in tabular form (1 mm x 5 mm) and larger nodules at 6,263.9 feet (5 mm x ½”). Abundant bioturbation is present from 6,263.7-6,263.9 feet.

**6,264-6,265:** Grayish black massive, poorly-laminated mudstone containing large silica clasts. Silica clasts from 6,264-6,264.6 feet consist of disseminated pyrite grains and calcite filled vertical fractures (1 mm-5 mm).

**6,265-6,266:** Grayish black massive, poorly laminated mudstone with silica clasts. Silica clasts occur from 6,265.5-6,266. The silica clasts consist of disseminated pyrite grains, vertical and ptygmatic calcite fractures (1 mm-1/2”), and stylolites.

**6,266-6,267:** Grayish black massive, poorly laminated mudstone with silica clasts and marcasite nodules. Silica clasts are present at the top of the interval from 6,266-6,266.1 feet and contain

disseminated pyrite grains and millimeter sized vertical calcite fractures. A cluster of marcasite nodules occurs at 6,266.7 feet.

**6,267-6,268:** Grayish black laminated mudstone with silica-cemented bands occurring at 6,267 (4 mm), 6,267.1 (4 mm), 6,267.4 (4 mm), 6,267.7 (6 mm), 6,267.8 (3 mm), and 6,267.9 (1/2”).

*Box 5 of 7*

**6,268-6,269:** Grayish black somewhat laminated mudstone with silica-cemented bands and carbonate laminae. A silica-cemented band (1/2”) occurs at the top of the interval, 6,268.4 (4 mm), and 6,268.5 (5 mm) feet containing numerous ptygmatic millimeter-sized calcite fractures. Silt-sized carbonate grains occur in a 3 mm high bundle at 6,268.4 feet and 6,268.9 feet.

**6,269-6,270:** Grayish black laminated mudstone with silica-cemented bands from 6,269-6,269.9 feet. Cyclical silica-cemented bands (~3 mm) occur from the top of the interval to 6,269.9 feet and consist of one 1 mm pyrite filled vertical fracture at 6,269.1 feet. A large silica clast occurs from 6,269.9-6,270 feet and contains numerous millimeter-sized ptygmatic calcite and natural fractures.

**6,270-6,271:** Grayish black massive mudstone consisting of a silica clast with numerous millimeter-sized ptygmatic calcite and natural fractures occurs from 6,270-6,270.1 feet. A grayish black laminated mudstone containing silica-cemented bands occurs from 6,270.1-6,271 feet. The silica cemented bands (4 mm-1”) occur throughout the interval and contain vertical and ptygmatic natural and calcite fractures that are limited to the height of the cemented interval.

**6,271-6,272:** Grayish black laminated mudstone with silica-cemented bands. The silica-cemented bands (2 mm-7 mm) are highly fractured intervals with vertical and ptygmatic calcite, pyrite, and natural fractures that are limited to the height of the cemented lamination. A phosphate nodule (2 mm x 4 mm) occurs at 6,271.7 feet.

**6,272-6,273:** Grayish black laminated mudstone with silica-cemented bands (4 mm-1”) occurs throughout the interval. The silica-cemented bands contain disseminated pyrite grains, natural fractures, and calcite to pyrite filled vertical and ptygmatic fractures that are limited to the height of the cemented lamination.

**6,273-6,274:** Grayish black laminated mudstone with silica-rich laminations occurring throughout the interval. The silica-rich laminations (1 mm-4 mm) are most abundant in the upper half of the interval. Ptygmatic pyrite filled fractures within silica-rich laminae occur at 6,273.6 feet.

**6,274-6,275:** Grayish black laminated mudstone with heavy bioturbation and pyrite to silica-rich laminations. A heavy bioturbated interval from 6,274.1-6,274.5 feet contains high concentrations of burrows and silica-rich laminations that have been disrupted to the bioturbation. The bioturbated area is bound on top and bottom by a 4 mm thick pyrite lamination

that is also bioturbated. A grayish black silica-rich laminated mudstone occurs from 6,274.5-6,275 feet.

**6,275-6,276:** Grayish black laminated mudstone with a silica-cemented band (1") and silica-rich laminae (2-3 mm) throughout the interval. A micro-normal fault occurs in a silica-rich lamina at 6,275.1 feet and exhibits 1 mm of displacement. Millimeter-sized calcite filled vertical fractures are present within the laminae and band.

**6,276-6,277:** Grayish black laminated mudstone with numerous silica-cemented bands occurring throughout the interval. The silica-cemented bands (1 mm-1") are dark black and contain numerous vertical and ptymatic calcite filled and natural fractures that are limited to the height of the cemented band. Disseminated pyrite grains also occur throughout the interval.

### ***Box 6 of 7***

**6,277-6,278:** Grayish black laminated mudstone consisting of silica-cemented bands. Silica-cemented bands are abundant throughout the interval and range from 6 mm to ½". The cemented bands contain high concentrations of vertical and ptymatic natural to calcite or pyrite filled fractures. A thick pyrite lamina (1") occurs at 6,277.1 feet and contains a ½" pyrite filled vertical fracture that splays off of the lamina.

**6,278-6,279:** Grayish black laminated mudstone consisting of silica-cemented bands and pyrite-to silica-rich laminae. A silica cemented band (1/2") occurs at 6,278.5 and 6,278.9 feet and contains high concentrations of vertical and ptymatic natural and calcite filled fractures that are commonly a few millimeters long. Silica-rich laminae (4 mm-1/2") occur at 6,278 and 6,278.9 and contain small millimeter-sized vertical calcite fractures. A 4 mm pyrite lamina occurs at 6,278.5 feet.

**6,279-6,280:** Grayish black laminated mudstone consisting of abundant silica-cemented bands in the upper half of the interval. The silica-cemented bands (3 mm-1") contain numerous vertical millimeter-sized calcite fractures.

**6,280-6,281:** Grayish black somewhat laminated mudstone consisting of abundant silica-cemented bands in the lower half of the interval. The silica-cemented bands (1/2"-1") contain an abundant number of ptymatic and vertical natural to calcite filled fractures that are limited to the cemented zone.

**6,281-6,282:** Grayish black somewhat laminated mudstone consisting of abundant silica-cemented bands in the upper half of the interval and a silica-rich lamina in the lower half. The silica-cemented bands (1"-2") contain ptymatic and vertical pyrite filled fractures that range in only a few millimeters in length. The silica-rich lamina that occurs at 6,281.9 feet contains two millimeter-sized disseminated pyrite grains within the lamination.



**6,282-6,283:** Grayish black laminated mudstone consisting of abundant silica-cemented bands in throughout the interval. The silica-cemented bands range from ½” to 2” high and contain high concentrations of vertical and ptygmatic pyrite and calcite filled fractures that range from a few millimeters up to the length of the cemented zone. A pyrite ring occurs at 6,282.5 feet.

**6,283-6,284:** Grayish black laminated mudstone consisting of abundant silica-cemented bands and silica-rich laminae in the lower half of the interval. The silica-cemented bands (2 mm-4 mm) contain millimeter-sized ptygmatic and vertical pyrite and calcite filled fractures. Finely laminated silica-rich laminae occur at 6,283.9 feet and contain vertical and ptygmatic calcite fractures that range from 4 mm to 1” long.

**6,284-6,285:** Grayish black finely laminated mudstone with silica-rich laminations occurs from 6,284-6,284.2 feet. The silica-rich laminations (1 mm-3 mm) contain numerous millimeter-sized vertical and ptygmatic calcite fractures. A thick (2”) silica-rich interval at 6,284.3 feet contains numerous burrows and pyrite and calcite filled vertical and ptygmatic fractures ranging from a few millimeters to 2” long. A grayish black laminated mudstone occurs from 6,284.5-6,285 feet containing silica-rich laminae (1 mm-4 mm) with minor vertical and ptygmatic calcite fractures (1 mm-3 mm).

**6,285-6,286:** Grayish black laminated mudstone consisting of abundant silica-cemented bands and silica-rich laminae in the upper and lower halves of the interval. Silica-cemented bands (2 mm-2”) occur in the upper half of the interval and contain numerous pyrites and calcite filled vertical and ptygmatic fractures (1 mm-1/2”). Silica-rich lamina (3 mm) occurs at 6,285.9 feet and contains small millimeter-sized vertical and ptygmatic pyrite and calcite filled fractures.

#### ***Box 7 of 7***

**6,286-6,287:** Grayish black somewhat laminated mudstone consisting of very minor millimeter-sized vertical calcite fractures.

**6,287-6,288:** Grayish black laminated mudstone consisting of silica-rich laminations. The silica-rich laminae (1 mm-1/2”) occur throughout the interval and contain small ptygmatic and vertical calcite fractures (1 mm-3 mm).

**6,288-6,289:** Grayish black laminated mudstone consisting of abundant silica-cemented bands in the lower half of the interval. Silica-cemented bands (1 mm-1/2”) occur from 6,288.7-6,289 feet and contain vertical and ptygmatic pyrite and calcite filled fractures (1 mm-1/2”).

**6,289-6,290:** Grayish black laminated mudstone consisting of abundant silica-cemented bands throughout the interval. The silica-cemented bands contain vertical and ptygmatic pyrite and calcite filled fractures (1 mm-1/2”).

**6,290-6,291:** Grayish black laminated mudstone consisting of silica-rich laminae throughout the interval. The silica-rich laminae contains small (1 mm) vertical and ptymatic calcite filled fractures. Abundant disseminated pyrite intervals at 6,290.9 feet are present within the interval.

**6,291-6,291.4:** Grayish black somewhat laminated mudstone transitions into blocky broken-up mudstone.

***Box 1 of 10***

**6,292-6,293:** Grayish black laminated mudstone consisting of silica-rich laminae throughout the interval. Silica-rich laminations (1 mm-1") contain abundant fracturing in the lower half of the interval. Vertical and ptymatic pyrite and calcite fractures (1 mm-1") can be seen within the silica-rich laminae.

**6,293-6,294:** Grayish black laminated mudstone consisting of silica-rich laminae throughout the interval. The silica-rich laminations (1-3 mm) contain minor vertical calcite fractures (1-2 mm).

**6,294-6,295:** Grayish black laminated mudstone consisting of abundant silica-cemented bands and silica-rich laminae throughout the interval. Silica-cemented bands (~1/2") occur from 6,294.2-6,294.4 feet and contain disseminated pyrite grains and numerous vertical and ptymatic calcite fractures (1 mm-1/2"). Finely laminated silica-rich lamina occurs in the lower half of the interval and contains smaller vertical calcite fractures (1-3 mm).

**6,295-6,296:** Grayish black laminated mudstone consisting of silica-rich laminae throughout the interval. Silica-rich lamina (1 mm-1/2") at 6,295.9 feet contains calcite and pyrite filled vertical and ptymatic fractures (2 mm-1/2").

**6,296-6,297:** Grayish black laminated mudstone consisting of silica-rich laminae throughout the interval. The silica-rich laminations (1-3 mm) contain minor vertical calcite fractures (1-2 mm).

**6,297-6,298:** Grayish black laminated mudstone consisting of silica-rich laminae throughout the interval. Numerous vertical calcite fractures (1 mm-1/2") exist within the silica-rich laminae.

**6,298-6,299:** Grayish black laminated mudstone consisting of silica-rich laminae throughout the interval. The silica-rich laminations (1-3 mm) contain minor vertical calcite fractures (1-2 mm).

**6,299-6,300:** Grayish black laminated mudstone consisting of silica-rich laminae throughout the interval. Higher concentrations of vertical calcite fractures (3 mm-1/2") are within the thicker silica-rich laminae (1/2"-1") in the upper half of the interval. Silica S (1 mm x 4 mm) are present at 6,299.3 feet.

**6,300-6,301:** Grayish black laminated mudstone consisting of fine silica-rich laminations throughout the interval. The silica-rich laminations (1-3 mm) occur in laminated intervals of 1/2-2" and contain ptymatic and vertical pyrite and calcite fractures (1-7 mm).

*Box 2 of 10*

**6,301-6,302:** Grayish black laminated mudstone consisting of silica-rich laminae throughout the interval. Silica clasts (1 mm x 5 mm) are present at 6,301.4 feet. High concentrations of disseminated pyrite grains appear throughout interval.

**6,302-6,303:** Grayish black laminated mudstone consisting of silica-rich laminae throughout the interval. Small (1 mm) pyrite ptymatic fractures appear in the silica-rich laminae in the lower half of the interval.

**6,303-6,304:** Grayish black laminated mudstone consisting of abundant silica-cemented bands and silica-rich laminae throughout the interval. Silica-cemented bands occur at 6,303 (1"), 6,303.1 (4 mm), and 6,303.9 (1/2") feet. The cemented bands contain numerous vertical and ptymatic calcite fractures ranging from 1 mm to 1/2" in length. Silica-rich laminae appear mostly in the middle of this interval and contain 1-3 mm vertical calcite fractures. Two silica clasts (1 mm x 3 mm) occur at 6,303.3 feet.

**6,304-6,305:** Grayish black finely laminated mudstone consisting of 1 mm silica-rich laminations. The fine silica-rich laminations contain vertical 1-5 mm calcite fractures with minor amounts of pyrite filled 1 mm fractures.

**6,305-6,306:** Grayish black laminated mudstone consisting of abundant silica-cemented bands and fractures throughout the interval. The silica-cemented bands (~7 mm) contain high concentrations of vertical and ptymatic calcite and pyrite filled fractures (1 mm-1/2"). The fractures within this interval are thicker than commonly seen throughout core.

**6,306-6,307:** Grayish black laminated mudstone consisting of abundant silica-cemented bands and fractures throughout the interval. The silica-cemented bands (~1/2") contain high concentrations of vertical and ptymatic calcite and pyrite filled fractures (1 mm-1"). The fractures within this interval are thicker than commonly seen throughout core.

**6,307-6,308:** Grayish black laminated mudstone consisting of silica-cemented bands throughout the interval. The silica-cemented bands (~4 mm) contain minor concentrations of vertical and ptymatic calcite fractures (1-4 mm). Three silica clasts (2 mm x 3 mm) occur at 6,307.2 feet.

**6,308-6,309:** Grayish black somewhat laminated mudstone consisting of silica-cemented bands and silt-sized carbonate grains throughout the interval. Silica-cemented bands occur at 6,308.5 (4 mm) and 6,308.7 (3 mm) feet. The cemented bands contain vertical calcite fractures (1-4 mm) that are limited to the height of the cemented band. Silt-sized carbonate burrows occur from 6,308.9-6,309 feet.

**6,309-6,310:** Grayish black somewhat laminated mudstone consisting of silica-cemented bands and silt-sized carbonate grains throughout the interval. Silt-sized disseminated carbonate grains occur at 6,309 feet and contain minor 6 mm calcite vertical fractures. A pyrite nodule (5 mm x 4

mm) occurs at 6,309 feet. Silica-cemented bands occur at 6,309 (5 mm) and 6,309.1 (1") and contain vertical calcite filled fractures (2 mm-1/2").

***Box 3 of 10***

**6,310-6,311:** Grayish black somewhat laminated mudstone consisting of silica-cemented bands in the lower 1/3 of the interval. Silica-cemented bands (~1/2") occur from 6,310.9-6,311 feet and contain high concentrations of vertical and pygmatic calcite fractures ranging from 1 mm to 1/2" long. Thin, compacted disseminated pyrite grains are abundant throughout the interval as well.

**6,311-6,312:** Grayish black somewhat laminated mudstone consisting of silica-cemented bands throughout the interval. Silica-cemented bands (2-3 mm) occur in the top and base of the interval and contain high concentrations of thin to thick pygmatic and vertical calcite filled fractures ranging from 1 mm to 1/2" long.

**6,312-6,313:** Grayish black laminated mudstone consisting of silica-cemented bands and silica-rich laminae throughout the interval. The silica-rich laminations (1-4 mm) contain small micro-sized vertical calcite fractures within the thin laminations. The silica-cemented bands occur more towards the base of the interval and are thicker (~1/2") than the laminations. The bands contain a higher concentration of vertical and pygmatic calcite fractures (1-4 mm). High concentrations of disseminated pyrite grains are evident throughout the interval.

**6,313-6,314:** Grayish black somewhat laminated mudstone consisting of silica-cemented bands throughout the interval. High concentration of calcite pygmatic and vertical fractures occur from 6,313.1-6,313.6 feet and range from 1 mm to 1/2" in length. Most of the thick fractures occur within a 1/2" silica-cemented band at 6,313.5 feet.

**6,314-6,315:** Grayish black laminated mudstone consisting of a silica-cemented zone at the top of the interval and fine silica laminations underlying the cemented zone. The silica-cemented band (1") at the top of the interval contains two sand-sized disseminated pyrite grains and numerous vertical and pygmatic calcite fractures ranging from 1 mm to 1" long. The silica-rich laminations occur from 6,314.1-6,315 feet and contain smaller vertical calcite fractures ranging from 1 mm to 3 mm long.

**6,315-6,316:** Grayish black somewhat laminated mudstone consisting of pyrite laminations and a silica-cemented band in the middle of the interval. A 1/2" silica-cemented band occurs at 6,315.6 feet and contains micro-sized disseminated pyrite grains. A 1 mm pyrite lamination at the base of the interval contains a thick 2 mm vertical calcite fracture.

**6,316-6,317:** Grayish black somewhat laminated mudstone consisting of pyrite laminations, disseminated pyrite grains, and minor silica laminations. A 3 mm pyrite lamination occurs at 6,316.4 feet.

**6,317-6,318:** Grayish black somewhat laminated mudstone consisting of pyrite laminations, disseminated pyrite grains, and minor silica laminations. A 4 mm pyrite lamination occurs at 6,317.2 feet.

**6,318-6,319:** Grayish black somewhat laminated mudstone consisting of minor silica-cemented bands in the upper 1/3 of the interval. Silica-cemented bands at 6,318.1 (6 mm) and 6,318.2 (6 mm) contain vertical calcite filled fractures (1-7 mm) and micro-sized disseminated grains.

***Box 4 of 10***

**6,319-6,320:** Grayish black massive, blocky mudstone containing scattered disseminated pyrite grains.

**6,320-6,321:** Grayish black massive, blocky mudstone containing scattered disseminated pyrite grains.

**6,321-6,322:** Grayish black massive, blocky mudstone containing scattered disseminated pyrite grains.

**6,322-6,323:** Grayish black massive, blocky mudstone containing scattered disseminated pyrite grains. Possible marcasite nodules occur from 6,322.8-6,323 feet.

**6,323-6,324:** Grayish black massive, blocky mudstone containing scattered disseminated pyrite grains. Pyritized sand-sized burrows occur from 6,323.9-6,324 feet.

**6,324-6,325:** Grayish black massive, blocky mudstone containing scattered disseminated pyrite grains occurs from 6,324-6,324.9 feet. A silica-cemented band occurs from 6,324.9-6,325 feet. Possible marcasite nodule at 6,324.95 feet.

**6,325-6,326:** Grayish black somewhat laminated mudstone consisting of minor silica-cemented bands at 6,325.2 feet. Minor disseminated pyrite grains occur throughout the interval.

**6,326-6,327:** Grayish black somewhat laminated mudstone consisting of pyrite laminations and a silica-cemented band at the base of the interval. Two marcasite nodules occur at 6,326.4 feet. 1 mm pyrite laminations occur at 6,326.2 and 6,326.5 feet. A 1" silica-cemented band occurs at 6,326.9 feet and contains numerous vertical and ptymatic calcite filled fractures ranging from 1 mm to 1" long.

**6,327-6,328:** Grayish black laminated mudstone consisting of silica-cemented bands in the upper and lower halves of the interval. Two silica-cemented bands (1" & 5 mm) are evident at the top of the interval and contain numerous vertical and ptymatic calcite fractures ranging from 2 mm to 1" long. Two pyrite nodules (4 mm x 4 mm) occur at 6,327.8 feet. Two more silica-cemented bands (4 mm & 7 mm) occur at 6,327.9 feet and also contain numerous vertical and ptymatic calcite fractures ranging from 2 mm to 7mm long.

*Box 5 of 10*

**6,328-6,329:** Grayish black somewhat laminated mudstone consisting disseminated pyrite grains.

**6,329-6,330:** Grayish black laminated mudstone consisting of silica-cemented bands in the middle half of the interval. Silica-cemented bands (~4 mm) occur from 6,329.5-6,329.8 feet and contain minor vertical calcite filled fractures ranging from 1 mm to 1.5”.

**6,330-6,331:** Grayish black laminated mudstone consisting of abundant silica-rich laminations and a silica-cemented band. The silica-rich laminations (1-5 mm) occur throughout the interval and contain ptygmatic calcite fractures within the laminations ranging from 1 mm to 5 mm long. A silica-cemented band (1/2”) occurs at 6,330.6 feet and contains three sand-sized disseminated pyrite grains as well as numerous vertical and ptygmatic calcite and pyrite filled fractures ranging from 1 mm to 1/2” in size.

**6,331-6,332:** Grayish black laminated mudstone consisting of abundant silica-cemented bands (1 mm-1/2”) containing numerous vertical and ptygmatic pyrite and calcite fractures that range from 1 mm to 1/2” in length. Disseminated pyrite grains are abundant throughout the interval as well.

**6,332-6,333:** Grayish black laminated mudstone consisting of abundant silica-cemented bands (1 mm-1”) containing numerous vertical and ptygmatic pyrite and calcite fractures that range from 1 mm to 1” in length.

**6,333-6,334:** Grayish black laminated mudstone consisting of abundant silica-cemented bands (1 mm-1/2”) containing numerous vertical and ptygmatic pyrite and calcite fractures that range from 1 mm to 1/2” in length.

**6,334-6,335:** Grayish black laminated mudstone consisting of abundant silica-cemented bands (1 mm-1”) containing numerous vertical and ptygmatic pyrite and calcite fractures that range from 1 mm to 1” in length.

**6,335-6,336:** Grayish black laminated mudstone consisting of minor silica-cemented bands (1 mm-1/2”) containing numerous vertical and ptygmatic natural and pyrite and calcite fractures that range from 1 mm to 1/2” in length. Minor 1 mm pyrite laminations and disseminated pyrite grains are evident throughout interval.

**6,336-6,337:** Grayish black laminated mudstone consisting of minor silica-cemented bands (1 mm-1”) containing numerous vertical and ptygmatic natural and pyrite and calcite fractures that range from 1 mm to 1” in length. A highly fractured cemented zone occurs at 6,336.9-6,337 feet.

***Box 6 of 10***

**6,337-6,338:** Grayish black somewhat laminated mudstone consisting of thin (1-3 mm) silica-rich laminations and a silica-cemented band (1"). The silica-rich laminations occur throughout the interval and contain vertical calcite fractures that range from 1 mm to 4 mm long. A marcasite nodule occurs at 6,337.4 feet. A silica-cemented band occurs at 6,337.9 feet and contains vertical calcite fractures that range from 3 mm to 1" long.

**6,338-6,339:** Grayish black somewhat laminated mudstone consisting of a silica-cemented band in the middle of the interval. A ½" silica-cemented band occurs at 6,338.5 feet and contains one vertical 7 mm calcite fracture. Two marcasite nodules occur at 6,338.9 feet.

**6,339-6,340:** Grayish black somewhat laminated mudstone consisting of a silica-cemented band and two 1 mm pyrite laminations. A 4 mm silica-cemented band occurs at 6,339.1 feet and contains small 1-2 mm vertical calcite fractures. Possible pyrites burrow at 6,339.3 feet.

**6,340-6,341:** Grayish black somewhat laminated mudstone consisting of a minor pyrite laminations and one carbonate-rich lamination. A carbonate-rich lamination (1 mm) occurs at 6,340.8 feet and contains a 2 mm thick and 7 mm long calcite filled fracture.

**6,341-6,342:** Grayish black somewhat laminated mudstone consisting of three carbonate-rich laminations at the top of the interval. Three silt-sized carbonate-rich laminations (3 mm, 1 mm, and 3 mm) occur at the top of the interval.

**6,342-6,343:** Grayish black somewhat laminated mudstone consisting of two silica-cemented bands. The two silica-cemented bands (2 mm) occur at 6,342.2 feet and contain small 1 mm vertical calcite fractures. A marcasite nodule occurs at 6,342.9 feet.

**6,343-6,344:** Grayish black laminated mudstone with silica-rich (1 mm) and silica-cemented bands (4 mm) occurring at the base of the interval. The silica-rich zones occur from 6,343.7-6,344 feet with the silica-rich laminations containing 1 mm vertical calcite fractures and the silica-cemented band containing numerous ptygmatic and vertical (1-6 mm) calcite fractures.

**6,344-6,345:** Grayish black somewhat laminated mudstone consisting of minor silica-cemented bands near the base of the interval. Minor disseminated pyrite occurs throughout the interval as well.

**6,345-6,346:** Grayish black somewhat laminated mudstone consisting of minor silica-rich laminations (1-4 mm) near the base of the interval.

***Box 7 of 10***

**6,346-6,347:** Grayish black somewhat laminated mudstone consisting of minor 1 mm pyrite laminations and a pyrite nodule (7 mm x 4 mm) at 6,346.1 feet.



**6,347-6,348:** Grayish black somewhat laminated mudstone consisting of two silica-cemented bands at 6,347.3 (7 mm) and 6,347.9 (7 mm) feet and minor 1 mm pyrite laminations. Two coarse disseminated pyrite grains occur at 6,347.4 feet.

**6,348-6,349:** Grayish black somewhat laminated mudstone consisting of disseminated pyrite grains and one 1 mm silica-rich lamination at 6,348.3 feet.

**6,349-6,350:** Grayish black poorly to somewhat laminated mudstone consisting of a ½" silica-cemented zone at 6,349.9 feet containing numerous vertical and ptigmatic natural fractures.

**6,350-6,351:** Grayish black poorly to somewhat laminated mudstone transitioning into a blocky broken up mudstone.

**6,351-6,352:** Grayish black somewhat laminated mudstone containing disseminated pyrite grains and minor 1 mm silica-rich laminations. A silica-rich lamination at 6,351.7 feet contains minor 1 mm vertical calcite fractures.

**6,352-6,353:** Grayish black laminated mudstone containing thin silica-rich laminations and minor disseminated pyrite grains. Silica rich laminations at 6,352.7 (1 mm), 6,352.8 (3 mm), and 6,352.9 (1 mm) contain numerous vertical and ptigmatic calcite and pyrite filled fractures ranging from 1 mm to ½" long.

**6,353-6,354:** Grayish black laminated mudstone containing thin silica-rich laminations and minor disseminated pyrite grains. Possible marcasite nodule occurs at 6,353.4 feet overlying a 1 mm x 1 mm pyrite grain. Two silica-rich laminations (1 mm & 5 mm) occur at 6,353.9 feet and contain three vertical pyrite filled (5 mm) fractures.

**6,354-6,355:** Grayish black laminated mudstone containing numerous very fine laminations of pyrite throughout the interval. Minor disseminated pyrite grains are evident throughout interval as well.

#### ***Box 8 of 10***

**6,355-6,356:** Grayish black laminated mudstone containing numerous very fine laminations of pyrite throughout the interval and two 4 mm silica-rich laminations. The two silica-rich laminations occur at 6,355.2 and 6,355.5 feet and contain vertical calcite and pyrite fractures that range from 1 mm to 5 mm long. A pyrite nodule (1/2"x1/2") occurs at the base of the interval.

**6,356-6,357:** Grayish black laminated mudstone containing numerous very fine laminations of pyrite throughout the interval. A 1 mm vertical calcite fracture occurs within two 1 mm pyrite laminations at 6,356.8 feet.

**6,357-6,358:** Grayish black laminated mudstone containing numerous very fine laminations of pyrite throughout the interval. Possible marcasite nodule occurs at the base of the interval.

**6,358-6,359:** Grayish black laminated mudstone containing numerous very fine laminations of pyrite throughout the interval. A 2 mm silica-rich lamination occurs at the base of the interval.

**6,359-6,360:** Grayish black laminated mudstone containing numerous very fine laminations of pyrite throughout the interval.

**6,360-6,361:** Grayish black laminated mudstone containing numerous very fine laminations of pyrite throughout the interval.

**6,361-6,362:** Grayish black somewhat laminated mudstone with minor silica-rich laminations occurring throughout the interval. A 3 mm silica-rich lamina occurs at 6,361.6 feet and a 4 mm silica-rich lamina occurs at 6,361.9 feet. Both silica-rich laminations contain vertical 1 mm calcite fractures.

**6,362-6,363:** Grayish black somewhat laminated mudstone with minor silica-rich laminations occurring throughout the interval. A 3 mm silica-rich lamina occurs at 6,361.7 feet and a 4 mm silica-rich lamina occurs at 6,361.9 feet.

**6,363-6,364:** Grayish black laminated mudstone containing numerous very fine laminations of pyrite throughout the interval and a 1 mm silica-rich lamination at 6,363.6 feet.

***Box 9 of 10***

**6,364-6,365:** Grayish black laminated mudstone containing numerous very fine laminations of pyrite throughout the interval and a 1 mm silica-rich lamination at 6,364.3 feet.

**6,365-6,366:** Grayish black laminated mudstone containing numerous very fine laminations of pyrite throughout the interval and two 1 mm silica-rich laminations at 6,365.6 feet and 6,365.9 feet, the latter containing two 3 mm vertical pyrite filled fracture.

**6,366-6,367:** Grayish black laminated mudstone containing numerous very fine laminations of pyrite throughout the interval and one 3 mm silica-rich lamination at 6,366.9 feet. A marcasite nodule occurs at 6,366.4 feet.

**6,367-6,368:** Grayish black laminated mudstone containing numerous very fine laminations of pyrite throughout the interval and one 5 mm silica-rich lamination at 6,367.7 feet containing four vertical calcite and pyrite fractures ranging from 1 mm to 4 mm in length.

**6,368-6,369:** Grayish black laminated mudstone containing numerous very fine laminations of pyrite throughout the interval as well as disseminated pyrite grains.

**6,369-6,370:** Grayish black laminated mudstone containing numerous very fine laminations of pyrite throughout the interval.

**6,370-6,371:** Grayish black laminated mudstone containing numerous very fine laminations of pyrite throughout the interval and one 2 mm silica-rich lamination at 6,370.9 feet containing four vertical calcite and pyrite fractures ranging from 1 mm to 4 mm in length.

**6,371-6,372:** Grayish black laminated mudstone containing numerous very fine laminations of pyrite throughout the interval. A 2 mm pyrite lamination occurring at 6,371.9 feet consists of four vertical 1 mm pyrite filled fractures.

**6,372-6,373:** Grayish black laminated mudstone containing fine laminations of pyrite throughout the interval as well as two (2 mm & 5 mm) silica-rich laminations occurring from 6,372.3-6,372.5 feet. The silica-rich laminations contain numerous vertical pyrite filled fractures ranging from 1 mm to 6 mm.

***Box 10 of 10***

**6,373-6,374:** Grayish black laminated mudstone containing numerous very fine laminations of pyrite throughout the interval. Marcasite nodule glob at the base of interval.

**6,374-6,375:** Grayish black laminated mudstone containing numerous very fine laminations of pyrite throughout the interval and one 2 mm silica-rich lamination at 6,374.2 feet.

**6,375-6,376:** Grayish black laminated mudstone containing numerous very fine laminations of pyrite throughout the interval as well as disseminated pyrite grains.

**6,376-6,377:** Grayish black laminated mudstone containing numerous very fine laminations of pyrite throughout the interval as well as disseminated pyrite grains. 2 mm pyrite lamination at 6,376.1 feet contains small vertical pyrite filled fractures (1 mm).

**6,377-6,378:** Grayish black laminated mudstone containing numerous very fine laminations of pyrite throughout the interval as well as disseminated pyrite grains.

**6,378-6,379:** Grayish black laminated mudstone containing numerous very fine laminations of pyrite throughout the interval as well as disseminated pyrite grains.

**6,379-6,380:** Grayish black laminated mudstone containing fine laminations of pyrite throughout the interval as well as disseminated pyrite grains. A 4 mm silica-rich lamination occurs at 6,379.6 feet containing small 1 mm vertical calcite fractures.

**6,380-6,381:** Grayish black laminated mudstone containing fine laminations of pyrite throughout the interval as well as disseminated pyrite grains. A 1 mm pyrite lamination at 6,380.5 feet contains small 1 mm vertical pyrite and calcite fractures.

**6,381-6,382:** Grayish black laminated mudstone containing fine laminations of pyrite and silica with 1-2 mm vertical calcite fractures transitions into a blocky, broken-up mudstone.

***Box 1 of 12***

**6,381.9-6,382:** Grayish black blocky, broken-up mudstone.

***Box 2 of 12***

**6,382-6,883:** Grayish black laminated mudstone containing fine laminations of pyrite and one 1 mm laminations of silica at 6,382.1 feet.

**6,383-6,384:** Grayish black laminated mudstone containing fine laminations of pyrite throughout the interval as well as disseminated pyrite grains.

**6,384-6,385:** Grayish black laminated mudstone containing fine laminations of pyrite throughout the interval as well as disseminated pyrite grains.

**6,385-6,386:** Grayish black laminated mudstone containing fine laminations of pyrite throughout the interval as well as disseminated pyrite grains. Two phosphate nodules (2 mm x 5 mm) occur from 6,385.4-6,385.5 feet. Marcasite nodules occur at the very base of the interval.

**6,386-6,387:** Grayish black laminated mudstone containing fine laminations of pyrite throughout the interval as well as marcasite nodules. A pyrite nodule (2 mm x 4 mm) occurs at 6,386.4 feet.

**6,387-6,388:** Grayish black laminated mudstone containing fine laminations of pyrite throughout the interval as well as minor marcasite nodules.

**6,388-6,389:** Grayish black laminated mudstone containing fine laminations of pyrite throughout the interval as well as disseminated pyrite grains. A phosphate nodule (1 mm x 1 mm) occurs at the very top of the interval.

**6,389-6,390:** Grayish black laminated mudstone containing fine laminations of pyrite throughout the interval as well as disseminated pyrite grains. Marcasite nodules occur at the very base of the interval.

**6,390-6,391:** Grayish black laminated mudstone containing minor laminations of pyrite and a 3 mm silica-cemented zone at the base of the interval.

***Box 3 of 12***

**6,391-6,392:** Grayish black laminated mudstone containing fine laminations of pyrite, disseminated pyrite grains, and a 7 mm silica-cemented band near the base of the interval containing numerous vertical natural fractures ranging from 5 to 7 mm.

**6,392-6,393:** Missing core

**6,393-6,394:** Grayish black laminated mudstone containing abundant silica-cemented bands. The silica-cemented bands range from 2 mm to 1" thick and contain numerous vertical and pygmatic natural and calcite filled fractures ranging from 1 mm to 1" long.

**6,394-6,395:** Grayish black laminated mudstone containing silica-cemented bands near the top of the interval. A 1" thick silica-cemented band at the top of the interval contains numerous 3 mm to 1" vertical natural fractures within the cemented band. Minor disseminated pyrite grains are evident throughout the interval as well.

**6,395-6,396:** Grayish black laminated mudstone containing silica-cemented bands near the lower half of the interval. The silica cemented bands (~1/2") contain numerous vertical and pygmatic natural fractures that are limited to the cemented bands height. A pyrite nodule (2 mm x 5 mm) occurs at 6,395.9 feet.

**6,396-6,397:** Grayish black laminated mudstone containing fine laminations of pyrite and disseminated pyrite grains.

**6,397-6,398:** Grayish black massive mudstone containing minor disseminated pyrite grains.

**6,398-6,399:** Grayish black massive mudstone containing minor disseminated pyrite grains. Possible pyrite burrows at the base of the interval.

**6,399-6,400:** Grayish black massive mudstone containing marcasite nodules.

***Box 4 of 12***

**6,400-6,401:** Grayish black massive mudstone containing marcasite nodules.

**6,401-6,402:** Grayish black massive mudstone containing marcasite nodules.

**6,402-6,403:** Grayish black massive mudstone containing marcasite nodules and disseminated pyrite grains.

**6,403-6,404:** Grayish black massive mudstone containing marcasite nodules and disseminated pyrite grains.

**6,404-6,405:** Grayish black massive mudstone containing marcasite nodules and disseminated pyrite grains.

**6,405-6,406:** Grayish black massive mudstone containing marcasite nodules and disseminated pyrite grains.

**6,406-6,407:** Grayish black massive mudstone containing marcasite nodules and disseminated pyrite grains.

**6,407-6,408:** Grayish black massive mudstone containing marcasite nodules and disseminated pyrite grains.

**6,408-6,409:** Grayish black massive mudstone containing marcasite nodules and disseminated pyrite grains.

***Box 5 of 12***

**6,409-6,410:** Grayish black massive mudstone containing marcasite nodules and disseminated pyrite grains.

**6,410-6,411.8:** Missing core

**6,411.8-6,412:** Grayish black massive mudstone containing marcasite nodules and disseminated pyrite grains.

**6,412-6,413:** Grayish black massive mudstone containing disseminated pyrite grains.

**6,413-6,414:** Grayish black massive mudstone containing disseminated pyrite grains.

**6,414-6,415:** Grayish black massive mudstone containing disseminated pyrite grains, marcasite nodules, and phosphate nodules (near base of interval).

**6,415-6,416:** Grayish black massive mudstone containing disseminated pyrite grains and small phosphate nodules.

**6,416-6,417:** Grayish black laminated mudstone containing disseminated pyrite grains and minor phosphate nodules (6,416.6 feet).

**6,417-6,418:** Grayish black laminated mudstone containing disseminated pyrite grains and marcasite nodules and one phosphate nodule (1 mm x 1 mm) at 6,417.1 feet.

***Box 6 of 12***

**6,418-6,427:** Medium dark gray to medium gray (N4-N5) limestone containing bioturbation and abundant skeletal fossils.

Williams 1H-7X Chemostratigraphy

Depth	Al	V	Cr	U	Zn	Cu	Ni	Ca	Ti	Si	K	Zr	Sr	V/Cr	V/(V+Ni)
12740.5	0.39	0.00	0.00	#VALUE!	0.01	0.00	#VALUE!	28.58	0.09	4.44	0.49	0.00	0.00	2.44	
12741.5	0.38	0.01	0.00	#VALUE!	0.01	#VALUE!	#VALUE!	25.84	0.08	4.80	0.52	0.00	0.00	2.67	
12742.5	0.98	0.01	0.00	#VALUE!	0.01	#VALUE!	#VALUE!	14.87	0.18	7.40	1.33	0.01	0.00	2.00	
12742.83	1.43	0.02	0.02	0.00	0.09	0.00	#VALUE!	2.92	0.29	10.58	2.08	0.01	0.00	1.18	
12743	1.62	0.02	0.01	#VALUE!	0.01	#VALUE!	#VALUE!	0.16	0.30	13.47	2.41	0.01	0.00	3.50	
12743.4	1.52	0.05	0.01	0.00	0.01	0.00	0.00	0.23	0.29	11.70	2.33	0.01	0.00	4.85	0.90
12744.17	1.19	0.07	0.01	0.00	0.03	0.00	#VALUE!	0.08	0.32	11.75	2.37	0.01	0.00	11.56	
12744.5	1.20	0.01	0.00	#VALUE!	0.00	#VALUE!	0.02	2.69	0.22	9.33	1.98	0.01	0.00	3.71	0.33
12744.75	1.33	0.01	0.00	#VALUE!	0.00	#VALUE!	#VALUE!	3.76	0.28	10.96	2.26	0.01	0.00	2.53	
12744.83	1.42	0.05	0.00	0.00	0.04	0.00	#VALUE!	4.97	0.27	10.80	2.31	0.01	0.00	35.71	
12745.5	0.93	0.10	0.00	0.01	0.03	0.00	0.00	4.53	0.21	9.29	1.80	0.01	0.00	32.71	0.98
12746.5	1.43	0.02	#VALUE!	#VALUE!	0.00	#VALUE!	#VALUE!	0.81	0.34	12.46	2.65	0.01	0.00	#VALUE!	
12747.5	1.46	0.02	0.00	0.00	0.00	#VALUE!	0.00	0.43	0.34	12.79	2.51	0.01	0.00	8.91	0.88
12748.5	1.37	0.02	#VALUE!	0.00	0.00	#VALUE!	0.03	2.15	0.26	10.76	1.96	0.01	0.00	#VALUE!	0.39



12749. 5	1.56	0.03	0.00	0.00	0.01	0.00	0.01	2.25	0.29	11.6 8	2.17	0.01	0.00	16.18	0.70
12750. 5	0.98	0.01	0.00	#VALU E!	0.00	#VALU E!	0.01	2.03	0.25	9.63	1.79	0.01	0.00	7.67	0.53
12751. 5	0.87	0.06	#VALU E!	0.00	0.04	0.00	#VALU E!	4.21	0.24	9.77	1.87	0.01	0.00	#VALU E!	
12752. 5	0.70	0.02	0.00	0.00	0.01	#VALU E!	0.00	1.16	0.15	14.9 3	1.16	0.01	0.00	63.00	0.88
12753. 5	0.53	0.18	0.00	0.00	0.58	0.00	#VALU E!	1.06	0.14	12.7 1	1.00	0.00	0.00	40.96	
12754. 5	0.91	0.01	0.00	#VALU E!	0.01	#VALU E!	#VALU E!	1.45	0.18	13.5 8	1.29	0.01	0.00	10.00	
12755. 5	0.46	0.01	0.00	#VALU E!	0.02	#VALU E!	#VALU E!	2.31	0.10	14.6 2	0.71	0.00	0.00	3.00	
12756. 5	0.32	0.01	0.00	#VALU E!	0.02	0.00	#VALU E!	1.44	0.09	12.7 3	0.63	0.00	0.00	4.00	
12757. 5	0.73	0.01	0.00	0.00	0.02	0.00	#VALU E!	1.63	0.16	13.6 6	1.09	0.01	0.00	3.22	
12758. 5	0.67	0.00	0.00	#VALU E!	0.00	#VALU E!	#VALU E!	4.83	0.14	12.8 0	1.09	0.01	0.00	5.20	
12759. 5	1.10	0.02	0.00	#VALU E!	0.01	0.00	#VALU E!	2.84	0.23	12.9 1	1.66	0.01	0.00	7.00	
12760. 5	1.01	0.02	0.00	#VALU E!	0.03	0.00	0.01	1.38	0.18	14.8 5	1.33	0.01	0.00	5.73	0.64
12761. 5	0.76	0.01	0.00	0.00	0.00	0.00	0.00	1.10	0.16	15.1 6	1.07	0.01	0.00	22.00	0.61
12762. 5	0.90	0.06	0.00	0.00	0.02	0.00	0.00	0.80	0.19	14.8 4	1.30	0.01	0.00	28.36	0.93
12763. 5	0.87	0.01	0.00	0.00	0.00	#VALU E!	0.00	1.52	0.18	15.0 4	1.21	0.01	0.00	14.00	0.67
12764. 5	0.81	0.02	#VALU E!	#VALU E!	0.01	#VALU E!	#VALU E!	1.36	0.18	13.8 0	1.28	0.01	0.00	#VALU E!	
12765. 5	0.92	0.15	0.00	0.00	0.12	0.00	#VALU E!	0.88	0.21	13.9 8	1.52	0.01	0.00	45.05	

12766. 5	0.81	0.05	0.00	0.00	0.12	0.00	#VALU E!	1.16	0.17	14.2 3	1.15	0.01	0.00	56.40	
12767. 5	0.41	0.01	0.00	0.00	0.01	0.00	#VALU E!	1.01	0.10	14.9 8	0.65	0.00	0.00	9.67	
12768. 5	0.42	0.00	0.00	0.00	#VALU E!	#VALU E!	#VALU E!	0.80	0.08	16.8 4	0.50	0.00	0.00	1.69	
12769. 5	0.33	0.00	#VALU E!	0.00	#VALU E!	#VALU E!	#VALU E!	0.48	0.04	20.0 8	0.31	0.00	0.00	#VALU E!	
12770. 5	1.08	0.04	0.00	0.00	0.02	0.00	0.00	1.22	0.21	15.0 6	1.42	0.01	0.00	23.20	0.92
12771. 5	0.83	0.03	0.00	#VALU E!	0.02	#VALU E!	0.01	1.51	0.19	13.2 1	1.28	0.01	0.00	32.00	0.81
12772. 5	0.24	0.03	0.00	0.00	0.01	0.00	#VALU E!	0.35	0.03	19.2 1	0.22	0.00	0.00	13.45	
12773. 5	0.88	0.03	#VALU E!	0.00	0.01	0.00	0.00	0.71	0.17	15.8 7	1.15	0.01	0.00	#VALU E!	0.94
12774. 5	0.91	0.06	0.00	0.00	0.03	0.00	#VALU E!	0.99	0.18	14.7 9	1.18	0.01	0.00	29.33	
12775. 5	0.70	0.01	0.00	0.00	0.03	0.00	#VALU E!	5.29	0.15	11.8 4	0.96	0.01	0.00	8.75	
12776. 5	1.03	0.02	0.00	0.00	0.01	0.00	#VALU E!	2.47	0.20	11.6 6	1.45	0.01	0.00	38.67	
12777. 5	0.57	0.02	0.00	0.00	0.01	0.00	#VALU E!	1.26	0.15	13.9 5	0.89	0.01	0.00	5.38	
12778. 5	0.93	0.01	0.00	0.00	0.00	#VALU E!	#VALU E!	0.65	0.19	15.5 5	1.26	0.01	0.00	6.57	
12779. 5	0.50	0.08	0.00	0.00	0.01	0.00	#VALU E!	0.77	0.13	15.5 6	0.77	0.00	0.00	28.00	
12780. 5	0.35	0.06	0.00	0.00	0.02	0.00	#VALU E!	0.74	0.15	10.7 0	0.79	0.01	0.00	42.00	
12781. 5	0.24	0.02	#VALU E!	0.00	0.01	0.00	#VALU E!	1.71	0.05	14.2 9	0.35	0.00	0.00	#VALU E!	
12782. 5	0.58	0.09	0.00	0.00	0.25	0.00	#VALU E!	2.35	0.13	13.8 8	0.75	0.00	0.00	37.38	

12783. 5	0.76	0.02	0.00	#VALU E!	0.02	0.00	#VALU E!	1.08	0.19	13.2 1	1.25	0.01	0.00	10.20	
12784. 5	0.92	0.01	0.00	0.00	0.01	0.00	#VALU E!	0.79	0.19	14.8 4	1.32	0.01	0.00	13.00	
12785. 5	0.00	0.02	0.00	#VALU E!	0.02	0.00	#VALU E!	0.00	#VALU E!	0.00	0.00	0.00	0.00	16.33	
12786. 5	0.57	0.04	0.00	#VALU E!	0.12	0.00	#VALU E!	0.86	0.13	14.1 5	0.80	0.00	0.00	14.75	
12787. 83	0.30	0.03	0.00	0.00	0.00	#VALU E!	#VALU E!	0.68	0.07	14.4 7	0.45	0.00	0.00	11.18	
12788. 5	0.63	0.02	0.00	0.01	0.01	0.00	#VALU E!	0.97	0.15	14.8 7	0.87	0.01	0.00	9.56	
12789. 5	0.00	0.01	0.00	0.01	0.02	0.00	#VALU E!	1.10	0.20	0.00	1.22	0.01	0.00	5.33	
12790. 5	0.86	0.01	0.00	0.00	0.02	0.00	#VALU E!	1.10	0.20	13.8 3	1.23	0.01	0.00	4.00	
12791. 3	0.69	0.01	0.00	0.00	0.03	0.00	#VALU E!	1.43	0.19	13.4 0	1.21	0.01	0.00	4.91	
12792. 5	0.00	0.01	0.00	0.00	0.02	0.00	#VALU E!	0.83	0.20	0.00	1.33	0.01	0.00	5.20	
12793. 5	0.85	0.01	0.00	0.00	0.02	0.00	#VALU E!	0.86	0.20	13.8 3	1.28	0.01	0.00	4.00	
12794. 5	0.91	0.00	#VALU E!	0.00	0.00	#VALU E!	0.00	0.83	0.22	13.2 1	1.31	0.01	0.00	#VALU E!	0.33
12795. 5	0.65	0.02	0.00	0.00	0.02	0.00	#VALU E!	3.85	0.18	12.6 2	1.06	0.01	0.00	9.20	
12796. 5	1.46	0.02	0.00	0.00	0.02	0.00	0.01	1.83	0.24	14.4 7	1.51	0.01	0.00	8.80	0.74
12797. 5	0.85	0.01	0.00	0.00	0.02	0.00	#VALU E!	1.06	0.21	13.2 9	1.29	0.01	0.00	8.00	
12798. 5	0.48	0.01	0.00	0.00	0.02	0.00	#VALU E!	0.83	0.17	12.4 7	1.01	0.01	0.00	4.17	
12799. 5	1.28	0.01	0.00	0.00	0.01	0.00	#VALU E!	2.65	0.24	14.6 8	1.60	0.01	0.00	2.63	

12800. 5	1.07	0.01	0.00	0.00	0.01	0.00	0.00	1.88	0.22	14.7 5	1.40	0.01	0.00	4.25	0.59
12801. 5	0.61	0.00	0.00	0.00	0.00	0.00	#VALU E!	1.01	0.14	15.4 2	0.92	0.01	0.00	2.22	
12802. 5	0.25	#VALU E!	0.00	#VALU E!	0.00	#VALU E!	#VALU E!	0.39	0.04	15.1 8	0.24	0.00	0.00	#VALU E!	
12803. 5	0.65	0.01	0.00	0.00	0.00	0.00	0.00	1.06	0.14	16.1 4	0.90	0.01	0.00	4.00	0.76
12804. 5	0.44	0.01	0.00	0.00	0.01	0.00	#VALU E!	0.83	0.09	14.9 2	0.59	0.00	0.00	3.45	
12805. 5	0.69	0.01	0.00	0.00	0.02	0.00	#VALU E!	0.71	0.14	16.0 8	0.91	0.01	0.00	3.82	
12806. 5	0.46	0.01	0.00	0.00	0.01	0.00	#VALU E!	1.58	0.13	12.7 4	0.77	0.01	0.00	3.18	
12807. 5	1.01	0.01	0.00	0.00	0.01	0.00	0.00	1.00	0.22	14.8 5	1.35	0.01	0.00	2.38	0.73
12808. 5	0.98	0.01	0.00	0.00	0.01	0.00	#VALU E!	0.59	0.19	16.1 6	1.21	0.01	0.00	4.18	
12809. 5	0.95	0.01	0.00	0.00	0.01	0.00	0.01	1.03	0.19	14.8 7	1.25	0.01	0.00	2.92	0.50
12810. 5	0.77	0.00	0.00	0.00	0.00	0.00	#VALU E!	1.76	0.18	15.3 0	1.16	0.01	0.00	2.40	
12811. 5	0.82	0.01	0.00	0.00	0.01	0.00	#VALU E!	1.13	0.16	16.0 3	1.09	0.01	0.00	3.40	
12812. 5	0.83	0.01	0.00	0.00	0.01	0.00	#VALU E!	0.56	0.17	15.3 4	1.30	0.01	0.00	3.80	
12813. 5	0.78	#VALU E!	#VALU E!	0.00	0.00	#VALU E!	#VALU E!	1.61	0.20	13.0 3	1.25	0.01	0.00	#VALU E!	
12814. 5	0.25	0.01	0.00	0.00	0.01	0.00	#VALU E!	0.79	0.03	20.0 2	0.21	0.00	0.00	2.92	
12815. 5	0.99	0.01	0.00	0.00	0.01	0.00	#VALU E!	1.05	0.21	14.8 2	1.38	0.01	0.00	2.91	
12816. 5	0.82	0.00	0.00	0.00	0.01	0.00	0.00	1.12	0.20	13.9 0	1.18	0.01	0.00	2.60	0.60

12817. 5	0.74	0.01	0.00	0.00	0.01	0.00	#VALU E!	1.24	0.17	13.1 5	1.09	0.01	0.00	3.07	
12818. 5	0.43	0.01	0.00	0.00	0.01	0.00	0.00	0.76	0.08	17.3 5	0.51	0.00	0.00	4.91	0.84
12819. 5	0.26	0.01	0.00	0.00	0.01	0.00	#VALU E!	0.81	0.05	17.7 5	0.31	0.00	0.00	2.86	
12820. 5	0.77	0.01	0.00	0.00	0.01	0.00	0.01	3.31	0.16	14.2 1	1.06	0.01	0.00	2.83	0.50
12821. 5	0.60	0.01	0.00	0.00	0.00	0.00	0.01	1.24	0.15	14.0 2	0.86	0.01	0.00	2.62	0.45
12822. 5	0.61	0.01	0.00	0.00	0.01	0.00	#VALU E!	2.87	0.12	15.4 3	0.82	0.00	0.00	4.60	
12823. 5	0.28	0.01	0.00	0.00	0.01	0.00	#VALU E!	0.57	0.06	16.4 5	0.37	0.00	0.00	3.38	
12824. 5	0.24	0.00	0.00	0.00	0.00	#VALU E!	0.00	0.98	0.05	12.3 8	0.35	0.00	0.00	2.00	0.33
12825. 5	0.84	0.01	0.00	0.00	0.02	0.00	#VALU E!	1.81	0.21	13.2 7	1.38	0.01	0.00	2.53	
12826. 5	0.78	0.00	0.00	0.00	0.01	#VALU E!	#VALU E!	1.61	0.16	15.7 7	1.08	0.01	0.00	1.50	
12827. 55	0.56	0.01	0.00	0.00	0.01	0.00	0.00	1.90	0.11	16.1 2	0.64	0.00	0.00	4.25	0.71
12828. 5	0.70	#VALU E!	0.00	0.00	#VALU E!	#VALU E!	0.00	1.66	0.16	13.2 1	1.05	0.01	0.00	#VALU E!	
12829. 5	0.77	0.00	#VALU E!	0.00	0.01	#VALU E!	#VALU E!	1.90	0.15	16.4 4	0.93	0.01	0.00	#VALU E!	
12830. 5	0.49	0.01	0.00	0.00	0.01	0.00	#VALU E!	1.92	0.14	12.0 1	0.82	0.01	0.00	3.20	
12831. 5	0.66	0.00	0.00	0.00	#VALU E!	#VALU E!	#VALU E!	0.77	0.17	12.2 7	1.08	0.01	0.00	0.86	
12832. 5	0.95	0.01	0.00	0.00	0.01	0.00	0.00	1.48	0.18	15.1 4	1.20	0.01	0.00	4.67	0.67
12833. 5	0.61	0.01	0.00	0.00	0.01	0.00	#VALU E!	3.41	0.18	12.1 2	1.05	0.01	0.00	2.59	

12834. 5	0.36	0.00	0.00	0.00	0.00	#VALU E!	#VALU E!	17.5 6	0.07	7.47	0.42	0.00	0.01	2.50	
12835. 5	0.82	0.01	0.00	0.00	0.01	0.00	#VALU E!	4.68	0.17	13.4 1	1.15	0.01	0.00	3.00	
12836. 5	0.68	0.00	0.00	0.00	0.00	#VALU E!	#VALU E!	3.36	0.17	10.5 1	1.09	0.01	0.00	2.25	
12837. 5	1.17	0.01	0.00	0.00	0.00	0.00	0.00	2.72	0.20	14.0 2	1.39	0.01	0.00	2.50	0.55
12838. 5	0.79	0.01	0.00	0.00	0.00	0.00	#VALU E!	2.42	0.19	12.7 3	1.21	0.01	0.00	2.31	
12839. 4	0.75	0.01	0.00	0.00	0.01	0.00	#VALU E!	4.19	0.19	9.63	1.45	0.01	0.00	4.00	
12840. 5	0.82	0.01	0.00	0.00	0.01	0.00	#VALU E!	2.81	0.20	11.6 0	1.40	0.01	0.00	3.00	
12841. 5	0.82	0.01	0.00	0.00	0.02	0.00	0.01	2.87	0.18	9.21	1.10	0.01	0.00	2.11	0.47
12842. 5	0.61	0.01	0.00	0.00	0.01	0.00	#VALU E!	2.84	0.22	8.54	1.46	0.01	0.00	3.69	
12843. 5	0.59	0.00	0.00	0.00	0.00	0.00	#VALU E!	11.4 3	0.14	7.51	1.01	0.01	0.01	2.60	
12844. 5	0.68	#VALU E!	0.00	#VALU E!	#VALU E!	#VALU E!	#VALU E!	0.74	0.18	12.7 8	1.09	0.01	0.00	#VALU E!	
12845. 5	1.13	0.00	0.00	0.00	0.00	0.00	#VALU E!	0.38	0.22	14.9 3	1.35	0.01	0.00	1.86	
12846. 5	0.85	0.01	0.00	0.00	0.01	0.00	#VALU E!	0.30	0.18	15.6 4	0.97	0.01	0.00	3.83	
12847. 5	0.74	0.01	0.00	0.00	0.01	0.00	#VALU E!	0.33	0.16	15.1 3	0.94	0.01	0.00	3.08	
12848. 5	0.66	0.01	0.00	0.00	0.00	0.00	#VALU E!	0.45	0.18	13.0 1	1.00	0.01	0.00	2.00	
12849. 5	0.57	0.01	0.00	0.00	0.00	0.00	#VALU E!	0.33	0.15	13.0 4	0.91	0.00	0.00	3.50	
12850. 5	0.46	0.01	0.00	0.00	0.01	0.00	#VALU E!	0.42	0.07	17.0 0	0.49	0.00	0.00	2.77	

12851. 6	0.27	0.01	0.00	0.00	0.01	0.00	#VALU E!	0.08	0.05	16.5 1	0.28	0.00	0.00	2.86	
12852. 5	0.80	0.01	0.00	0.00	0.01	0.00	0.01	0.69	0.18	14.3 9	0.99	0.01	0.00	2.00	0.56
12853. 5	0.75	0.01	0.00	0.00	0.01	0.00	0.00	0.36	0.17	15.5 2	0.96	0.01	0.00	2.53	0.65
12854. 5	0.25	0.01	0.00	0.00	0.01	0.00	#VALU E!	0.14	0.07	13.5 2	0.37	0.00	0.00	3.08	
12855. 5	0.82	0.00	0.00	0.00	0.00	#VALU E!	#VALU E!	0.53	0.17	16.0 3	0.94	0.01	0.00	1.18	
12856. 5	0.59	0.01	0.00	0.00	0.01	0.00	0.00	0.21	0.14	14.2 8	0.82	0.00	0.00	3.38	0.81
12857. 5	0.36	0.01	0.00	0.00	0.01	0.00	#VALU E!	2.12	0.13	7.59	0.77	0.00	0.00	3.13	
12858. 5	0.69	0.00	0.00	0.00	0.00	#VALU E!	#VALU E!	0.18	0.16	14.3 1	0.98	0.00	0.00	2.00	
12859. 5	0.64	0.00	0.00	0.00	0.00	0.00	#VALU E!	0.48	0.13	14.9 3	0.89	0.00	0.00	3.67	
12860. 5	0.65	0.01	0.00	0.00	0.01	0.00	#VALU E!	2.03	0.12	15.7 8	0.83	0.00	0.00	2.21	
12861. 5	0.35	0.01	0.00	0.00	0.01	0.00	#VALU E!	2.48	0.14	10.0 4	0.90	0.00	0.00	2.18	
12862. 5	0.85	0.01	0.00	0.00	0.01	0.00	#VALU E!	1.45	0.16	15.3 3	0.98	0.01	0.00	2.80	
12863. 3	0.86	0.01	0.00	0.00	0.01	0.00	#VALU E!	1.32	0.17	15.8 1	1.02	0.01	0.00	3.00	
12864. 5	0.44	0.01	0.00	0.00	0.01	0.00	#VALU E!	0.35	0.10	15.2 9	0.65	0.00	0.00	2.78	
12865. 5	0.17	0.01	0.00	0.00	0.01	0.00	#VALU E!	0.13	0.01	19.5 9	0.11	#VALU E!	#VALU E!	2.67	
12866. 5	0.38	0.01	0.00	0.00	0.00	#VALU E!	#VALU E!	0.37	0.07	14.6 4	0.51	0.00	0.00	2.40	
12867. 5	0.70	0.01	0.00	0.00	0.01	0.00	0.00	0.39	0.14	15.4 4	0.89	0.00	0.00	2.29	0.70



12868. 5	0.39	0.01	0.00	0.00	0.01	0.00	0.01	0.33	0.13	11.6 9	0.77	0.00	0.00	2.14	0.47
12869. 5	0.56	0.01	0.00	0.00	0.01	0.00	0.00	0.42	0.13	14.2 0	0.79	0.00	0.00	2.32	0.76
12870. 5	0.47	0.01	0.00	0.00	0.01	0.00	0.02	0.56	0.11	12.7 6	0.69	0.00	0.00	2.33	0.31
12871. 5	0.41	0.01	0.00	0.00	0.00	0.00	0.00	0.32	0.08	14.1 4	0.59	0.00	0.00	2.50	0.74
12872. 5	0.35	0.01	0.00	0.00	0.01	0.00	#VALU E!	0.24	0.10	14.9 9	0.62	0.00	0.00	2.63	
12873. 5	0.18	0.01	0.00	0.00	0.00	0.00	#VALU E!	0.23	0.04	11.7 8	0.24	0.00	0.00	3.09	
12874. 5	0.50	0.01	0.00	0.00	0.00	0.00	0.00	0.25	0.13	12.7 3	0.90	0.00	0.00	2.29	0.54
12875. 5	0.14	0.00	0.00	0.00	#VALU E!	#VALU E!	#VALU E!	0.23	0.02	14.9 7	0.16	#VALU E!	0.00	1.56	
12876. 5	0.34	0.01	0.00	0.00	0.00	0.00	#VALU E!	1.13	0.11	10.1 8	0.66	0.00	0.00	2.00	
12877. 5	0.56	0.01	0.00	0.00	0.01	0.00	0.00	0.34	0.11	16.0 2	0.65	0.00	0.00	2.86	0.70
12878. 5	0.12	0.01	0.00	0.00	0.01	0.00	#VALU E!	0.08	0.02	17.6 8	0.13	#VALU E!	0.00	2.09	
12879. 5	0.51	0.01	0.00	0.00	0.00	#VALU E!	0.01	0.33	0.12	12.8 7	0.77	0.00	0.00	2.00	0.29
12880. 5	0.20	0.00	0.00	0.00	0.00	0.00	#VALU E!	0.09	0.02	20.0 4	0.14	#VALU E!	0.00	2.89	
12881. 5	0.07	0.01	0.00	0.00	0.01	0.00	#VALU E!	0.10	0.01	18.0 7	0.06	#VALU E!	#VALU E!	2.38	
12882. 5	0.48	0.00	0.00	0.00	0.00	0.00	0.01	0.16	0.10	15.0 9	0.62	0.00	0.00	3.00	0.44
12883. 5	0.22	0.01	0.00	0.00	0.00	0.00	#VALU E!	0.12	0.06	13.3 5	0.36	0.00	0.00	3.60	
12884. 5	0.50	0.01	0.00	0.00	0.01	0.00	0.01	0.20	0.15	15.0 6	0.66	0.00	0.00	2.80	0.50

12885. 5	0.19	0.00	0.00	0.00	0.00	0.00	#VALU E!	0.13	0.03	17.4 1	0.18	#VALU E!	0.00	1.78	
12886. 5	0.51	0.00	0.00	0.00	#VALU E!	0.00	0.01	0.19	0.10	14.2 3	0.70	0.00	0.00	1.33	0.23
12887. 5	0.54	0.01	0.00	0.00	0.01	0.00	0.01	0.28	0.11	16.2 7	0.69	0.00	0.00	4.44	0.56
12889. 5	0.29	0.01	0.00	0.00	0.01	0.00	#VALU E!	4.49	0.07	11.9 9	0.49	0.00	0.01	2.50	
12890. 5	0.45	0.01	0.00	0.00	0.01	0.00	0.00	0.23	0.10	15.6 3	0.61	0.00	0.00	4.00	0.74
12891. 5	0.47	0.00	0.00	#VALU E!	#VALU E!	#VALU E!	#VALU E!	0.16	0.10	15.4 9	0.61	0.00	0.00	2.50	
12892. 5	0.67	0.00	0.00	0.00	0.00	0.00	0.00	3.79	0.12	14.5 2	0.72	0.00	0.01	2.86	0.42
12893. 5	0.62	0.01	0.00	0.00	0.01	0.00	0.00	0.60	0.13	14.5 8	0.86	0.00	0.00	2.50	0.59
12894. 5	0.30	0.01	0.00	0.00	0.01	0.00	#VALU E!	0.18	0.07	15.7 6	0.41	0.00	0.00	3.60	
12895. 5	0.43	0.01	0.00	0.00	0.01	0.00	#VALU E!	0.23	0.08	16.0 9	0.53	0.00	0.00	6.18	
12896. 5	0.43	#VALU E!	#VALU E!	#VALU E!	0.00	#VALU E!	0.00	0.18	0.09	14.6 5	0.58	0.00	0.00	#VALU E!	
12897. 5	0.10	0.01	0.00	0.00	0.00	0.00	#VALU E!	0.13	0.01	20.4 7	0.06	#VALU E!	0.00	3.71	
12898. 5	0.70	0.01	0.00	0.00	0.00	0.00	0.00	1.31	0.12	16.3 1	0.85	0.00	0.01	6.18	0.77
12899. 4	0.53	0.01	0.00	0.00	0.01	0.00	#VALU E!	0.30	0.09	15.6 4	0.60	0.00	0.00	4.80	
12900. 5	0.33	0.01	0.00	0.00	0.00	0.00	#VALU E!	0.17	0.07	16.3 1	0.44	0.00	0.00	4.20	
12901. 5	0.51	0.01	0.00	0.00	0.00	0.00	0.00	0.14	0.11	15.0 3	0.72	0.00	0.00	3.71	0.79
12902. 5	0.59	0.02	0.00	0.00	0.01	0.00	0.00	0.37	0.13	15.4 9	0.71	0.00	0.00	8.36	0.82

12903. 5	0.30	0.01	0.00	0.00	0.02	0.00	#VALU E!	1.61	0.09	12.3 9	0.53	0.00	0.00	5.82	
12904. 5	0.67	0.01	0.00	0.00	0.00	0.00	#VALU E!	0.80	0.15	13.9 6	0.88	0.00	0.01	3.17	
12905. 5	0.57	0.01	0.00	0.00	0.01	0.00	0.00	0.18	0.12	14.8 0	0.74	0.00	0.00	9.67	0.74
12906. 5	0.46	0.01	0.00	0.00	0.00	0.00	#VALU E!	0.11	0.11	14.7 4	0.72	0.00	0.00	2.55	
12907. 5	0.49	0.01	0.00	0.00	0.01	0.00	#VALU E!	0.04	0.08	15.8 8	0.57	0.00	0.00	6.86	
12908. 5	0.10	0.01	0.00	0.00	0.00	0.00	#VALU E!	0.15	0.01	15.3 9	0.08	#VALU E!	0.00	4.00	
12909. 5	0.39	0.01	0.00	0.00	0.00	0.00	#VALU E!	10.5 7	0.07	10.3 6	0.46	0.00	0.01	5.20	
12910. 5	0.36	0.01	0.00	0.00	0.01	0.00	#VALU E!	0.16	0.07	16.7 3	0.48	0.00	0.00	5.50	
12911. 33	0.43	0.01	0.00	0.00	0.00	0.00	#VALU E!	0.47	0.12	12.7 1	0.84	0.00	0.00	5.83	
12912. 5	0.69	0.01	0.00	0.00	0.01	0.00	#VALU E!	0.70	0.15	15.4 4	1.11	0.00	0.00	5.85	
12913. 5	0.61	0.01	0.00	0.00	0.01	0.00	#VALU E!	0.34	0.11	16.0 5	0.88	0.00	0.00	4.13	
12914. 5	0.70	0.01	0.00	0.00	0.02	0.00	#VALU E!	0.40	0.15	16.1 1	0.98	0.01	0.00	3.40	
12915. 5	0.79	0.01	0.00	0.00	0.00	0.00	0.00	0.45	0.15	16.1 0	1.02	0.01	0.00	2.77	0.64
12916. 5	0.12	0.01	0.00	0.00	0.01	0.00	#VALU E!	0.16	0.01	18.8 1	0.07	#VALU E!	0.00	3.25	
12917. 5	0.64	#VALU E!	#VALU E!	0.00	0.01	0.00	0.01	0.13	0.14	12.5 2	0.90	0.01	0.00	#VALU E!	
12917. 5	0.69	0.01	0.00	0.00	0.01	0.00	0.01	0.15	0.14	15.7 2	0.88	0.00	0.00	3.57	0.59
12918. 5	0.55	0.01	0.00	0.00	0.00	0.00	0.01	0.81	0.11	14.5 6	0.63	0.00	0.00	3.00	0.31

12919. 5	0.52	0.01	0.00	0.00	0.01	0.00	0.01	0.14	0.13	11.3 8	0.81	0.00	0.00	4.00	0.42
12919. 5	0.98	0.01	0.00	0.00	0.01	0.00	0.01	0.89	0.16	15.6 6	1.03	0.01	0.00	3.67	0.38
12920. 5	0.00	0.01	0.00	0.00	0.01	0.00	0.01	38.2 1	0.02	2.09	0.13	0.01	0.05	4.44	
12921. 5	1.33	0.00	0.00	0.00	0.01	0.00	#VALU E!	0.10	0.29	13.4 0	1.88	0.01	0.00	1.50	
12922. 5	0.57	#VALU E!	#VALU E!	#VALU E!	#VALU E!	#VALU E!	#VALU E!	0.18	0.10	15.6 4	0.83	0.00	0.00	#VALU E!	
12922. 5	0.27	0.01	0.00	0.00	0.01	0.00	#VALU E!	0.10	0.04	18.2 3	0.30	0.00	0.00	7.60	
12923. 3	0.45	0.01	0.00	0.00	0.01	0.00	#VALU E!	7.19	0.08	12.8 7	0.55	0.00	0.01	5.80	
12924. 5	0.29	0.01	0.00	0.00	0.01	0.00	#VALU E!	0.31	0.05	19.4 9	0.31	0.00	0.00	4.14	
12925. 5	0.84	0.01	0.00	0.00	0.00	0.00	#VALU E!	0.36	0.14	17.1 3	0.95	0.00	0.00	3.00	
12926. 5	0.29	0.00	0.00	0.00	0.00	#VALU E!	#VALU E!	0.08	0.04	19.5 0	0.27	0.00	0.00	1.80	
12927. 5	0.44	0.01	0.00	0.00	0.01	0.00	0.00	0.14	0.07	17.9 6	0.53	0.00	0.00	3.00	0.67
12928. 5	0.63	0.01	0.00	0.00	0.01	0.00	0.01	0.12	0.13	15.4 6	0.85	0.00	0.00	4.60	0.37
12929. 5	0.12	0.01	0.00	0.00	0.01	0.00	#VALU E!	0.06	0.02	18.2 8	0.11	#VALU E!	0.00	9.00	
12930. 5	0.57	0.01	0.00	0.00	0.00	0.00	0.01	0.65	0.12	13.9 7	0.85	0.00	0.00	3.67	0.59
12931. 5	0.34	0.01	0.00	0.00	0.00	0.00	0.00	0.09	0.05	19.4 3	0.31	0.00	0.00	3.85	0.74
12932. 5	0.34	0.01	0.00	0.00	0.00	0.00	0.00	1.39	0.06	14.1 8	0.36	0.00	0.00	2.80	0.67
12933. 5	0.63	0.01	0.00	0.00	0.01	0.00	0.01	0.12	0.13	15.6 3	0.88	0.00	0.00	3.29	0.43

12934. 5	0.28	0.01	0.00	0.00	0.02	0.00	#VALU E!	0.07	0.03	19.6 6	0.24	0.00	0.00	4.55	
12935. 3	0.79	#VALU E!	0.00	#VALU E!	0.00	0.00	0.00	0.15	0.16	16.2 8	0.96	0.01	0.00	#VALU E!	
12936. 5	0.16	0.01	0.00	0.00	0.03	0.00	#VALU E!	0.09	0.03	19.1 4	0.18	0.00	0.00	3.75	
12937. 5	0.54	0.01	0.00	0.00	0.01	0.00	0.01	0.15	0.11	16.7 1	0.67	0.00	0.00	4.92	0.48
12938. 5	0.17	0.00	0.00	0.00	0.01	0.00	#VALU E!	0.23	0.02	20.6 7	0.10	#VALU E!	0.00	4.00	
12939. 5	0.10	0.01	0.00	0.00	0.02	0.00	#VALU E!	0.20	0.02	14.9 3	0.13	#VALU E!	0.00	3.00	
12940. 5	0.65	0.01	0.00	0.00	0.00	0.00	#VALU E!	0.40	0.12	17.5 4	0.73	0.00	0.00	3.00	
12941. 5	0.38	0.01	0.00	0.00	0.01	0.00	#VALU E!	0.16	0.07	16.4 7	0.43	0.00	0.00	2.88	
12942. 5	0.68	0.01	0.00	0.00	0.01	0.00	0.01	0.15	0.14	15.2 9	0.96	0.00	0.00	5.43	0.61
12943. 5	0.16	0.01	0.00	0.00	0.01	0.00	#VALU E!	0.13	0.02	20.6 4	0.11	#VALU E!	0.00	4.00	
12944. 5	0.13	0.01	0.00	0.00	0.01	0.00	#VALU E!	0.07	0.01	18.8 0	0.08	#VALU E!	0.00	4.00	
12945. 5	0.65	0.01	0.00	0.00	0.01	0.00	0.01	0.16	0.14	16.0 0	0.89	0.00	0.00	5.08	0.58
12946. 5	0.37	0.01	0.00	0.00	0.01	0.00	#VALU E!	0.41	0.07	18.9 0	0.40	0.00	0.00	4.55	
12947. 7	0.74	0.01	0.00	0.00	0.01	0.00	#VALU E!	0.35	0.12	17.7 8	0.91	0.00	0.00	4.77	
12948. 5	0.33	0.01	0.00	0.00	0.01	0.00	#VALU E!	11.2 0	0.07	8.63	0.39	0.00	0.01	5.43	
12949. 5	0.18	0.01	0.00	0.00	0.00	0.00	#VALU E!	0.09	0.03	19.1 0	0.17	0.00	0.00	2.55	
12950. 5	0.80	0.01	0.00	0.00	0.00	0.00	0.00	1.35	0.16	14.4 4	1.08	0.01	0.00	3.14	0.76

12951. 5	0.58	0.01	0.00	0.00	#VALU E!	0.00	#VALU E!	4.74	0.12	13.9 7	0.68	0.00	0.01	2.15	
12952. 5	0.20	0.01	0.00	0.00	0.00	0.00	#VALU E!	0.15	0.04	16.5 7	0.21	#VALU E!	#VALU E!	2.31	
12953. 5	0.25	0.01	0.00	0.00	0.01	0.00	#VALU E!	0.05	0.04	19.8 6	0.25	0.00	0.00	3.69	
12954. 5	0.77	0.01	0.00	0.00	0.01	0.00	0.00	0.21	0.18	13.6 7	1.15	0.01	0.00	4.18	0.63
12955. 5	0.14	0.01	0.00	0.00	0.01	0.00	#VALU E!	0.28	0.02	20.0 9	0.10	#VALU E!	0.00	5.60	
12956. 5	0.23	0.02	0.00	0.00	0.03	0.00	#VALU E!	0.11	0.03	20.0 6	0.22	0.00	0.00	6.25	
12957. 5	0.08	0.02	0.00	0.00	0.03	0.00	#VALU E!	0.15	0.01	18.5 8	0.05	#VALU E!	0.00	5.14	
12958. 5	0.42	0.02	0.00	0.00	0.03	0.00	0.01	19.2 1	0.07	4.60	0.44	0.00	0.01	6.38	0.75
12959. 35	0.21	0.04	0.00	0.01	0.04	0.00	#VALU E!	0.11	0.02	19.7 9	0.17	0.00	0.00	11.90	
12960. 5	0.12	0.03	0.00	0.00	0.03	0.00	#VALU E!	0.20	0.02	16.7 3	0.14	#VALU E!	0.00	12.00	
12961. 5	0.15	0.03	0.00	0.00	0.00	0.00	#VALU E!	0.25	0.01	19.7 1	0.10	#VALU E!	0.00	9.41	
12962. 5	0.50	0.01	0.00	0.00	0.01	0.00	0.06	0.72	0.15	9.14	0.86	0.00	0.00	4.00	0.17
12963. 5	0.29	0.01	0.00	0.00	0.02	0.00	0.03	0.22	0.07	16.5 0	0.42	0.00	0.00	4.13	0.26
12964. 5	0.07	0.01	0.00	0.00	0.01	0.00	#VALU E!	0.04	0.01	15.5 6	0.08	#VALU E!	0.00	3.50	
12965. 5	0.09	0.02	0.00	0.00	0.02	0.00	#VALU E!	0.53	0.02	16.2 0	0.10	#VALU E!	0.00	4.75	
12966. 5	0.75	0.01	0.00	0.00	0.01	0.00	#VALU E!	11.5 8	0.21	9.56	1.09	0.01	0.01	2.87	
12967. 5	1.55	0.02	0.00	0.00	0.02	0.00	#VALU E!	0.74	0.31	13.5 6	1.93	0.01	0.00	6.11	

12967. 92	1.32	0.01	0.00	0.00	#VALU E!	#VALU E!	#VALU E!	0.43	0.30	14.0 0	1.85	0.01	0.00	2.82	
12968	0.85	0.01	0.00	#VALU E!	0.00	#VALU E!	0.02	4.53	0.08	11.5 8	1.55	0.00	0.00	2.71	0.30
12968. 5	0.83	0.01	0.00	#VALU E!	#VALU E!	#VALU E!	#VALU E!	0.21	0.21	15.7 2	1.02	0.01	0.00	1.75	
12969. 5	0.90	0.00	0.00	#VALU E!	#VALU E!	#VALU E!	#VALU E!	0.51	0.27	14.4 7	1.26	0.01	0.00	1.40	
12970. 5	0.59	0.00	0.00	#VALU E!	0.00	#VALU E!	#VALU E!	4.46	0.19	14.7 4	0.69	0.01	0.00	1.43	



McDonald 2H-16E Chemostratigraphy

Depth	Al	V	Cr	U	Zn	Cu	Ni	Ca	Ti	Si	K	Zr	Sr	V/Cr	V/(V+Ni)
6416.5	0.18	#VALUE!	0.00	#VALUE!	0.00	#VALUE!	#VALUE!	33.44	0.07	3.91	0.35	0.01	0.00	#VALUE!	
6419.5	0.31	0.00	0.00	#VALUE!	0.01	#VALUE!	#VALUE!	24.64	0.10	5.41	0.55	0.01	0.00	1.43	
6418.8	0.51	0.00	0.00	#VALUE!	#VALUE!	#VALUE!	#VALUE!	17.69	0.13	8.20	0.70	0.02	0.00	2.50	
6417.8	0.80	0.06	0.00	0.00	0.07	0.01	0.02	1.36	0.19	10.08	1.52	0.01	0.00	25.71	0.74
6416.5	0.95	0.03	0.00	0.01	0.03	0.01	0.02	1.14	0.19	12.10	1.63	0.01	0.00	10.33	0.65
6415.5	1.38	0.04	0.00	0.00	0.05	0.00	0.01	0.63	0.29	12.21	2.28	0.01	0.00	9.74	0.81
6414.5	1.13	0.03	0.00	0.00	0.06	0.00	0.01	0.70	0.26	11.33	2.11	0.01	0.00	6.89	0.84
6413.5	1.02	0.03	0.00	0.00	0.02	0.00	0.00	0.98	0.23	12.42	1.69	0.01	0.00	11.63	0.93
6412.5	1.08	0.04	0.00	0.00	0.06	0.00	0.00	1.05	0.23	11.34	1.81	0.01	0.00	9.42	0.92
6411.8	1.29	0.01	0.00	0.00	0.01	0.00	#VALUE!	2.08	0.29	11.77	2.16	0.01	0.00	4.59	
6409.5	1.40	0.02	0.00	0.00	0.01	0.00	#VALUE!	2.08	0.29	12.07	2.17	0.01	0.00	5.22	
6408.5	1.31	0.02	0.00	0.00	0.02	0.00	0.01	1.88	0.26	11.03	2.01	0.01	0.00	6.53	0.63

6407.5	1.23	0.02	0.00	0.00	0.02	0.00	0.01	1.88	0.27	10.46	1.98	0.01	0.00	4.26	0.70
6406.5	1.56	0.01	0.00	0.00	0.01	0.00	#VALUE!	2.63	0.31	12.33	2.26	0.01	0.00	4.56	
6405.5	1.57	0.01	0.00	0.00	0.01	0.00	#VALUE!	1.76	0.32	12.49	2.21	0.01	0.00	3.58	
6404.5	1.55	0.02	0.00	0.00	0.02	0.00	0.01	2.32	0.29	11.82	2.12	0.01	0.00	4.26	0.67
6403.5	1.45	0.01	0.00	0.00	0.02	0.00	#VALUE!	2.77	0.31	11.71	2.21	0.01	0.00	3.76	
6402.5	1.56	0.01	0.00	0.00	0.01	0.00	#VALUE!	2.65	0.32	12.61	2.16	0.01	0.00	3.88	
6401.5	1.19	0.01	0.00	0.00	0.01	0.00	#VALUE!	2.86	0.30	10.74	2.04	0.01	0.00	4.47	
6400.5	1.58	0.02	0.00	0.00	0.03	0.00	0.01	1.09	0.31	11.71	2.53	0.01	0.00	6.00	0.79
6399.5	1.22	0.02	0.00	0.00	0.01	0.00	0.00	2.90	0.26	9.81	1.86	0.01	0.00	5.58	0.79
6398.5	1.08	0.02	0.00	0.00	0.02	0.00	0.01	1.07	0.22	10.90	1.72	0.01	0.00	5.41	0.71
6397.5	0.95	0.01	0.00	0.00	0.01	0.00	#VALUE!	0.98	0.19	12.90	1.41	0.01	0.00	3.87	
6396.5	0.40	0.00	0.00	0.00	0.00	0.00	#VALUE!	1.87	0.08	16.15	0.57	0.00	0.00	4.00	
6395.5	0.33	0.00	0.00	0.00	0.00	0.00	#VALUE!	1.16	0.07	16.89	0.43	0.00	0.00	3.60	
6394.5	0.94	0.01	0.00	0.00	0.01	0.00	#VALUE!	0.86	0.20	13.74	1.32	0.01	0.00	3.63	
6393.5	0.98	0.01	0.00	0.00	0.01	0.00	#VALUE!	0.92	0.18	15.42	1.17	0.01	0.00	4.17	
6391.5	0.79	0.01	0.00	0.00	0.01	0.00	#VALUE!	1.27	0.15	15.38	0.90	0.01	0.00	3.08	
6390.5	0.97	0.01	0.00	0.00	0.01	0.00	#VALUE!	1.55	0.20	14.31	1.30	0.01	0.00	3.33	

6389.5	1.10	0.01	0.00	0.00	0.01	0.00	#VALUE!	3.73	0.23	10.80	1.74	0.01	0.00	2.95	
6388.5	1.30	0.01	0.00	0.00	0.02	0.00	0.01	0.90	0.27	10.38	1.79	0.01	0.00	3.45	0.63
6387.5	1.30	0.02	0.00	0.01	0.02	0.00	0.01	0.50	0.28	10.23	1.84	0.01	0.00	5.00	0.60
6386.5	1.59	0.01	0.00	0.00	0.01	0.00	#VALUE!	2.85	0.29	11.66	2.20	0.01	0.00	3.63	
6385.5	1.69	0.02	0.00	0.00	0.02	0.00	0.02	0.57	0.27	12.16	1.84	0.01	0.00	3.78	0.51
6384.5	1.34	0.02	0.00	0.00	0.02	0.00	0.01	1.46	0.24	10.64	1.66	0.01	0.00	3.46	0.65
6383.5	1.23	0.01	0.00	0.00	0.01	0.00	0.01	1.39	0.23	13.77	1.51	0.01	0.00	3.88	0.68
6382.5	1.18	0.01	0.00	0.00	0.01	0.00	0.00	0.96	0.22	11.67	1.47	0.01	0.00	2.52	0.81
6381.5	0.29	0.01	0.00	0.00	0.01	0.00	#VALUE!	2.00	0.17	4.56	1.07	0.01	0.00	2.00	
6381.33	1.18	0.01	0.00	0.00	0.00	0.00	#VALUE!	1.35	0.21	13.32	1.46	0.01	0.00	2.89	
6380.5	1.32	0.01	0.00	0.00	0.01	0.00	#VALUE!	2.66	0.22	12.88	1.57	0.01	0.00	3.00	
6379.5	1.35	0.01	0.00	0.00	0.01	0.00	#VALUE!	1.43	0.22	14.14	1.65	0.01	0.00	3.18	
6378.5	1.19	0.01	0.00	0.00	0.01	0.00	#VALUE!	3.51	0.20	12.65	1.64	0.01	0.00	2.59	
6377.5	1.31	0.01	0.00	0.00	0.00	0.00	#VALUE!	2.02	0.23	13.04	1.78	0.01	0.00	2.84	
6376.5	1.48	0.01	0.00	0.00	0.00	0.00	#VALUE!	1.71	0.21	14.15	1.80	0.01	0.00	3.07	
6375.5	1.42	0.01	0.00	0.00	0.00	0.00	#VALUE!	0.94	0.22	14.47	1.70	0.01	0.00	3.47	
6374.5	1.14	0.01	0.00	0.00	0.01	0.00	#VALUE!	1.40	0.22	12.67	1.60	0.01	0.00	2.63	

6373.5	1.01	0.01	0.00	0.00	0.01	0.00	#VALUE!	3.07	0.18	12.94	1.40	0.00	0.00	2.80
6372.5	1.14	0.01	0.00	0.00	0.00	0.00	#VALUE!	1.35	0.20	14.35	1.47	0.01	0.00	3.54
6371.5	1.26	0.01	0.00	0.00	0.00	0.00	#VALUE!	1.14	0.20	14.77	1.56	0.01	0.00	3.29
6370.5	1.14	0.01	0.00	0.00	0.00	0.00	#VALUE!	1.13	0.21	13.83	1.52	0.01	0.00	2.93
6369.5	0.76	0.01	0.00	0.00	0.00	0.00	#VALUE!	1.52	0.18	12.02	1.35	0.00	0.00	2.47
6368.5	0.95	0.01	0.00	0.00	0.00	0.00	#VALUE!	0.87	0.19	14.00	1.38	0.01	0.00	2.93
6367.5	1.24	0.01	0.00	0.00	0.00	0.00	#VALUE!	1.00	0.21	14.61	1.51	0.01	0.00	2.88
6366.5	1.13	0.01	0.00	0.00	0.00	0.00	#VALUE!	1.62	0.19	14.36	1.43	0.01	0.00	3.00
6365.5	0.99	0.01	0.00	0.00	0.00	0.00	#VALUE!	1.13	0.18	14.49	1.27	0.01	0.00	2.71
6364.5	0.67	0.01	0.00	0.00	0.00	0.00	#VALUE!	1.55	0.16	13.58	1.03	0.00	0.00	2.12
6363.5	0.97	0.01	0.00	0.00	0.00	0.00	#VALUE!	1.43	0.20	13.25	1.36	0.01	0.00	2.70
6362.5	0.88	0.01	0.00	0.00	0.01	0.00	#VALUE!	1.53	0.20	12.23	1.32	0.01	0.00	2.63
6361.5	0.77	0.01	0.00	0.00	0.00	0.00	#VALUE!	1.64	0.18	12.08	1.30	0.01	0.00	2.67
6360.5	1.12	0.01	0.00	0.00	0.01	0.00	#VALUE!	1.28	0.23	13.12	1.46	0.01	0.00	2.82
6359.5	1.16	0.01	0.00	0.00	0.01	0.00	#VALUE!	1.21	0.22	13.14	1.56	0.01	0.00	2.56
6358.5	0.46	0.01	0.00	0.00	0.01	0.00	#VALUE!	1.12	0.18	8.78	1.11	0.01	0.00	2.18
6357.5	0.78	0.01	0.00	0.00	0.01	0.00	#VALUE!	1.44	0.20	12.09	1.32	0.01	0.00	2.42

6356.5	1.01	0.01	0.00	0.00	0.01	0.00	#VALUE!	1.14	0.20	13.39	1.32	0.01	0.00	2.53	
6355.5	0.51	0.01	0.00	0.00	0.00	0.00	#VALUE!	1.34	0.17	10.33	0.98	0.01	0.00	2.11	
6354.5	1.10	0.01	0.00	0.00	0.00	0.00	#VALUE!	2.14	0.20	15.03	1.28	0.01	0.00	3.23	
6353.5	1.25	0.01	0.00	0.00	0.01	0.00	#VALUE!	2.18	0.24	13.46	1.47	0.01	0.00	2.74	
6352.5	0.98	0.01	0.00	0.00	0.01	0.00	#VALUE!	2.53	0.19	15.08	1.19	0.01	0.00	3.33	
6351.5	0.95	0.01	0.00	0.00	0.01	0.00	0.00	1.48	0.24	11.85	1.36	0.01	0.00	3.10	0.86
6350.5	0.35	0.01	0.00	0.00	0.01	0.00	#VALUE!	0.99	0.17	7.67	0.94	0.01	0.00	2.40	
6349.5	1.00	0.01	0.00	0.00	0.01	0.00	0.00	0.89	0.20	14.56	1.21	0.01	0.00	3.38	0.72
6348.5	0.61	0.01	0.00	0.00	0.01	0.00	#VALUE!	0.59	0.14	15.22	0.82	0.00	0.00	3.00	
6347.5	0.93	0.01	0.00	0.00	0.01	0.00	0.01	0.77	0.21	13.73	1.19	0.01	0.00	3.44	0.62
6346.5	0.95	0.01	0.00	0.01	0.01	0.00	0.00	1.39	0.20	13.43	1.20	0.01	0.00	2.95	0.73
6345.5	0.73	0.01	0.00	0.00	0.01	0.00	0.00	0.93	0.19	11.22	1.25	0.01	0.00	2.67	0.84
6344.5	0.12	0.00	0.00	#VALUE!	#VALUE!	#VALUE!	#VALUE!	0.20	0.03	16.76	0.16	#VALUE!	0.00	0.57	
6343.5	0.86	0.01	0.00	0.00	0.00	0.00	#VALUE!	3.83	0.15	13.86	1.16	0.00	0.00	3.00	
6342.5	1.06	0.01	0.00	0.00	0.01	0.00	0.00	1.09	0.21	13.21	1.34	0.01	0.00	3.14	0.76
6341.5	0.94	0.01	0.00	0.00	0.01	0.00	0.00	0.88	0.20	14.11	1.15	0.01	0.00	3.11	0.80
6340.5	1.00	0.01	0.00	0.00	0.01	0.00	0.00	1.22	0.20	12.81	1.24	0.01	0.00	2.36	0.79

6339.5	0.93	0.01	0.00	0.00	0.01	0.00	0.01	1.27	0.20	12.75	1.18	0.01	0.00	2.43	0.60
6338.5	0.21	0.00	0.00	0.00	0.00	#VALUE!	#VALUE!	0.43	0.04	18.25	0.27	0.00	0.00	1.33	
6337.5	0.80	0.01	0.00	0.00	0.01	0.00	#VALUE!	0.46	0.18	13.38	1.26	0.00	0.00	2.30	
6336.5	0.34	0.01	0.00	0.00	0.00	0.00	#VALUE!	0.49	0.11	11.69	0.71	0.00	0.00	1.79	
6335.5	0.14	#VALUE!	0.00	0.00	#VALUE!	#VALUE!	#VALUE!	0.34	0.02	18.06	0.14	#VALUE!	0.00	#VALUE!	
6334.5	0.30	0.00	0.00	0.00	0.00	#VALUE!	#VALUE!	0.22	0.05	19.06	0.33	0.00	0.00	2.00	
6333.5	0.75	0.01	0.00	0.00	0.01	0.00	#VALUE!	0.78	0.12	17.21	0.85	0.00	0.00	3.00	
6332.5	0.38	0.00	0.00	0.00	0.00	#VALUE!	#VALUE!	0.43	0.05	16.06	0.36	0.00	0.00	2.29	
6331.5	0.37	0.00	0.00	0.00	0.00	#VALUE!	#VALUE!	0.48	0.07	14.07	0.47	0.00	0.00	1.33	
6330.5	0.86	0.01	0.00	0.00	0.01	0.00	0.01	0.54	0.17	15.43	1.14	0.01	0.00	2.88	0.60
6329.5	0.32	0.00	0.00	0.00	0.00	#VALUE!	#VALUE!	0.96	0.08	15.35	0.52	0.00	0.00	1.33	
6328.5	0.43	0.00	0.00	0.00	0.00	0.00	#VALUE!	1.21	0.07	15.47	0.55	0.00	0.00	2.50	
6327.5	0.80	0.01	0.00	0.00	0.01	0.00	0.01	1.27	0.14	13.91	0.98	0.00	0.00	2.33	0.43
6326.5	0.78	0.01	0.00	0.00	0.01	0.00	#VALUE!	1.18	0.17	12.23	1.24	0.01	0.00	2.38	
6325.5	1.31	0.01	0.00	0.00	0.01	0.00	#VALUE!	0.88	0.23	13.72	1.64	0.01	0.00	3.38	
6324.5	0.76	0.01	0.00	#VALUE!	0.01	0.00	#VALUE!	1.12	0.18	13.17	1.29	0.01	0.00	2.38	
6323.5	1.18	0.01	0.00	#VALUE!	0.01	0.00	#VALUE!	0.78	0.25	12.27	1.89	0.01	0.00	2.33	

6322.5	1.51	0.01	0.00	#VALUE!	0.01	0.00	#VALUE!	0.87	0.26	14.68	1.89	0.01	0.00	2.22	
6321.5	1.12	0.01	0.00	#VALUE!	0.01	0.00	#VALUE!	0.84	0.23	13.60	1.67	0.01	0.00	2.25	
6320.5	0.85	0.01	0.00	#VALUE!	0.01	0.00	#VALUE!	0.80	0.21	12.68	1.41	0.01	0.00	2.00	
6319.5	1.30	0.01	0.00	#VALUE!	0.00	0.00	#VALUE!	0.89	0.23	14.95	1.63	0.01	0.00	2.11	
6318.5	1.21	0.01	0.00	#VALUE!	0.01	0.00	#VALUE!	0.62	0.21	15.51	1.68	0.01	0.00	4.89	
6317.5	0.89	0.01	0.00	0.00	0.01	0.00	#VALUE!	2.81	0.16	15.14	1.10	0.01	0.00	4.91	
6316.5	1.18	0.01	0.00	0.00	0.01	0.00	#VALUE!	2.12	0.24	13.35	1.61	0.01	0.00	4.67	
6315.5	0.84	0.01	0.00	0.00	0.00	0.00	#VALUE!	1.48	0.18	15.46	1.09	0.01	0.00	4.18	
6314.5	0.98	0.01	0.00	0.00	0.01	0.00	#VALUE!	2.07	0.20	14.94	1.21	0.01	0.00	5.60	
6313.5	0.36	0.01	0.00	0.00	0.00	#VALUE!	#VALUE!	2.35	0.09	14.51	0.55	0.00	0.00	2.50	
6312.5	0.58	0.01	0.00	0.00	0.01	0.00	#VALUE!	0.45	0.13	13.76	0.99	0.00	0.00	2.67	
6311.5	0.73	0.01	0.00	0.00	0.01	0.00	#VALUE!	0.70	0.17	14.24	1.12	0.01	0.00	3.86	
6310.5	0.30	0.00	#VALUE!	#VALUE!	0.00	#VALUE!	#VALUE!	0.26	0.03	19.95	0.23	0.00	0.00	#VALUE!	
6309.5	1.01	0.01	0.00	0.00	0.01	0.00	0.00	1.24	0.18	15.83	1.27	0.01	0.00	4.15	0.80
6308.5	0.17	0.00	0.00	#VALUE!	0.00	#VALUE!	#VALUE!	0.05	0.03	18.41	0.23	#VALUE!	0.00	0.73	
6307.5	0.17	0.00	0.00	#VALUE!	0.00	#VALUE!	#VALUE!	0.09	0.04	14.90	0.29	0.00	0.00	0.75	
6306.5	1.10	0.01	0.00	0.00	0.01	0.00	#VALUE!	4.88	0.22	14.36	1.39	0.01	0.01	4.00	



6305.5	0.38	0.00	0.00	#VALUE!	0.01	0.00	#VALUE!	2.72	0.05	18.06	0.34	0.00	0.00	4.00	
6304.5	1.17	0.01	0.00	#VALUE!	0.01	0.00	#VALUE!	0.51	0.22	16.45	1.45	0.01	0.00	4.00	
6303.5	0.39	0.00	0.00	#VALUE!	0.01	0.00	#VALUE!	0.57	0.09	16.34	0.62	0.00	0.00	1.67	
6302.5	0.34	0.00	0.00	#VALUE!	0.01	0.00	#VALUE!	0.62	0.08	15.40	0.53	0.00	0.00	1.07	
6301.5	0.82	0.01	0.00	0.00	0.01	0.00	#VALUE!	8.32	0.20	11.90	1.07	0.01	0.01	3.00	
6300.5	0.57	0.01	0.00	#VALUE!	0.01	0.00	#VALUE!	0.51	0.15	14.36	0.97	0.01	0.00	2.14	
6299.5	0.86	0.01	0.00	0.00	0.02	0.00	#VALUE!	2.46	0.20	12.69	1.36	0.01	0.00	3.88	
6298.5	0.31	0.00	0.00	#VALUE!	0.01	0.00	#VALUE!	0.63	0.05	18.50	0.35	0.00	0.00	1.60	
6297.5	0.49	0.00	0.00	#VALUE!	0.02	0.00	#VALUE!	0.56	0.08	18.38	0.59	0.00	0.00	2.33	
6296.5	0.90	0.01	0.00	#VALUE!	0.01	0.00	#VALUE!	0.83	0.19	15.15	1.23	0.01	0.00	2.62	
6295.5	0.32	0.00	0.00	#VALUE!	0.01	0.00	#VALUE!	0.63	0.06	13.00	0.43	0.00	0.00	0.90	
6294.5	0.25	0.00	0.00	#VALUE!	0.01	0.00	#VALUE!	0.93	0.04	17.21	0.28	0.00	0.00	0.75	
6293.5	0.72	0.00	0.00	#VALUE!	0.01	0.00	#VALUE!	1.69	0.14	16.21	0.96	0.00	0.00	2.00	
6292.5	1.00	0.01	0.00	0.00	0.01	0.00	#VALUE!	1.49	0.20	15.22	1.34	0.01	0.00	3.64	
6291.4	0.26	0.00	0.00	#VALUE!	0.01	0.00	#VALUE!	1.36	0.12	6.99	0.64	0.00	0.00	1.29	
6290.5	0.70	0.01	0.00	#VALUE!	0.01	0.00	#VALUE!	1.04	0.19	12.76	1.29	0.01	0.00	2.50	
6289.5	0.68	0.00	0.00	#VALUE!	0.02	0.00	#VALUE!	0.84	0.14	15.42	0.97	0.00	0.00	2.60	

6288.5	0.68	0.01	0.00	#VALU E!	0.01	0.00	#VALU E!	1.46	0.16	13.9 2	1.12	0.01	0.00	2.62	
6287.5	0.48	0.00	0.00	#VALU E!	0.01	0.00	#VALU E!	1.62	0.09	16.5 0	0.60	0.00	0.00	2.00	
6286.5	0.69	0.00	0.00	#VALU E!	0.02	0.00	#VALU E!	1.06	0.14	16.1 5	0.95	0.00	0.00	2.60	
6285.5	0.61	0.01	0.00	#VALU E!	0.01	0.00	#VALU E!	1.28	0.15	13.4 1	1.04	0.00	0.00	2.31	
6284.5	1.12	0.01	0.00	0.00	0.02	0.00	#VALU E!	1.00	0.20	15.5 9	1.45	0.01	0.00	3.33	
6283.5	0.22	0.00	0.00	#VALU E!	0.01	0.00	#VALU E!	1.65	0.05	16.7 5	0.34	0.00	0.00	1.00	
6282.5	0.77	0.01	0.00	0.00	0.03	0.00	#VALU E!	4.56	0.19	10.7 7	1.37	0.01	0.01	2.78	
6281.5	0.91	0.01	0.00	0.00	0.02	0.00	#VALU E!	3.77	0.16	14.8 7	1.17	0.01	0.01	2.91	
6280.5	1.02	0.01	0.00	0.00	0.02	0.00	#VALU E!	1.98	0.17	15.4 0	1.29	0.01	0.00	3.33	
6279.5	0.60	0.01	0.00	0.00	0.01	0.00	#VALU E!	2.28	0.12	14.6 0	0.92	0.00	0.00	2.43	
6278.5	0.69	0.01	0.00	#VALU E!	0.02	0.00	#VALU E!	0.99	0.16	13.5 1	1.21	0.00	0.00	2.24	
6277.5	0.90	0.01	0.00	#VALU E!	0.01	0.00	#VALU E!	1.12	0.19	14.2 3	1.36	0.01	0.00	2.77	
6276.5	0.91	0.01	0.00	0.00	0.03	0.00	#VALU E!	8.71	0.16	12.9 4	1.12	0.01	0.01	3.38	
6275.5	0.53	0.00	0.00	#VALU E!	0.01	0.00	#VALU E!	1.85	0.10	16.0 9	0.75	0.00	0.00	2.22	
6274.5	0.81	0.01	0.00	#VALU E!	0.01	0.00	#VALU E!	1.30	0.16	14.9 2	1.12	0.00	0.00	3.00	
6273.5	0.45	0.00	0.00	#VALU E!	0.01	0.00	#VALU E!	1.37	0.09	16.2 1	0.60	0.00	0.00	1.64	
6272.5	0.23	0.00	0.00	#VALU E!	0.01	#VALU E!	#VALU E!	2.09	0.04	16.5 8	0.29	0.00	0.00	1.09	

6271.5	0.22	#VALUE!	#VALUE!	#VALUE!	0.01	#VALUE!	#VALUE!	2.57	0.02	20.25	0.15	#VALUE!	0.00	#VALUE!	
6270.5	0.35	0.00	0.00	#VALUE!	0.01	0.00	#VALUE!	1.85	0.05	18.83	0.38	0.00	0.00	1.67	
6269.5	0.68	0.01	0.00	#VALUE!	0.02	0.00	#VALUE!	1.37	0.19	11.50	1.29	0.01	0.00	2.78	
6268.5	0.39	0.00	0.00	#VALUE!	0.01	0.00	#VALUE!	1.50	0.07	18.89	0.40	0.00	0.00	2.00	
6267.5	1.15	0.01	0.00	#VALUE!	0.02	0.00	#VALUE!	0.80	0.24	14.61	1.58	0.01	0.00	3.00	
6266.5	0.00	#VALUE!	#VALUE!	#VALUE!	0.06	0.00	#VALUE!	0.00	#VALUE!	0.00	0.00	0.00	0.00	#VALUE!	
6266.5	0.00	#VALUE!	#VALUE!	#VALUE!	0.06	#VALUE!	#VALUE!	0.00	#VALUE!	0.00	0.00	0.01	0.00	#VALUE!	
6266.5	0.00	0.00	0.00	#VALUE!	0.06	0.00	#VALUE!	0.44	0.13	0.00	0.92	0.00	0.00	3.00	
6266.5	0.77	0.00	0.00	#VALUE!	0.06	0.00	#VALUE!	0.43	0.13	18.50	0.91	0.00	0.00	3.00	
6265.5	0.91	0.01	0.00	0.00	0.01	0.00	#VALUE!	10.65	0.20	11.47	1.01	0.01	0.00	2.57	
6264.5	0.09	0.00	0.00	#VALUE!	0.00	0.00	#VALUE!	1.80	0.03	14.92	0.16	0.00	0.00	0.62	
6264	0.82	0.01	0.00	#VALUE!	0.01	0.00	#VALUE!	0.77	0.20	12.99	1.24	0.01	0.00	2.53	
6263.917	0.70	0.01	0.00	0.00	0.01	0.00	0.00	11.46	0.14	12.74	0.72	0.01	0.01	3.20	0.70
6263.5	1.35	0.01	0.00	0.00	0.01	0.00	#VALUE!	5.98	0.29	14.26	1.52	0.01	0.01	3.18	
6263	1.69	0.01	0.00	0.00	0.02	0.00	#VALUE!	0.40	0.35	13.78	2.03	0.01	0.00	2.96	
6262.917	1.03	0.02	0.00	0.00	0.02	0.00	#VALUE!	3.26	0.30	10.12	1.74	0.01	0.00	4.09	
6262.5	1.13	0.01	0.00	0.00	0.01	0.00	#VALUE!	6.87	0.29	11.41	1.52	0.01	0.01	3.26	

6261.5	1.16	0.01	0.00	0.00	0.02	0.00	0.01	3.27	0.30	9.85	1.94	0.01	0.00	3.28	0.53
6260.917	1.17	0.02	0.00	0.00	0.01	0.01	0.01	3.37	0.32	9.73	2.00	0.01	0.00	3.26	0.66
6260.75	1.10	0.02	0.00	0.00	0.00	0.00	0.00	2.67	0.33	9.34	2.03	0.01	0.00	3.36	0.83
6260.5	2.06	0.02	0.01	0.00	0.01	0.00	#VALUE!	1.59	0.38	13.00	2.46	0.01	0.00	3.42	
6260	0.60	0.01	0.00	0.00	0.01	0.00	0.00	14.23	0.16	6.38	0.90	0.01	0.01	4.29	0.69
6259.5	0.67	0.04	0.02	#VALUE!	0.05	0.00	0.30	2.82	0.21	7.70	1.40	0.02	0.00	2.84	0.13
6258.5	0.91	0.03	0.05	#VALUE!	0.02	0.00	0.02	3.05	0.18	8.34	1.53	0.01	0.00	0.61	0.63
6258.17	0.72	0.01	0.01	0.00	0.01	#VALUE!	0.00	19.11	0.17	8.78	0.61	0.01	0.00	1.03	0.65
6256.5	1.04	0.01	0.01	#VALUE!	0.02	0.00	#VALUE!	10.58	0.25	11.60	1.30	0.02	0.00	1.36	
6256.17	0.92	0.00	0.00	#VALUE!	0.00	#VALUE!	#VALUE!	15.85	0.23	9.28	0.90	0.02	0.00	1.73	
6255.5	0.61	0.00	0.00	#VALUE!	0.00	#VALUE!	#VALUE!	23.30	0.15	6.88	0.55	0.01	0.00	1.82	
6254.5	0.21	#VALUE!	0.00	#VALUE!	0.00	#VALUE!	#VALUE!	38.84	0.08	3.86	0.15	0.01	0.01	#VALUE!	
6253.5	0.19	#VALUE!	0.00	#VALUE!	#VALUE!	#VALUE!	#VALUE!	40.52	0.08	3.54	0.13	0.01	0.00	#VALUE!	

## VITA

Eli Christian Reese

Candidate for the Degree of

Master of Science

Thesis: LITHOFACIES AND CHEMOSTRATIGRAPHIC EVALUATION OF THE  
WOODFORD SHALE IN THE WESTERN ARKOMA AND EASTERN ANADARKO  
BASINS, OKLAHOMA

Major Field: Geology

Biographical: Born in Nardin, Oklahoma, on March 26, 1990, the son of Ken and Lynn Reese.  
Married Weslee Ann Simpson on May 23, 2014.

Education: Graduated from Deer Creek-Lamont High School, Lamont, Oklahoma in May 2009;  
received Bachelor of Science degree in Geology from Oklahoma State University,  
Stillwater, Oklahoma, in December 2013. Completed requirements for the Master of  
Science degree with a major in Geology at Oklahoma State University in December  
2016.

Experience: Interned for Samson Resources in Tulsa, Oklahoma, May 2014 to August 2014;  
Interned for Newfield Exploration in Tulsa, Oklahoma and The Woodlands, Texas,  
May 2015 to August 2015 and May 2016 to August 2016; employed as a teaching  
assistant for two years by Oklahoma State University, teaching laboratories for  
introductory geology.

Professional Memberships: American Association of Petroleum Geologists